Fall 2017

Precipitation and Sea Level Rise Impacts on Groundwater Levels in Virginia Beach, Virginia

Brett A. Buzzanga
Old Dominion University, bbuzz001@odu.edu

PRECIPITATION AND SEA LEVEL RISE IMPACTS

ON GROUNDWATER LEVELS IN VIRGINIA BEACH, VIRGINIA

by

Brett A. Buzzanga
B.A. May 2011, Rutgers University
A.S. December 2013, Brookdale Community College

A Thesis Submitted to the Faculty of
Old Dominion University in Partial Fulfillment of the
Requirements for the Degree of

MASTER OF SCIENCE

OCEAN AND EARTH SCIENCES

OLD DOMINION UNIVERSITY
December 2017

Approved by:

Hans-Peter Plag (Director)

Richard G. Whittecar (Member)

Hua Liu (Member)

ABSTRACT

PRECIPITATION AND SEA LEVEL RISE IMPACTS ON GROUNDWATER LEVELS IN VIRGINIA BEACH, VIRGINIA

Brett A. Buzzanga
Old Dominion University, 2017
Director: Dr. Hans-Peter Plag

Global sea level rise (SLR) is one of the most immediate impacts of climate change, and poses a significant threat to low-lying coastal communities worldwide. The metropolitan region of Hampton Roads in Southeastern Virginia is one such community, and one where knowledge surrounding SLR is rapidly accumulating. However, most of the research is focused exclusively on surface water processes despite the presence of a shallow groundwater table closely connected to them. SLR will continue to cause the groundwater table to rise in tidally influenced areas of Hampton Roads, and thereby decrease storage capacity of the unsaturated zone.

This study investigates the spatial and temporal response of the groundwater table to SLR and precipitation. A tidal watershed, West Neck Creek, in Hampton Roads was chosen to conduct a conceptual yet realistic simulation of the hydrologic cycle using historical precipitation data with SLR scenarios from 0 m (current) to 2 m in 1 m intervals. Groundwater infiltration from the land surface, recharge, and evapotranspiration are modeled using the Unsaturated-Zone Flow package with MODFLOW-NWT. Groundwater rise is simulated by increasing the stage of the tidal stream that drains the watershed. Precipitation and overland runoff are simulated using the surface water model SWMM. The two models are coupled to permit the exchange of boundary condition values at each time step. An ensemble approach is taken to test model sensitivity to a variety of parameters.

The findings of the study demonstrated the potential for the effects of SLR-induced groundwater rise to become a damaging hazard to Virginia Beach communities and ecosystems. Most of the potential damages arose from increased interactions of groundwater levels with subsurface infrastructure. Additional runoff was found to be of lesser concern, because the prevalent soils in West Neck Creek are characterized by slow infiltration rates. The results of the sensitivity analysis provided encouraging results, in that changes in parameters did not have excessively large effects on forcing variables. Overall, this study provides a foundation to guide future scientific and engineering efforts to mitigate and adapt to the increasing threat of SLR-induced groundwater rise.

This thesis is dedicated to my Grandfathers.

ACKNOWLEDGMENTS

First, thank you to my advisor Dr. Hans-Peter Plag. Your guidance and patience have been essential in helping me through this thesis, and your wisdom has instilled in me a scientific frame of mind that will be invaluable for all my future endeavors.

Additional thanks to the following people:

- Dr. Rich Whittecar, for his seemingly unlimited hydrological and local knowledge that provided the foundation for this project,
- Dr. Hua Liu and the ODU Center for Geospatial & Visualization Computing for teaching me how to effectively use ArcGIS,
- Kurt McCoy (USGS) for data and information,
- Drs. Ben Hamlington and John Klinck, and Sean O'Brien for IT support,
- Dr. Eileen Hofmann and the Department of Coastal and Physical Oceanography for fostering interdisciplinary research,
- my fellow graduate students for laughter, empathy, and coffee,
- and my parents for perpetual, unwavering support.

TABLE OF CONTENTS

Page

Chapter Page

LIST OF TABLES

Table Page

LIST OF FIGURES

Figure Page

CHAPTER 1

INTRODUCTION

As humanity continues to push the Earth out of the relatively stable Holocene into the Anthropocene, there is an urgent need to create the knowledge necessary to adapt to this transition (Rockstrom et al. 2009; Steffen et al. 2015). The warming planet is already resulting in rising seas, and with nearly half the global population living within 100 km of an ocean, SLR poses a significant threat to low-lying coastal communities worldwide (Harbaugh 2005; Small 2003). Further, the latest research suggests that minimum and maximum estimates of SLR projected for this century and beyond are higher than previously determined, and could occur sooner than expected due to instabilities in the Greenland and Antarctic ice sheets (Sweet et al. 2017). As shown in Figure 1, under the red 'business-as-usual' emissions scenario, a 2.5 m increase in global sea levels has a 90% conditional probability to occur before the end of this century.

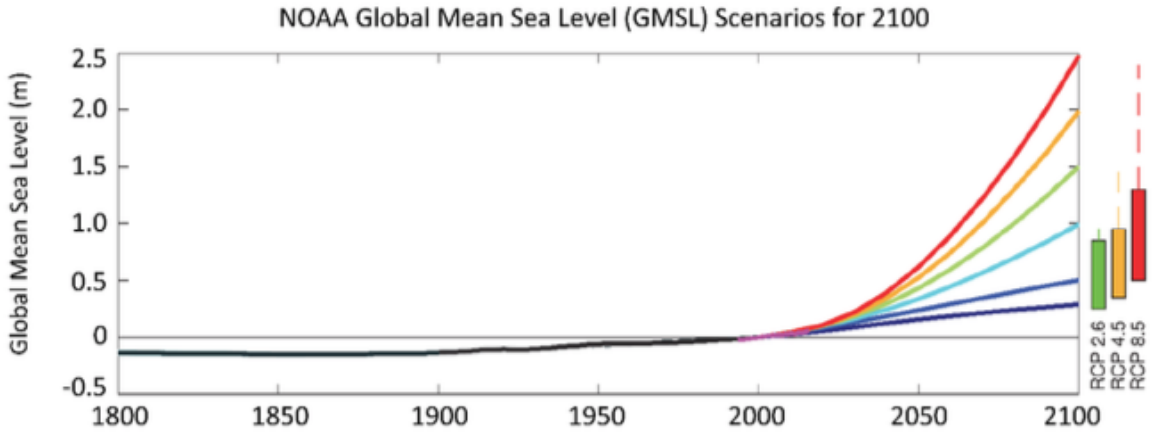

Figure 1: Global Mean Sea Level Rise Scenarios for 2100. The lowest scenario is based on historical data, projecting the current rate of 3 mm/yr constantly into the future. Ice sheet dynamics and greater ocean/atmospheric warming are included as the scenarios increase in magnitude (source: Sweet et al. 2017).

Despite this understanding, there is still much uncertainty in future SLR. Ice sheet melt rates are not well understood (Alley et al. 2015), and changes in ocean currents may accelerate SLR well beyond predicted levels in some regions (Ezer et al. 2013). Further, the probability of rapid sea level rise is recently thought to be increasing (Hansen et al. 2016). Regardless of extent, localities experience SLR differently than global averages, with some experiencing much faster rates (Fig. 2).

The metropolitan region of Hampton Roads in Southeastern Virginia, home to over 1.5 million people (U.S. Census Bureau 2012) and the world's largest naval base, is one such community. Large parts of it have low relief, and the entire region is experiencing land subsidence from ground-water (GW) withdrawals and post-glacial adjustment (Scott

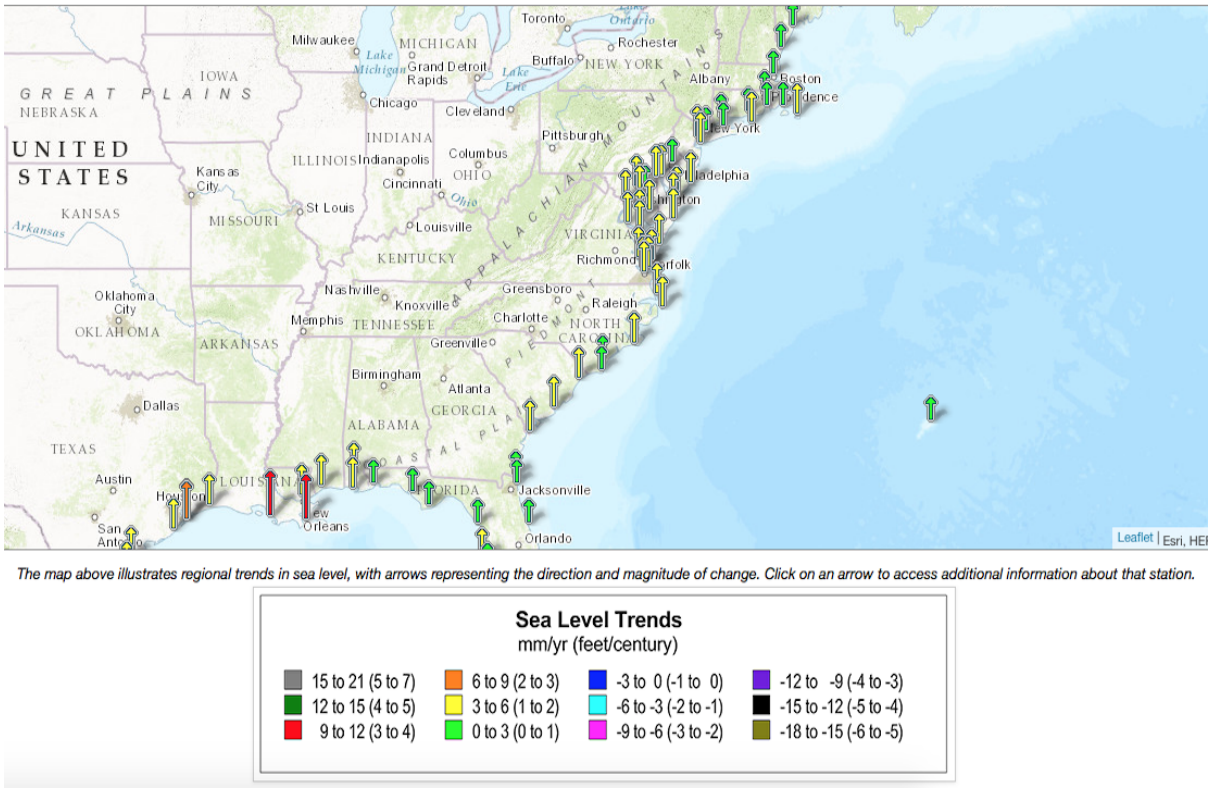

Figure 2: Local rates of sea level rise on the Atlantic and gulf coasts of the US (source: NOAA 2017).

et al. 2010; Eggleston & Pope 2013). These characteristics contribute to Hampton Roads experiencing the highest rates of local SLR on the Atlantic Coast of the United States (Zervas 2009).

Negative impacts of SLR felt already today, such as inundation, flooding, and GW contamination, will continue to affect Hampton Roads' environments. Inundation and erosion may cause valuable infrastructure, including the Virginia Port Authority and Norfolk Naval Base to become unusable (Wright & Hogan 2008; Li et al. 2012). Storm surge flooding poses an increasing threat to the human populations of coastal neighborhoods (Kleinosky et al. 2006; McFarlane 2011), and to thousands of acres of protected lands (McFarlane 2012). Freshwater aquifers are vulnerable to vertical migration of contaminants from inundation and overland flooding (Masterson & Garabedian 2007), and to the horizontal movement of salt water into fresh GW aquifers – the process known as saltwater intrusion (SWI).

While the body of knowledge surrounding SLR in Hampton Roads is rapidly accumulating, most of the research is focused on surface water processes. However, water tables in coastal unconfined aquifers are increasing in connection with SLR (Masterson 2004; Rotzoll & Fletcher 2012; Bjerklie et al. 2012). When the GW table intersects the land surface or infiltrates subsurface infrastructure, it causes localized GW flooding (Fig. 3) (Rotzoll & Fletcher 2012).

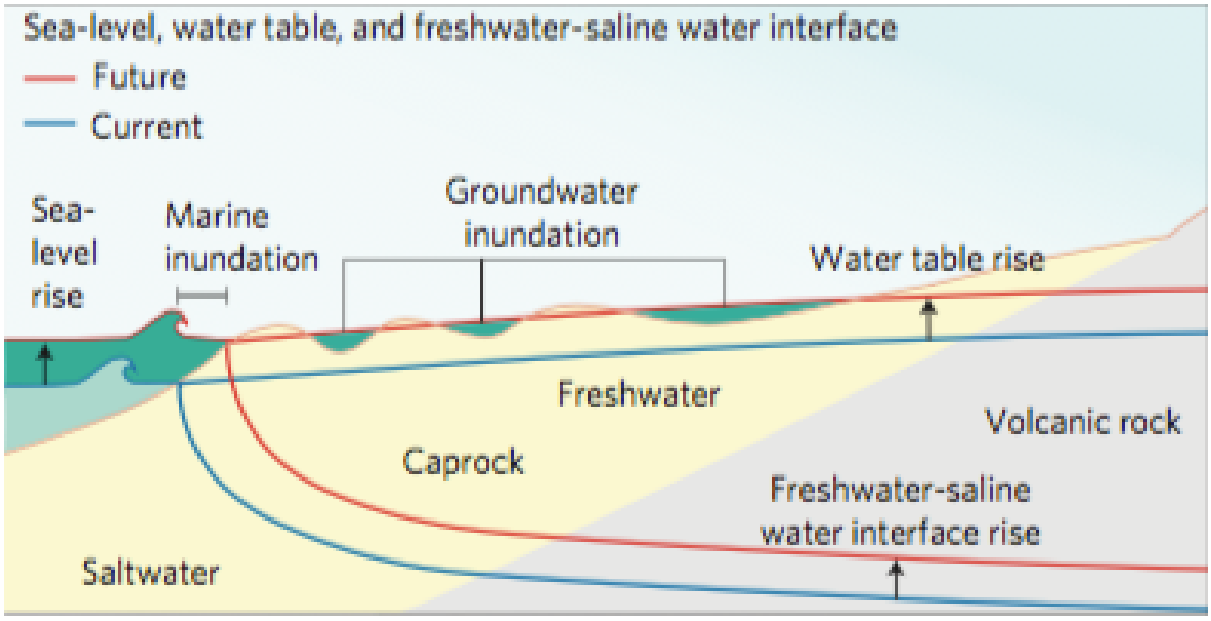

Figure 3: Flooding occurring as SLR forces GW levels above the land surface in Honolulu, Hawaii (source: Rotzoll & Fletcher 2012).

Though it is conceptually clear that the GW levels rise in response to precipitation-induced infiltration, how a specific aquifer reacts depends on numerous factors, such as antecedent soil-water conditions, rainfall characteristics, and subsurface flow (Fetter 2014, p. 54). At locations with a shallow depth to water (DTW), the potential exists for precipitation events to saturate the vadose zone, preventing infiltration and causing overland runoff (Dunne & Leopold 1978). This inability of precipitation to infiltrate has become a significant problem in the United Kingdom (UK), where widespread and long-term GW flooding can result during winter months with above average rainfall (Morris et al. 2015).

To properly account for future risk of GW flooding, potential effects of climate change also must be considered to understand how the water table response to rainfall will be altered in the future. Several studies have explored the water table response to changed rainfall characteristics, but neglected to consider SLR, such as Pinault et al. (2005); Kidmose et al. (2013). Others have modeled changes in recharge with increases in SLR, but stopped short of analyzing specific rainfall scenarios (Bjerklie et al. 2012; Vandenbohede et al. 2008). Fordyce (2014) united these approaches in a study of storm events and SLR scenarios to demonstrate an increase in flood frequency for equal rainfall amounts under higher sea levels. While that study effectively determined the spatial extent of GW flooding, it did not consider the effects of a higher water table on runoff generation.

Even in areas where a shallow GW table does not rise above the land surface to cause flooding, a higher water table inhibits the ability of precipitation to infiltrate into the subsurface, potentially interacting with subsurface infrastructure and/or causing increased stormwater runoff (Sophocleous 2004; Bjerklie et al. 2012). To explore these effects, this

thesis undertook an investigation into how SLR-induced GW rise responds to historical precipitation by:

1. Developing a steady-state GW flow model representative of present day conditions,
2. Simulating changes in GW levels for future SLR scenarios using the historic rainfall record, and
3. Performing a sensitivity analysis on the model parameters to discern the impact of SLR in various model configurations

To achieve these objectives, first a three-dimensional GW flow model was constructed using a Newton Formulation for MODFLOW-2005 (MODFLOW-NWT) that delineated the spatial extent of a SLR-induced increase in GW levels (Niswonger et al. 2011). Next, a surface water model was built using the Environmental Protection Agency (EPA)'s storm water management model (SWMM) to separate precipitation events into infiltration and runoff (Rossman 2015). The unsaturated-zone flow (UZF1) package for MODFLOW-NWT simulated the movement of this infiltration through the unsaturated zone of an unconfined aquifer (Niswonger et al. 2006). Finally, runoff was routed by the land surface capabilities of SWMM, until it exited the system via evapotranspiration (ET), infiltration, or as flow into a surface water body. These processes are fundamentally linked, so an interface was developed using the programming language Python 2.7 to couple MODFLOW-NWT and SWMM, enabling the exchange of information at each time step.

West Neck Creek (WNC) watershed in southern Virginia Beach was chosen for the investigation of these relationships. It has a relatively simple hydrogeologic structure that enables results to be extrapolated to other catchments. Further, it is largely undeveloped land, which permits a better representation of natural processes. Finally, the importance of adaptation to climate change in the Hampton Roads region accents the usefulness of this study area.

CHAPTER 2

HYDROLOGICAL BACKGROUND

2.1 INTRODUCTION

The hydrologic cycle is the collection of processes by which water moves through different reservoirs above, within, and upon the earth. (Fig. 4). The largest of these reservoirs are the oceans, with 97.2% of the world's water supply (Feth 1973). Others include ice caps and glaciers, GW, surface water, soil moisture, and the atmosphere.

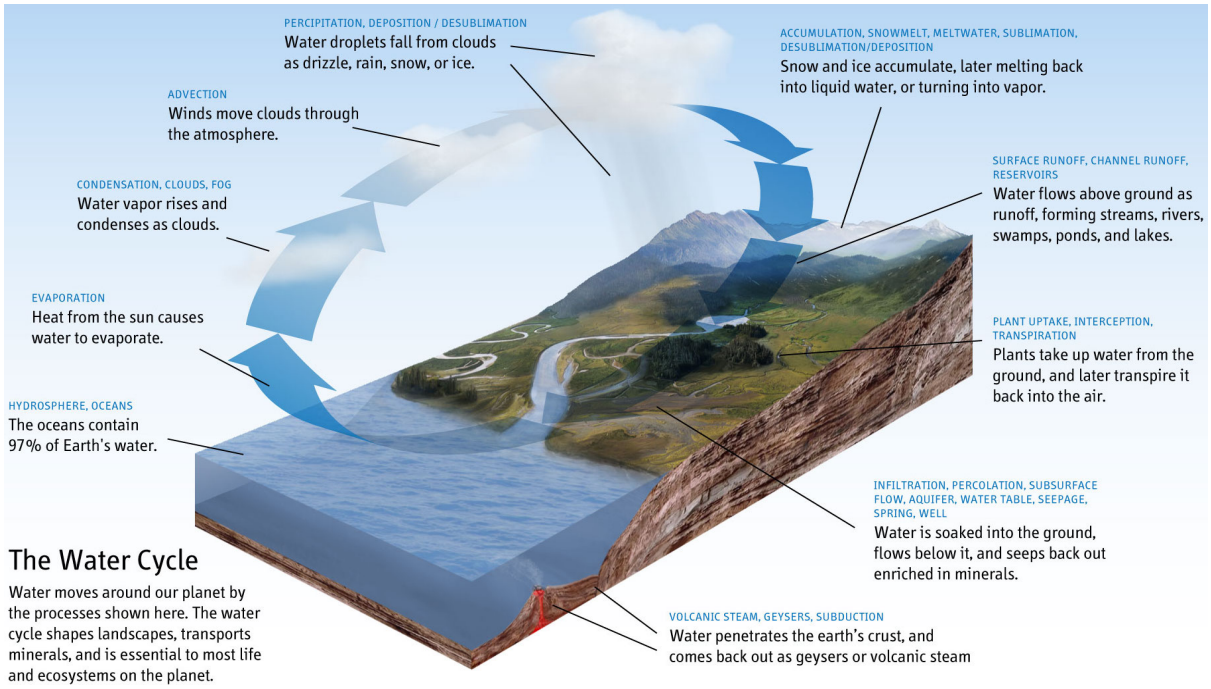

Figure 4: Movement of water through the hydrologic cycle (source: Tal 2016)

The cycle has no beginning or end, but for convenience we start with water stored as vapor in the atmosphere. As air becomes saturated, vapor condenses into droplets or ice crystals to fall under gravity as precipitation. If this precipitation reaches the ground, it infiltrates into the subsurface, is held temporarily as storage, or flows overland as runoff. Eventually, this water returns to the atmosphere via evaporation and transpiration.

For a specific area and time, these processes are most simply quantitatively evaluated with the law of mass conservation (Fetter 2014, p. 20):

$$Inflow = outflow \pm changes\ in\ storage \tag{1}$$

Most often, rainfall is the dominant inflow and ET, the lumped term for the processes of evaporation and transpiration, the dominant outflow (Xu & Singh 1998). Water is mainly stored in surface water, such as oceans and lakes, in solid form as part of the cryosphere,

or below ground in subsurface rock or sediment formations. These underground geologic units are broadly classified into aquifers or confining units (sometimes called aquitards) depending on how easily they transmit water (Fetter 2014, p. 113). Aquifers are further subdivided into confined aquifers, whose upper boundary is a confining unit, or unconfined aquifers, whose upper boundary is called the water table (Fig. 5). Generally, the water table is the top of the saturated zone where the pore water and atmospheric pressure are equivalent. Between the water table and land surface exists the unsaturated, or vadose, zone.

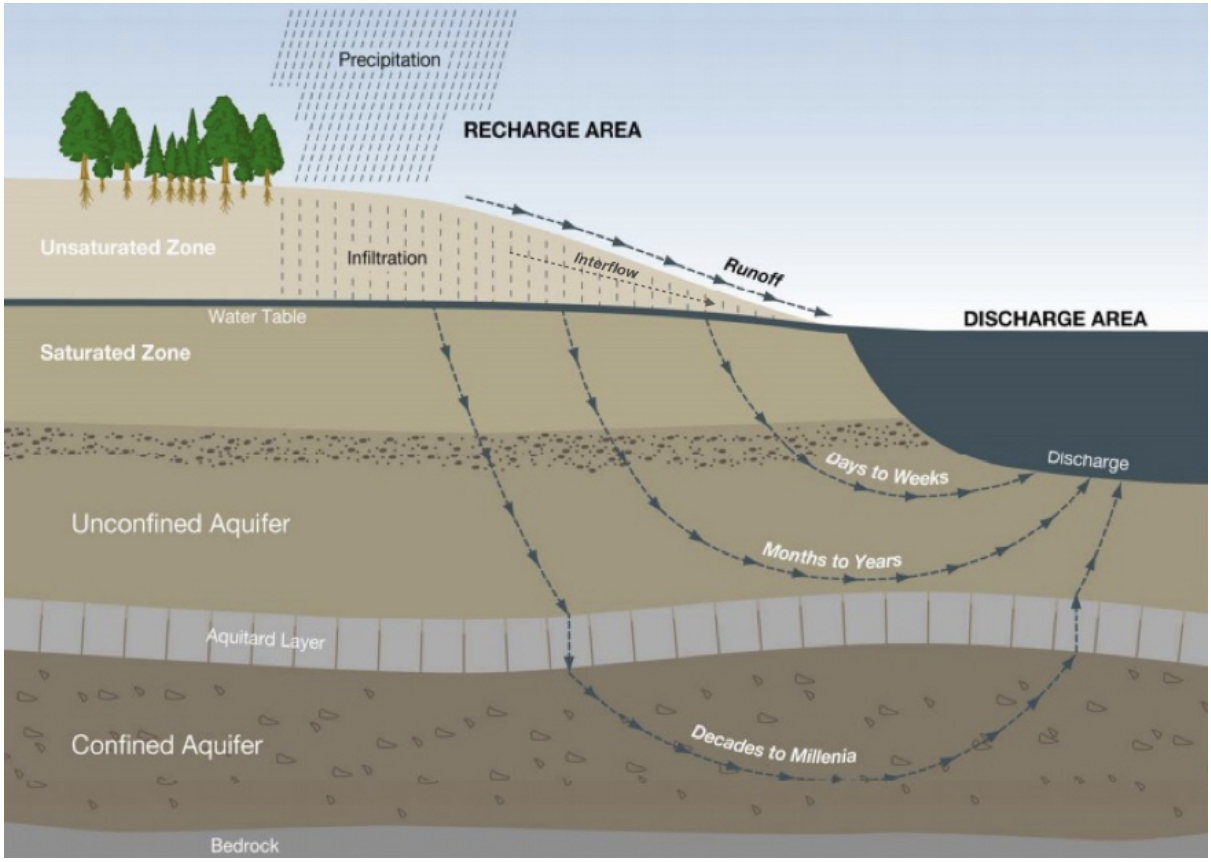

Figure 5: Diagram depicting a typical aquifer layout with local and regional flow systems. Adapted from Wehrmann (2008).

The amount of water in the unsaturated zone (UZ), known as soil-moisture or soil-water content, exerts a strong influence on the transition of water from above to below ground. It is vital to understand these processes and their relationships with the storage reservoirs because they are fundamentally important to human societies.

Understanding the GW resources is particularly important because they contain over 98% of the planet's available freshwater (Gleick 1996), and are increasingly threatened by overuse and climate change (Ferguson & Gleeson 2012; Richey et al. 2015). Of these resources, shallow unconfined aquifers are most used simply because they are much easier to access than those beneath them. For the same reason, these are most easily recharged by rainfall that percolates through the soil and unsaturated zone, uninhibited

by a confining unit, to become saturated flow. In this way, the position of the water table that forms the upper boundary of the saturated zone in such shallow unconfined aquifers is strongly influenced by precipitation (Healy & Cook 2002; van Gaalen et al. 2013; Viswanathan 1983). However, the position of the water table is also subject to a number of natural and anthropogenic factors, such as seasonal changes and GW withdrawals that can significantly impact the shallow GW system (Khaled et al. 2011). Additionally, a shallow depth to the water table (DTW) is often the controlling factor in what plant species can inhibit an area, and can pose a hazard to underground infrastructure (Rodriguez-Iturbe et al. 2001; Vázquez-Suñé et al. 2005). Water table position is thus an important factor in understanding the shallow GW system and how it interacts with other parts of the hydrological cycle.

Therefore, the research presented in this thesis seeks to add to the body of knowledge investigating the position of the water table and how its positions affects the natural and built environment. This chapter proceeds by summarizing the hydrologic processes that contribute to GW recharge. It describes the general properties of aquifers, specifically those that interact with surficial and coastal processes to affect the water table. Next, an overview is given of the current state of knowledge related to SLR, with specific consideration given to issues related to GW. The chapter concludes with a brief restatement of the research objective and the challenges of meeting it.

2.2 GROUNDWATER RECHARGE

As shown in Figure 5 (p. 6), land surface is connected to subsurface GW via the UZ. Water originating as precipitation must infiltrate through the land surface and pass through the UZ before adding to the saturated zone of an aquifer. Overland runoff occurs when the rate of precipitation exceeds that of infiltration, or there is an an absence of available UZ space to store additional water. In some circumstances, laterally flowing infiltrated water (interflow) will resurface and join overland runoff. Water that seeps downward and reaches the saturated zone serves as recharge to GW, and depending on where it enters the flow system, will follow a local, intermediate or regional flow path (Toth 1963). Generally, GW flow paths reflect topography, with water moving from upland recharge zones to low-elevation discharge zones (Toth 1963). Within these systems, flow gradients are determined by changes in hydraulic head, which is a measure of the total energy available to move GW. However, for recharge to occur, infiltrating water must overcome losses that occur in the UZ due to ET (Earman & Dettinger 2011).

Infiltration into the subsurface vadose zone is the result of the vertical forces of gravity and capillary action. Capillary action, or capillarity, is a combination of surface tension and adhesive forces between water and soil molecules that generally acts in the upward direction. Before these forces can act upon infiltrated water, precipitation must penetrate the land surface. Impervious surfaces, such as paved roads or parking lots and compacted

soils prevent infiltration, increasing overland runoff. Conversely, vegetated land-cover can facilitate infiltration by protecting the soil from compaction upon raindrop impact, breaking it up through root action, and promoting the presence of biota which create space through motion (Horton 1941, p. 54). Furthermore, during a precipitation event, infiltration rate decreases over time, as shown in Figure 6. Once in the subsurface,

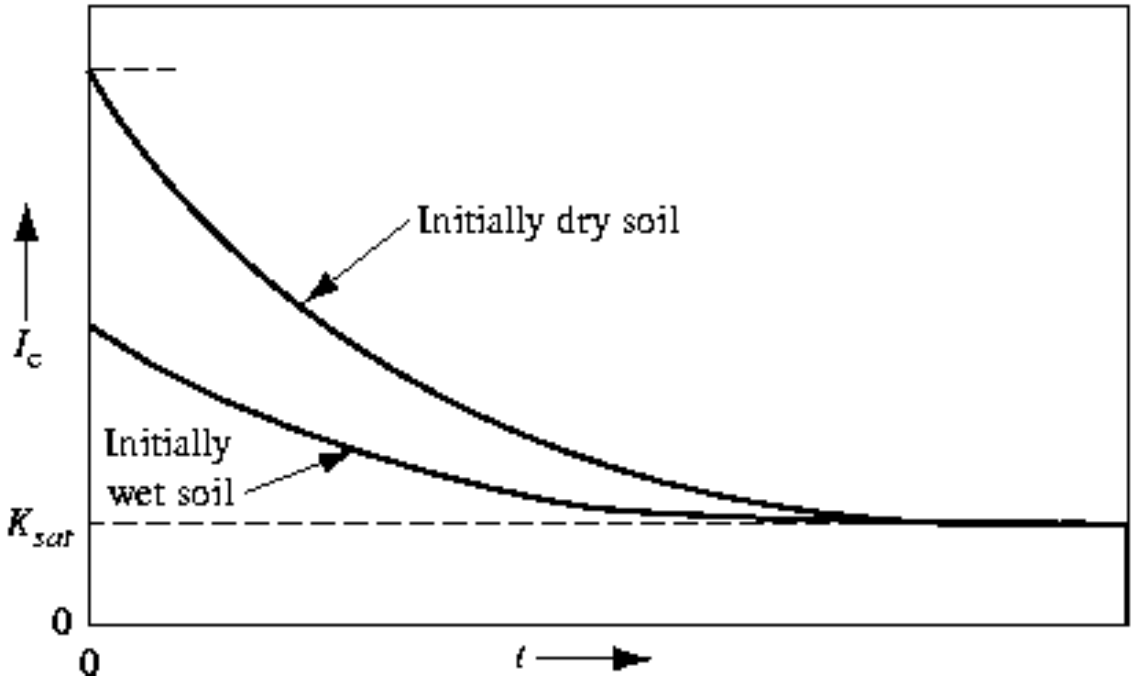

Figure 6: Infiltration capacity curves for soils with different antecedent conditions. The infiltration capacity (I_c) of a soil decreases exponentially with time (t) until the soil is fully saturated (K_{sat}) (source: Bear 1999).

infiltrated water is predominantly vertically-flowing fluid with a rate dependent on soil properties, water content of the soil, and depth to the water table (Gregory et al. 1999).

The soil properties of porosity and hydraulic conductivity determine the volume available to accept infiltration. Porosity is the percentage of sediment that is void space, calculated as the volume of void space in a sediment divided by the total volume of the sediment. It is dependent upon the shape and orientation of the grains, and decreases with differences in grain size (Fetter 2014, p. 88). Hydraulic conductivity is the rate at which a fluid can move through a permeable medium. It is dependent on both the fluid itself and the material the fluid is passing through; more viscous fluids will move more slowly through materials with smaller pore diameters. If the precipitation rate applied to a soil is higher than this rate, water will temporarily be prevented from infiltrating, and result in unsaturated runoff, known as Hortonian overland flow (Horton 1933). Further, because hydraulic conductivity is impacted by the fluid itself, infiltration rate depends on the amount of water present in the soil.

The water content of a soil is expressed as the ratio of the volume of water to the

volume of void space (Fig. 7). The antecedent conditions, or the amount of water present in the subsurface before a precipitation event, exert a strong control on infiltration by dictating the initial infiltration capacity of the soil (Fig. 6). Field capacity and wilting point are determined by the opposing forces of gravity and capillarity. Water content at field capacity, though not constant over time, is practically defined as the maximum amount of water that can be held against gravity (Veihmeyer & Hendrickson 1931; Gregory et al. 1999). Thus, only when the water content of the soil within the UZ is above field capacity can it percolate downwards to recharge GW. However, not all the water above field capacity may reach the saturated zone because water content greater than the wilting point can be removed via ET (Earman & Dettinger 2011).

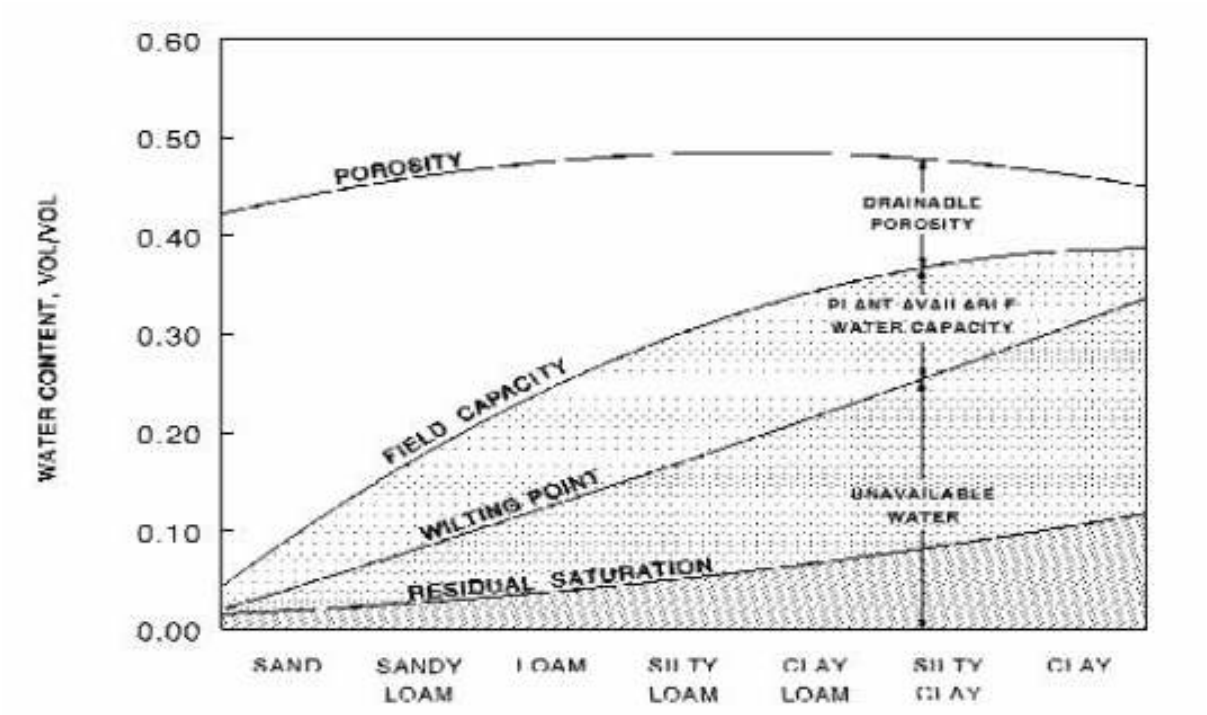

Figure 7: Conceptual soil moisture profile in which soil water content varies by soil type, and ranges from oven dry (0) to completely saturated (1). Intermediate values of wilting point and field capacity include values of the energy potential of water as indicated by the moisture tension in the soil (source: Schroeder et al. 1994).

Infiltrated water that does eventually reach the saturated zone will cause the water table to rise, having a complex feedback on GW recharge. A higher water table decreases porosity by filling the void spaces in the vadose zone from below (Gregory et al. 1999). If the water table reaches the land surface, no water can infiltrate, and subsequent precipitation flows overland as Dunnian runoff (Dunne & Black 1970). However, increasing the water content of the soil reduces the capillary pressures that cause water to cling to sediment, inhibiting flow (Horton 1933). Therefore as the water table rises, there are simultaneously void spaces in the UZ being filled while new ones are opening up as

water flows faster away from the surface. Recharge in shallow unconfined aquifers is thus impacted by processes at the land surface, and in both the vadose and saturated zones.

2.3 COASTAL AQUIFERS

2.3.1 TRANSITION ZONE

Shallow aquifers are often found in coastal areas, where the land elevation approaches sea level and GW discharges to the oceans (Glover 1959). Recharge rates are especially important in coastal aquifers because they are the responsible for this discharge, which is the major factor in determining the landward extent of saline ocean waters (Barlow 2003). Over geologic time, GW discharge, known as submarine groundwater discharge (SGD), is balanced by mean sea level, which establishes average GW levels and the corresponding water table position (Horn 2002). However, the relative positions of freshwater and saltwater are not static, but subject to mixing and other coastal oceanic processes.

The transition zone, or zone of dispersion, is where freshwater flows seaward from beneath the ground to mix with salty ocean water (Fig. 8). Due to its mixed nature, there is no exact method for defining it, but it can generally be considered where there is a range of total dissolved solids between 1,000 and 35,000 mg/L and chloride ranging from ∼250 to 19,000 mg/L (Barlow 2003). Mixing occurs by dispersion and diffusion due to the heterogeneities and hydraulic properties of the aquifer, and dynamical forces, such as waves and tides.

Changes in ocean levels cause oscillations in the location of the transition zone, which can propagate through aquifers to influence GW levels (Turner 1998). With distance inland, lag time between movements in ocean levels and related GW fluctuations increases, while amplitude of the GW changes decreases (Jacob 1950; Carr & Van Der Kamp 1969). This decrease is rapid, thus the effects of a fluctuating body rarely alter GW conditions further than 1 km away (Rotzoll & Fletcher 2012). However, the actual distance GW is effected is highly dependent on the aquifer and confining unit properties of the GW system in question (Li et al. 1999). Further, it is increasingly being shown that GW recharge pathways are impacted by dynamic near-shore processes of wave-setup and seawater recirculation (Robinson et al. 2007). Thus, processes in the transition zone are related to GW levels in complex, nonlinear ways.

2.3.2 SALTWATER INTRUSION

To manage the complexity of the transition zone, it is often envisioned as a sharp boundary, known as the fresh water/saltwater interface (FW/SWI), which separates freshwater above from denser saline water below (Bear 1999). This simplification can facilitate scientific inquiries, especially into matters concerned with the freshwater resources of coastal aquifers, which are relied upon by over a billion people worldwide (Kundzewicz

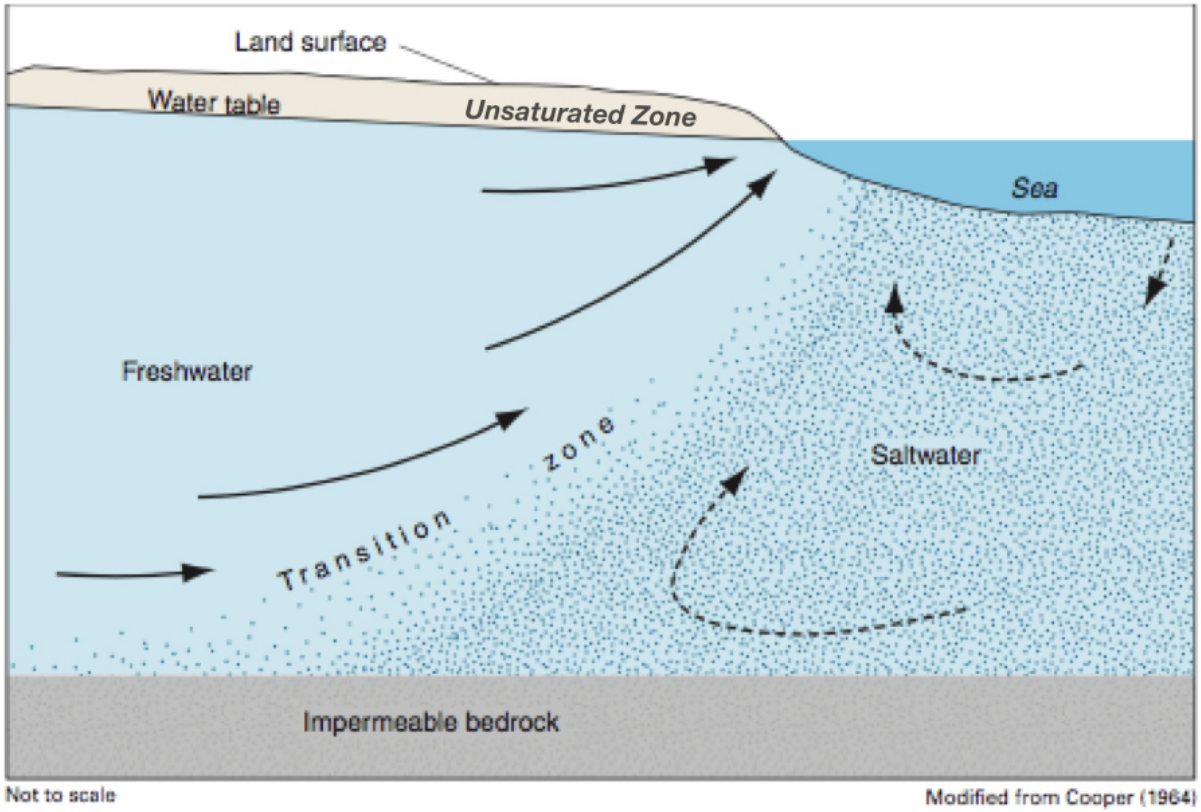

Figure 8: Fresh discharging GW mixes with saline ocean water within the transition zone to form a fresh water/saltwater interface. Adapted from: Barlow (2003).

& Doell 2009). The natural processes just discussed, along with anthropogenic influences such as withdrawal of fresh GW, can lead to contamination of these resources by saltwater. This movement of saline seawater into freshwater aquifers is known as SWI, and has been an active area of research since it was recognized in 1854 (Bear 1999; Barlow 2003) (Fig. 9).

There are several mechanisms which cause SWI, whose severity depends on local and regional factors, such as GW use, topography, and vertical land motion. Upconing is the vertical movement of saltwater in response to GW withdrawals (Reilly & Goodman 1987). As water is extracted from a freshwater aquifer, a 'cone of depression' forms around a pumping well, reversing the natural hydraulic gradient from seaward to inland (Theis 1938). If this cone spreads deep enough, seawater will flow into the well, contaminating the freshwater supplies. Fresh GW can also be contaminated vertically from above when saline water infiltrates from the ground surface. This process, known as land surface inundation (LSI), most often occurs due to storm surges that flood coastal lands with saline overwash (Anderson 2014). Several case studies have shown that chloride concentrations can exceed safe levels for months after an inundation event, indicating that this is a particularly hazardous form of SWI. (Anderson 2002; Illangasekare et al. 2006; Holding & Allen 2015).

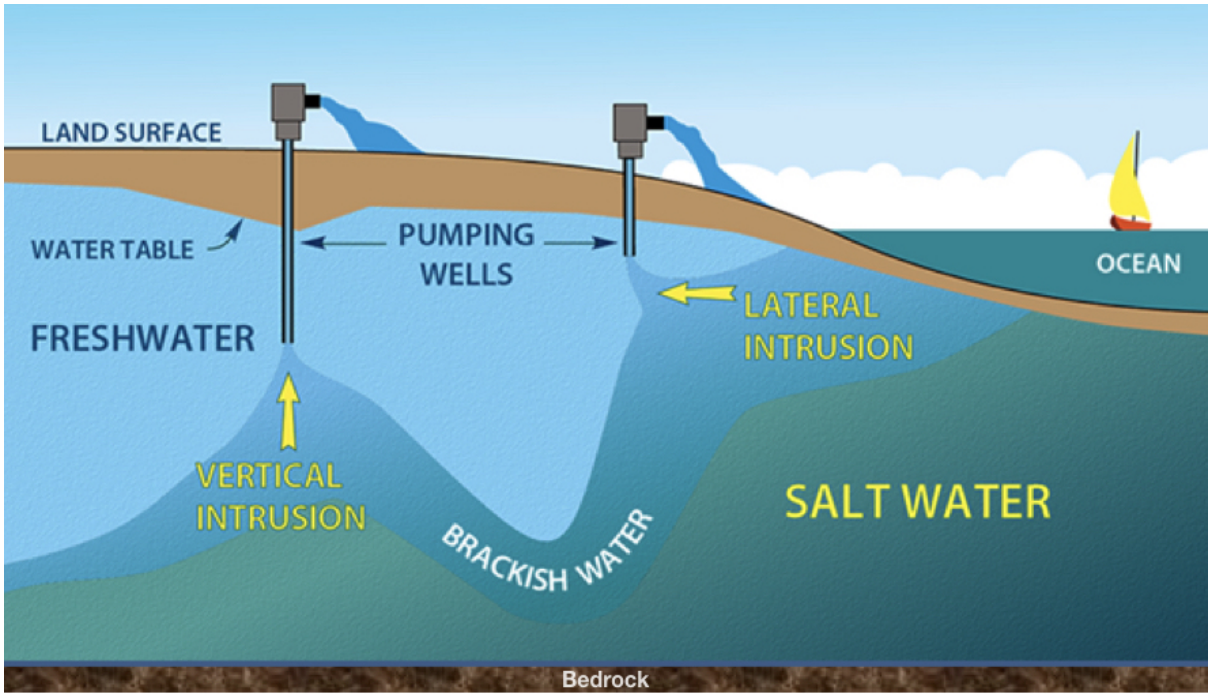

Figure 9: Saltwater intrusion occurring vertically and horizontally in a coastal aquifer. Adapted from Feltgen (2015).

Saltwater may also intrude laterally, as the toe of the FW/SWI migrates landward in response to warm climates that increase global mean sea level (Fig. 9). As sea levels rise, saline water heads increase at the ocean boundary of the transition zone that induce more saltwater into the freshwater zones of coastal aquifers (Bear 1999). Although others have shown both overpumping and LSI to be more severe forms of SWI (Ferguson & Gleeson 2012; Ataie-Ashtiani et al. 2013), lateral movement of the FW/SWI can have grave long-term consequences that are receiving renewed attention (Werner & Simmons 2009; Watson et al. 2010; Oude Essink et al. 2010). Many of these recent inquiries are due to increasing mean sea levels, which are forcing the saltwater wedge inland at timescales relevant to water resource managers (Watson et al. 2010; Feseker 2007).

2.3.3 SEA LEVEL RISE

Climate change induced SLR (Fig. 1, p. 1) is expected to increase the potential for SWI. Not only will saltwater transgress laterally, but higher water levels more easily surge landward to contaminate GW from above. Due to spatial differences in rates of local SLR (Fig. 2, p. 2) and the importance of local hydrogeology, most studies have focused on specific aquifers and relied on numerical models to simulate complex subsurface processes (Sherif & Singh 1999; Masterson 2004; Sanford et al. 2009; Oude Essink et al. 2010; Rozell & Wong 2010). The Netherlands is particularly vulnerable to SWI because a third of its flat lands lie below mean sea-level (Huisman et al. 1998). Several studies have shown it is already taking place, and will be exacerbated by future SLR (Oude Essink

2001; Oude Essink et al. 2010). Global investigations do exist, such as those taken by Werner & Simmons (2009) and Holly et al. (2013). The former found that the movement of the FW/SWI interface depended greatly on the inland boundary condition: if GW levels rose with SLR to maintain GW discharge rates there was minimal SWI, whereas if GW levels remained constant the salt water toe migrated kilometers inland. Holly et al. (2013) determined that aquifer properties, rather than uncertainties in the magnitude of SLR, are the most important factor in determining the extent of SWI.

Along with SWI, coastal flooding is a major hazard that is increasing due to SLR. Coastal flooding occurs in two main forms: marine and GW inundation (Fig. 3, p. 3). Marine inundation is overland flooding that results from coastal processes such as storm surges and tides. While this type of coastal flooding has been the subject of extensive inquiries, the main modeling technique only utilizes land surface elevations to identify areas vulnerable to flooding (Romah 2012). This oversimplification does not account for the possibility of the water table to rise with SLR above the land surface, thus resulting in GW inundation.

In recent years, several case studies have shown that GW inundation can be a major part of coastal flooding. Rotzoll & Fletcher (2012) used an analytical model to show that for a 0.33 m SLR scenario flooding from GW would contribute over 50% to the total flooded area. Manda et al. (2015) investigated GW rise in Bogues Bank, North Carolina, using a geographic information system (GIS) and concluded that the proportion of land inundated by GW will be comparable to that subject to marine inundation. In the Hampton Roads region of Virginia, Moss (2016) also used a GIS to determine that over 70% of the total flooded area would be from GW inundation for a SLR of $\sim$0.5 m. Numerical simulations have produced similar results (Bjerklie et al. 2012; Rekker 2012; Masterson et al. 2014), indicating the flooding will occur from below the ground, as well from overtop, due to SLR.

Even when GW levels don't rise high enough to overtop the land surface to cause flooding, an elevated water table can have detrimental effects on the built environment. Underflooding occurs when high water table conditions come in contact with the foundations of structures. This can reduce their load carrying capacity by corroding their foundations, especially in older buildings (Lerner & Barrett 1996; Vázquez-Suñé et al. 2005; Morrison & Taylor 1994). Underground infrastructure, such as storm water and wastewater pipes, and communications networks are also susceptible to deterioration via underflooding (Johnson et al. 2001). When GW infiltrates pipes through cracks in the casing, the networks experience loads beyond their designed capacity, increasing risks such as sewer overflow, and decreasing the efficiency of the overall system (Ellis 2001; Heywood 1997). With the higher tides produced by SLR, these potential risks become chronic hazards (Dahl et al. 2017).

High GW levels will also have consequences for the natural environment. Many plant

species rely on the uptake of GW for their water needs, and thus changing the depth to water may cause water-tolerant plants to dominate an ecosystem (Rodriguez-Iturbe et al. 2001). While some lands that are currently wetlands will become permanently submerged, others will expand and new ones will emerge (Rotzoll & Fletcher 2012). However, the GW in some areas may be excessively saline, stunting or preventing plant growth (Wong et al. 2014). Finally, higher GW levels will limit infiltration, which can lead to increased runoff rates that may deliver contaminants to water bodies, intensify erosion, and/or cause precipitation induced flooding as runoff ponds on the land surface.

To minimize the threats caused by GW rise it is essential to understand how shallow GW levels in coastal aquifers will respond to SLR. Because the position of the water table is dependent on recharge rates as well as sea level, it is valuable to understand how past precipitation and infiltration have controlled the height of the water table. With this knowledge as a foundation, it becomes possible to make projections about how future SLR scenarios could impact GW levels.

However, the complex, nonlinear relationships between these various processes makes the understanding of coastal systems challenging. This is complicated by the underground nature of aquifer systems, which presents difficulties in data collection. Further, what data is collected may not be an accurate representation of an aquifer due to the high level of heterogeneity of coastal systems. And of course, developing an understanding of the future depends upon the primary assumption of uniformity, which is often not the case, especially given climate change is changing the state of the earth system to one which we have very little information about.

Nevertheless, water resources are a vital resource that must be managed using the best knowledge we can create. Thus, there is a long history of attempts to understand surface and GW systems using a variety of modeling techniques. Such tools are essential not for predicting the future, but for developing foresight that enables us to consider possible scenarios, such as different rates of SLR, and the impacts they may have on the future. The next chapter presents a review of those particularly relevant to this research.

CHAPTER 3

BACKGROUND-MODELING

3.1 INTRODUCTION

Abstracting reality to a simpler model to aid in understanding is a necessary and useful enterprise in the hydrological sciences. Models of different types are needed because we are limited in our ability to perfectly represent reality by a lack of measurements, and a lack of techniques with which to gather and assimilate the needed data.

However, the models themselves are fundamentally limited by epistemic uncertainty, our lack of complete understanding of the processes and characteristics of the system we're trying to represent. Nevertheless, as shown in Chapter 2, a detailed understanding of future hydrological changes is needed to protect freshwater resources, ecosystems, and communities from water-related hazards. When used as tools to explore possible futures, models can provide useful insights for achieving such tasks

Hydrological models can generally be divided into three categories based on which aspect of the water cycle they are concerned with: rainfall-runoff, GW, or integrated surface/subsurface flow. The former must have a runoff generation component that partitions rainfall into runoff or infiltration, and a runoff routing component that accounts for the contributions of runoff to the catchment outlet (Beven 2011, p. 16). GW models are generally concerned with GW flow, solute transport, heat flow, aquifer deformation, or some combination of the above (Fetter 2014, p. 516). The advent of digital computers has enabled different surface water/ground-water (SW/GW) models to be integrated in complicated ways to represent the interdependencies of surface processes, infiltration in the UZ, and GW flows (Sophocleous 2002; Furman 2008). Computers are continuously facilitating the solution or approximation of quantitative, equation-based models and will be the focus of the following review.

At the most basic level, quantitative models can be subdivided based on the scale at which they aggregate measurements into variables (Beven 1989). At one end of the spectrum are 'lumped' models, which essentially treat an area of inquiry, or catchment, as a single unit. Using this approach it is relatively easy to build a model that produces the desired outputs given a set of input data. However, it is generally considered a 'blackbox' model in that there is no insight into the processes that produce the output. The other end of the spectrum, 'distributed' models, divide a catchment into smaller units and distribute properties, called parameters, that vary heterogeneously. These models are still effectively 'lumped' at the resolution of the representative unit, but can represent processes between unit and catchment scales (Singh & Woolhiser 2002). However, because each unit will need to have representative parameters, it is often difficult to gather enough data to build distributed models that produce accurate results.

Calibration is the process of adjusting the parameters in a model such that it produces results that best match observations. However, due to spatial and temporal differences in measurements and required parameters values, it can be difficult or impossible to gather the data required for their estimation (Beven 1989). Even when measurements are considered to be reliable parameter values, a large amount of diverse observations are required to show that the model is well calibrated (Gupta & Sorooshian 1985; Yapo et al. 1996). Further, in most cases there is no optimal parameter set, and thus multiple models with different parameters can reproduce observations for a certain input dataset, but likely differ greatly in their representation of reality (Beven 1993). This principle of equifinality, in conjunction with the many results showing that models always perform worse for independent data than calibrated data, leads to the need for verification and validation (V&V) of hydrological models (Gupta et al. 1998; Refsgaard & Henriksen 2004).

In their seminal paper on V&V, Oreskes et al. (1994) defined verification as demonstrating that a model is true, and a valid model as one that "does not contain known or detectable flaws, and is internally consistent". They conclude that true V&V is impossible because knowledge of the necessary input parameters cannot be perfectly known for natural systems. Nevertheless, models can be valuable heuristic tools if model performance is within an acceptable uncertainty range as compared to independent observations, i.e., observations not used in calibration (Oreskes et al. 1994; Refsgaard & Henriksen 2004). In this way, validation is limited to a 'domain of applicability', and can be determined good enough when it meets accuracy criteria that are established by not only modelers and researchers, but also by those who use the model to make decisions (Refsgaard & Henriksen 2004). Thus, despite that all models are wrong, some can be useful (Box & Draper 1987).

Aside from decision making and prediction, models can be useful in a variety of ways, such as bounding outcomes or challenging paradigms (Epstein 2008). This research develops and uses a model to illustrate the core relationships between SLR induced GW rise, rainfall/runoff, and infiltration. It intends to demonstrate first principles, and highlight uncertainties that could be resolved with future data-collection efforts. To demonstrate the interactions of these principles, a rainfall/runoff model (SWMM) and GW model (Modular Three-Dimensional Finite-Difference Ground-Water Flow Model (MODFLOW)), are coupled to connect processes at the land surface, in the UZ, and in the saturated zone of a coastal aquifer. The remainder of this chapter is devoted to summarizing the three major types of hydrological models described above: rainfall/runoff, GW, and coupled SW/GW. Each section begins with a brief summary of major developments in the field and then is followed by a more detailed analysis of the models used for this investigation.

3.2 RAINFALL/RUNOFF MODELS

Dozens, if not hundreds, of models have been created to investigate the two main processes of surface hydrology: runoff generation and runoff routing (Singh & Woolhiser 2002). Early constructions, such as the Rational Method, developed by Thomas Mulvaney (1851, reproduced in Loague 2010), and the unit hydrograph concept (Sherman 1932), use lumped approaches in which the runoff routing component is determined by relating the peak of a stream flow time series (hydrograph) to a rainfall event. Within a channel, stream-flow is considered to behave according to the shallow water equations (Saint-Venant 1871). These Saint-Venant equations, after their original deriver, include mass and momentum components that model unsteady flow in a channel (or overland) of arbitrary geometry. While these methods are commonly used together to model surface water dynamics, they neglect the component of runoff generation and thus the role of infiltration.

In his seminal paper, Horton (1933) empirically determined a maximum infiltration capacity of soils. He argued surface and soil characteristics would cause an exponential decline in the amount of precipitation infiltrating the subsurface according to:

$$f_p = f_\infty + (f_0 - f_\infty)e^{-k_d t} \tag{2}$$

where:

f_p is the infiltration capacity into soil

f_∞ is the minimum or equilibrium value of f_p

f_0 is the maximum or initial value of f_p

k_d is the decay coefficient, and

t is the time from beginning of storm (Horton 1933; adapted from Rossman & Huber 2016).

Rainfall in excess of this maximum capacity is prevented from infiltrating, thus resulting in runoff.

In contrast to (and earlier than) Horton, Green & Ampt (1911) developed a physically based model of infiltration known as the Green-Ampt Method. This method separates a vertical column of soil into two zones separated by a 'wetting front' (Fig. 10). These zones have different, but constant amounts of water content: saturated and initial moisture conditions. Rate of infiltration then results from the difference in hydraulic head (after accounting for the opposite pressure at the wetting front due to capillary action) at the surface and wetting front.

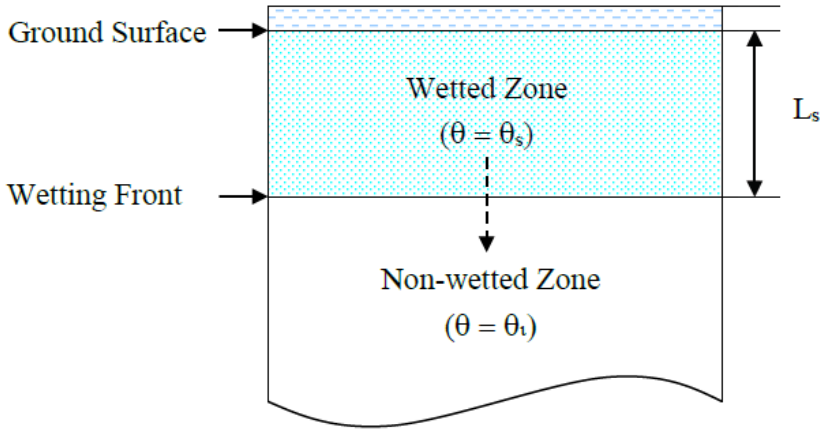

Figure 10: Zonal depiction of the Green-Ampt infiltration model from Rossman & Huber (2016). Original adapted from Nicklow et al. (2006).

Therefore, the Green-Ampt method accounts for capillary tension and differences in water content, but oversimplifies the latter by discretizing to only two divisions and neglecting horizontal flow. Moreover, the Green-Ampt model assumes an unrealistic infinite vertical soil profile (Liu et al. 2010).

The most rigorous quantitative model of infiltration was developed in the early 20^{th} century by Richards (1931). He described the movement of water through the UZ in one vertical dimension as the partial differential equation:

$$\frac{\partial \theta}{\partial t} = \frac{\partial}{\partial z}[K(\theta)(\frac{\partial \psi}{\partial z} + 1)] \, , \tag{3}$$

where:

K is the hydraulic conductivity of the material in the direction of flow

ψ is the pressure head

z is the elevation above a vertical datum

θ is the volumetric water content, and

t is time (Richards 1931).

This model accounts for the continuously changing relationship of water content with depth, and that of hydraulic conductivity with degree of saturation. However, these relationships are nonlinear and a only a few solutions have been developed under ideal lab conditions (Serrano 2004). Nevertheless, simplifications can be made to approximate solutions, such as those developed by Serrano (2004) and (Niswonger et al. 2006).

Today, computing power has enabled the creation of models capable of simulating all these aspects of the hydrological cycle - rainfall/runoff, infiltration, and channel/overland flow (Singh & Woolhiser 2002). The first to do so was the Stanford Watershed Model (now Hydrological Simulation Program - Fortran (HSPF)) (Crawford & Linsley 1966; Johanson & Davis 1980), and others such as HEC-HMS, GSSHA, and SWAT have followed (Feldman 2000; Downer &

Ogden 2002; Arnold et al. 2012). Many others models make simplifications in catchment designation (Beven et al. 1984; Neitsch et al. 2001) and/or physical processes (Neitsch et al. 2001; Markstrom et al. 2015) to focus on certain aspects of the hydrological cycle at the expense of others. SWMM, for example, is capable of high resolution flow routing, but reduces GW flow to a simple storage compartment governed by mass balance (Rossman 2015).

Nevertheless, SWMM has been used successfully to simulate runoff quantity and quality for both single and long-term continuous events (Rossman 2015). The applications of SWMM are far reaching, with a variety of uses documented by Gironás et al. (2009). This manual, complete with worked-out examples, demonstrates the use of SWMM for such tasks as calculating runoff for a residential site before and after it was developed, and assessing performance of a detention pond subject to a ten year period of historical rainfall (Gironás et al. 2009). It has been used in a variety of site-specific case studies (Temprano et al. 2005; Peterson & Wicks 2006; Jang et al. 2007; Tian et al. 2015) that have varied from small urban catchments (Tsihrintzis & Hamid 1998) to larger rural watersheds (Davis et al. 2007). While SWMM was originally designed for areas smaller than 1 km^2, it has been used with some success in areas over 200 km^2 (Barco et al. 2008).

SWMM is so versatile because it conceptualizes the hydrological cycle as four separate, but interrelated components: atmosphere, land, sub-surface, and conveyance. The processes that occur within and between these compartments are shown in Figure 11.

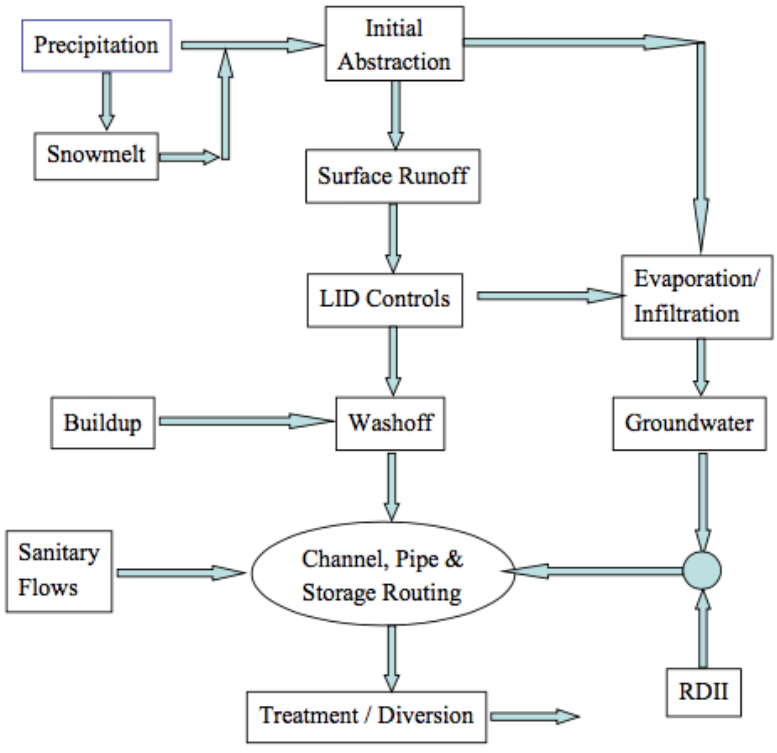

Figure 11: Conceptual model of the hydrological cycle in SWMM. The controls facilitate the simulation of engineered structures designed to manage stormwater runoff using natural features. The component can be used to model the movement of rain or subsurface water into and through a sewer network (source: Rossman & Huber 2016).

Generally, precipitation falls from the atmosphere component to the land surface, where it evaporates back to the atmosphere, infiltrates into the sub-surface compartment, or flows as runoff into the conveyance system. The conveyance compartment consists of a network of structures that transport water to terminal endpoints. Importantly, these components do not necessarily rely on one another, which allows a model to be built without using them all.

This study made particular use of the land surface compartment of SWMM to partition precipitation into infiltration and runoff. In SWMM, the land surface is discretized into homogeneous two dimensional rectangular areas called subcatchments which receive precipitation and generate runoff (Rossman & Huber 2016). The discretization can be based on characteristics such as land-cover, surface elevation, or drainage boundaries. Runoff is estimated using the nonlinear reservoir model shown in Figure 12 (Chen & Shubinski 1971).

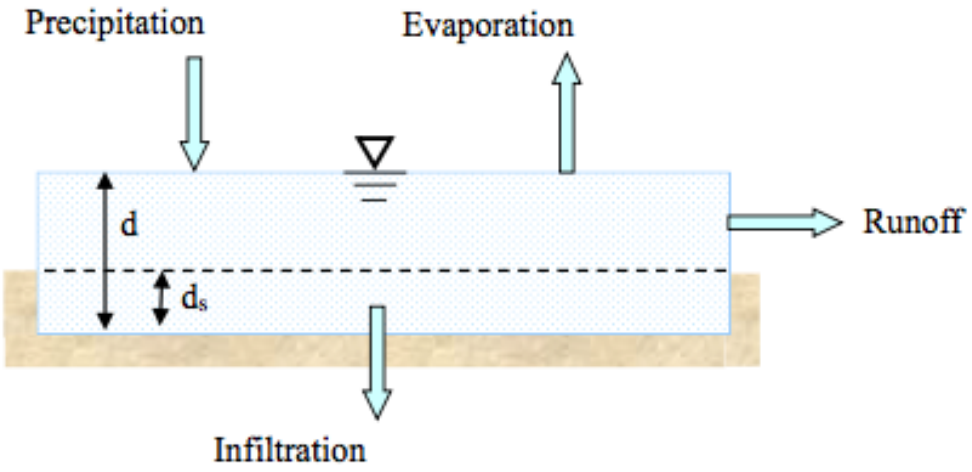

Figure 12: Nonlinear reservoir model of a subcatchment. The subcatchment receives inflow from precipitation and losses from evaporation and infiltration. Excess water ponds atop the surface to depth (d) and becomes runoff when it exceeds depression storage depth (d_s) (source: Rossman & Huber 2016).

Infiltration can be simulated using one of several methods, including Horton's Method and the Green-Ampt Method. When runoff is produced, it is routed to the conveyance network or to another subcatchment at a rate calculated via Manning's equation using water depth and land surface slope (Rossman 2015). By enabling overland re-routing between subcatchments, one can simulate runoff through heterogeneous subcatchments.

This re-routing capability, along with the compartmentalized and open-source nature of SWMM were the primary reasons for choosing it for this study. The former enables infiltration to vary spatially during and after a precipitation event, which emphasizes the processes in the UZ. Because it is open source, components of the model code could be easily changed to facilitate coupling with a GW model. And because the SWMM compartments function independently, a small change to one component does not have an affect on unconnected parts. Additionally, SWMM has been successfully coupled to a GW model in several previous studies (Rowan 2001; Uchrin et al. 2002; Bulatewicz Jr 2006; Yergeau 2010).

3.3 GROUNDWATER

GW modeling is a much more homogeneous field than rainfall/runoff modeling. While there are exceptions, such as the commercial programs HYDRUS (2D/3D) and FEFLOW (Sejna & Simunek 2007; Diersch 2002), subsurface modeling is dominated by the family of open source MODFLOW (Harbaugh 2005) programs written primarily in the Fortran programming language. Originally developed by the United States Geological Survey (USGS) to consolidate GW simulation capabilities into one program, MODFLOW uses numerical methods to calculate a mass balance on water flow, where the flux values are hydraulic heads according to Darcy's law:

$$Q = -\frac{KA(h_1 - h_2)}{L}\ , \tag{4}$$

where:

Q is the volumetric flow,

K is the hydraulic conductivity of the material in the direction of flow

A is the cross-sectional area perpendicular to the flow,

$h_1 - h_2$ is the head difference parallel to flow, and

L is the length of the prism parallel to the flow path (Darcy 1856). Adapted from Harbaugh (2005).

MODFLOW solves the finite-difference equation over a grid of rectangular cells by calculating the hydraulic head at the center of each (Fig. 13). Since head is a function of time as well as space, time is discretized into individuals steps and head is calculated at each one (Harbaugh 2005).

Until the late 1990s, updates to MODFLOW were relatively minor changes intended to improve its ease of use (Harbaugh 2005). Conversely, MODFLOW-2000 was a major development which broadened the capabilities of MODFLOW beyond the realm of GW flow by incorporating pre/post processing techniques (Hill et al. 2000), solute transport modeling (Konikow et al. 1996), and support for decision making (Ahlfeld et al. 2005). Most recently, MODFLOW-2005 has improved internal data management by using global Fortran modules that allow sharing of data between subroutines (Harbaugh 2005). These updates have managed to maintain the original design criteria of being easy to use and modify, cementing MODFLOW's status as the most used GW model (Barlow & Harbaugh 2006).

Continual improvement of MODFLOW has been ensured by its modular structure, which enables the coupling of new packages that add functionality, such as saltwater intrusion (Bakker et al. 2013), without having to rewrite the source code (Barlow & Harbaugh 2006). Packages are continually being developed that link GW and surface water, such as the streamflow-routing packages SFR1 and SFR2 (Prudic et al. 2004; Niswonger & Prudic 2005; Barlow & Harbaugh 2006). Further, the creation of unsaturated zone packages such as UZF1 (Niswonger et al. 2006), and variable saturated flow (VSF) (Thoms et al. 2006) enable iterative coupling between surface and subsurface models (Furman 2008; Markstrom et al. 2008).

Unfortunately even the most recent version, MODFLOW-2005, is not capable of robustly

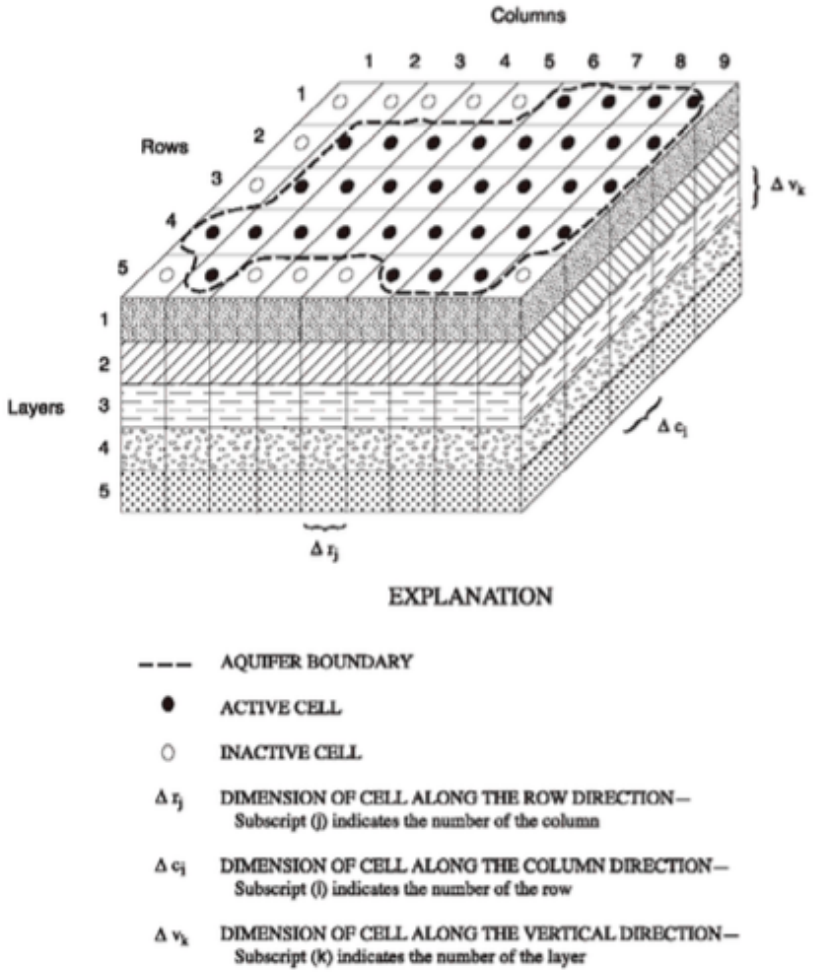

Figure 13: Discretization of an aquifer system into rows and columns in the horizontal plane, and layers in the vertical dimension (source: Harbaugh 2005).

handling these UZ processes. This is mainly due to problems associated with a fluctuating water table in an unconfined aquifer (Hunt & Feinstein 2012). Originally in MODFLOW-2005, if the water table dropped below the bottom a cell, that cell would become dry, and remain so for the remaining duration of the simulation. Subsequently, attempts were made that enabled 're-wetting' in order to overcome this inaccurate representation of reality, but these were numerically unstable and often prevented the model from converging to a solution (Doherty 2001).

In response to these limitations, Niswonger et al. (2011) developed MODFLOW-NWT. In MODFLOW-NWT, the Newton method replaces the Picard method used in MODFLOW-2005 for solving the systems of nonlinear equations that arise when modeling unconfined aquifers. Since the Newton method can only be applied to continuous functions, the Upstream-Weighting (UPW) package was developed to smooth the horizontal-conductance and storage-change functions that are otherwise discrete during wetting and drying of a cell. This formulation requires a different method for computing the conductance and storage terms, thus the UPW package is a replacement for the internal flow packages used in MODFLOW-2005 (Niswonger et al. 2011).

The use of MODFLOW-NWT with the UZF1 package, also developed by Niswonger et al. (2006), enables a robust simulation of interacting saturated and unsaturated zone processes. The UZF1 package models unsaturated flow by approximating Richards Equation in the vertical dimension (Eq. 3). First, the package converts a specified precipitation intensity[1] to water content and then subjects it to unsaturated flow. The unsaturated flow equation is solved by using a lead wave and trailing wave to simulate an increase or decrease, respectively, in the infiltration rate. These waves propagate with time, elongate due to gravity, and interact with one another to set water content at each time and depth. The Brooks-Corey function (Brooks & Corey 1966) is used to convert saturated hydraulic conductivity into unsaturated hydraulic conductivity $K(\theta)$. Precipitation is prevented from infiltrating not only when the precipitation rate exceeds the saturated vertical hydraulic conductivity (Hortonian unsaturated excess runoff), but also as the water table rises. Moreover, when the water table is higher than the land elevation as set in MODFLOW-NWT, GW is discharged to the land surface where it can contribute to stream flow (Dunnian saturation excess runoff) (Markstrom et al. 2008). However, overland flow of this GW discharge is not considered; rather, the water is routed instantaneously to a specified water body. While the predominance of the MODFLOW family and availability of UZF1 are a natural fit for the research presented in this thesis, the absence of this overland routing functionality within MODFLOW-NWT or its packages necessitates the addition of a surface water component.

3.4 SURFACE WATER/GROUNDWATER

In reality, GW and surface water form a continuous system in which water is exchanged in complex ways between the components (Winter & Rosenberry 1998). Freeze & Harlan (1969) were the first to formalize it as such in their seminal paper which linked the equations for different surface and subsurface flow processes via a shared boundary condition. This structure remains as the basis of the most advanced SW/GW models of today, but differences in temporal and spatial scales, and the complicated nature of the individual systems alone have historically led to the components being modeled separately (Winter 1999; Furman 2008; Markstrom et al. 2008; Fleckenstein et al. 2010). Such simplifications, which often reduce an entire system to a boundary condition, can be beneficial for increasing our knowledge and for some management concerns, but there has been a growing desire to manage GW and surface water as a single entity (Bouwer & Maddock III 1997; Sophocleous 2002; Furman 2008). This need to model the hydrological system holistically has led in recent times to a variety of numerical methods intended to enhance our ability to effectively manage these resources together (Fleckenstein et al. 2010).

These techniques can generally be divided by their level of coupling between surface and subsurface processes (Fig. 14) (Morita & Chie Yen 2000; Furman 2008). At the first level each system is solved independently at each time step.

[1]This is somewhat confusingly called infiltration rate by Niswonger et al. (2006), but clarified in Markstrom et al. (2008).

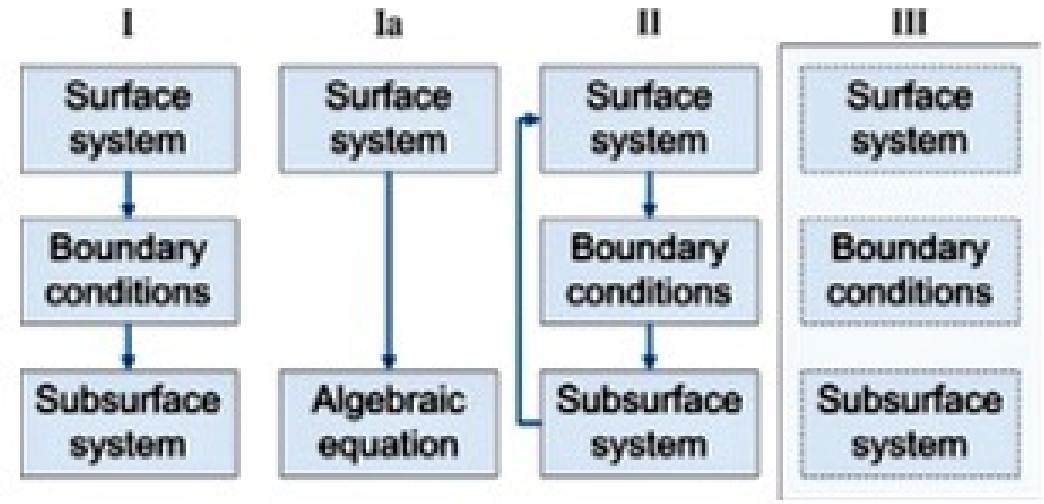

Figure 14: The four different numerical coupling schemes: (I) uncoupled; (Ia) degenerated uncoupled; (II) iterative coupling; and (III) fully coupled (source: Furman 2008).

Here, the solution of one system provides the input boundary condition for the second system. Since there is no feedback from the second system on the first, this is considered an uncoupled approach (Morita & Chie Yen 2000; Furman 2008). A subgroup of this approach, called degenerative uncoupling, models one of the systems as an algebraic equation, rather than as a numerical model. The iterative coupling approach extends the uncoupled approach by using the solution of the second system as an input to the first in subsequent time steps. The final coupling level, fully coupled, solves all equations simultaneously. While this is the most complete approach, it is not necessarily the most superior because numerical difficulties often arise in attempting to reconcile differences in the equations (Furman 2008).

The first uncoupled approach that did not use a degenerative approximation was likely that of Smith & Woolhiser (1971). They solved the 1D Richards Equation (Eq. 3) to link the surface and subsurface systems, but greatly simplified the system by setting the surface boundary condition to a zero pressure head upon precipitation-induced ponding (Smith & Woolhiser 1971). More recently, Yergeau (2010) integrated SWMM and MODFLOW in an uncoupled fashion by passing infiltration and evaporation loss values from SWMM to MODFLOW. An iteratively coupled model was developed by Govindaraju & Kavvas (1991) to investigate runoff produced from saturated zones adjacent to streams. With dozens of documented uses, Groundwater and Surface-water FLOW (GSFLOW) is likely the most widely used iteratively coupled model.

GSFLOW is an open source SW/GW model designed to simulate flow simultaneously overland, within the saturated and unsaturated compartments of the subsurface, and through surface water bodies (Markstrom et al. 2008). It utilizes MODFLOW for the GW component, the UZF1 package for representing processes in the UZ, and the rainfall/runoff model Precipitation-Runoff Modeling System (PRMS), also developed by the USGS. As shown in Figure 15, flux between the compartments is controlled by soil moisture and hydraulic head. Rainfall characteristics, soil properties, and antecedent moisture conditions dictate the rate at which water flows from the soil zone (Region 1) to streams and lakes (Region 2). Water flows overland in

the cascading wave module of PRMS. This approach routes water through an acyclic network, usually by starting at the highest upslope point and traversing downwards until reaching a surface water body (Markstrom et al. 2015).

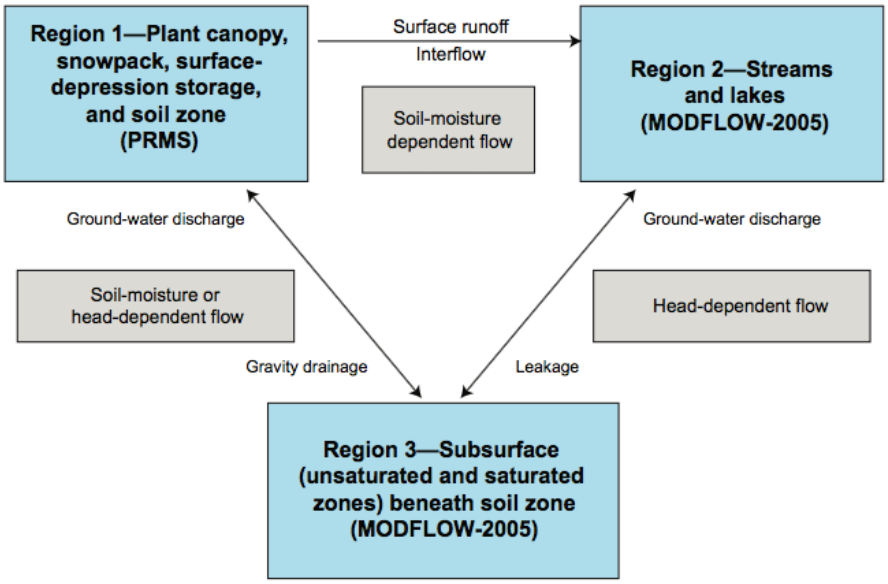

Figure 15: Conceptual model for the exchange of water between the three regions in GSFLOW (source: Markstrom et al. 2008).

Interactions between surface water bodies and GW is determined by hydraulic head. When the head at a water body is higher than that of the saturated GW zone, water will 'leak' from the surface water to the GW. In the reverse situation, GW flows as discharge to the surface water body. Flow through channels is governed either by using a steady uniform flow solution developed by Prudic et al. (2004), or a kinematic wave approximation of the Saint-Venant equations. At the interface between Regions 1 and 3 is a 'gravity reservoir', which consists of water content between field capacity and soil saturation (See Fig. 7 on p. 9). Gravity drainage to the subsurface (i.e. infiltration into the UZ) that occurs is dependent upon head and the hydraulic conductivities of the unsaturated and saturated zone. If infiltration causes the hydraulic head in an underlying MODFLOW cell to rise above the base of the soil zone, the gravity reservoir receives GW discharge that can contribute to overland flow. While GSFLOW is an integrated model that effectively conserves water mass through its components, it is not fully coupled in the sense that these components and the equations that govern the flow of water through them are separate, coupled only through iteration.

A true fully-coupled simulation models both unsaturated and saturated flow by solving the full three-dimensional form of Richards Equation. HydroGeoSphere (HGS), developed from a GW flow and solute transport model built at the University of Waterloo, follows this approach (Therrien & Sudicky 1992). To make HGS a complete hydrologic model, a surface component was added in 2002 that models flow through channels using the most complete, diffusive wave, approximations of the Saint-Venant equations. These equations, along with Richards Equation, are solved simultaneously over a finite-element grid and have been applied in over 40 peer-

reviewed publications (Brunner & Simmons 2012) to a variety of problems, such as large-scale watershed modeling (Li et al. 2008) and river bank storage processes (Doble et al. 2012). However, HGS is limited by a steep learning curve and problems common of proprietary software, including hidden functionality, software bugs, discrepancies in versions, and price (Brunner & Simmons 2012). Further, it is argued that iteratively coupled models may be better suited for simulating flow through regional hydrologic systems because the full Richards equation requires spatial and temporal discretization that may not accurately reflect saturated flow conditions (Furman 2008; Markstrom et al. 2008).

3.5 OBJECTIVES REVISITED

At the most basic level, all the models described here are different attempts to answer the defining question of the hydrological sciences: where does the rain go? (Penman 1961). While the question appears simplistic, the variety of techniques outlined here demonstrate its complexity, and the great deal of uncertainty that surrounds the topic. This uncertainty extends beyond a lack of understanding of physical processes to fundamental epistemological questions about how to deal with this lack of understanding itself. On the one hand, advances in computing power have led to the development of more and more complicated models that strive to account for every process and parameter of a system, following the blueprint developed by Freeze & Harlan (1969). However, it is often infeasible, or indeed impossible, to gather the data at the scales necessary for such a model to accurately represent a natural system (Beven 2002). This has led to another school of thought that seeks to let the available data dictate which model best fits a study area (Beven 1993). Moreover, some of the simplest models, such as the Rational and unit hydrograph methods are still used today because they can enable effective decision making. However, such simplified models may not offer sufficient physical insights, fundamentally limiting their usefulness (Brunner & Simmons 2012).

Thus in its current state, this debate is unsettled and unwinnable. Ultimately, model choice must be decided by how well it answers the question(s) it was designed for. Especially in hydrology, due to the heterogeneity of the natural processes and properties, local conditions are an important determinant in a model's performance. The model designed for this thesis essentially seeks to investigate how SLR effects the GW table of a coastal aquifer, and how historic precipitation could have caused this changed water table to interact with the land surface.

Thus, a fully-coupled approach was decided against, following the argument of Markstrom et al. (2008), that precipitation, infiltration, and GW flow operate at different timescales, and the equations that model them should be separated. Since precipitation and infiltration can affect GW levels on sub-daily time scales, GSFLOW was not used, which currently operates at a daily step (Markstrom et al. 2008). Additionally, the flow routing functionality of PRMS is not suitable for urban environments because it is unable to simulate flow through infrastructure. Although the setting for this study is primarily undeveloped, there are residential areas that could benefit from the use of SWMM's excellent flow transport capabilities. Therefore, a coupled approach is taken here that integrates SWMM and MODFLOW-NWT via the UZF1 package in

an iterative schematic, whereby a time step in SWMM is followed by a time step in MODFLOW-NWT.

CHAPTER 4

STUDY AREA AND DATA COLLECTION

4.1 INTRODUCTION

WNC watershed is located in the southern portion of Virginia Beach, part of the Hampton Roads region (Fig. 16). It is a USGS hydrologic unit distinguished by West Neck Creek, a tidal creek that runs approximately north-south through the center of the watershed. WNC is hydraulically connected to the Chesapeake Bay in the north via the London Bridge Creek and Bypass Canal, and to the Currituck Sound in the south via the North Landing River. Land use in the ∼87 km^2 watershed is comprised mainly of agricultural and wetlands that have been protected from urban development since 1979. While largely flat, changes in relief mark the boundaries of the hydrologic unit, most notably the Pungo Ridge to the east which rises ∼5 m above NAVD88. The average elevation of WNC is ∼2.85 m above NAVD88, but is decreasing due to land subsidence from aquifer compaction and glacial rebound (Holdahl & Morrison 1974; Scott et al. 2010; Eggleston & Pope 2013). These factors contribute to the area experiencing some of the the highest rates of relative SLR in the country, and are already beginning to impact valuable infrastructure (Zervas 2009; Wright & Hogan 2008; Li et al. 2012).

Virginia Beach has a humid subtropical climate characterized by mild, wet winters, and hot, humid summers. Precipitation and temperature data recorded at Norfolk International Airport and Back Bay Wildlife Refuge indicate averages temperatures range from 4.1° C in January to 26.2° C in July over the period 1981-2010.[2] From December 12, 1953 to April 30, 2012 the precipitation has averaged 114.7 cm per year.[3] Rainfall amount is fairly constant between seasons, but intense storms with higher rainfall in shorter time periods are more prevalent in the summer.

4.2 HYDROGEOLOGIC FRAMEWORK

The study area lies within the Coastal Plain Physiographic Province. Most of the present landscape consists of unconsolidated to partly consolidated Pleistocene deposits of the Tabb formation (Mixon et al. 1989). The Sedgefield is the oldest Member of the Tabb formation, rising about 7 m above sea level to form the Oceana Ridge in the northeastern corner of the WNC watershed (Johnson & Berquist 1989). The bottom of the Sedgefield Member is 15 m of what is most likely paleochannel fill; the tidal wetlands adjacent to the creek are soft muds, further indicative of a paleochannel. The younger Lynnhaven Member covers most of the study area and forms flat, poorly drained surficial deposits that are generally less than 6 m deep. The Poquoson Member is the youngest part of the Tabb formation and forms the sand deposits of the Pungo Ridge, which is the eastern boundary of the study area.

Beneath these Quaternary sediments is a wedge of Tertiary and Cretaceous strata that

[2]Season climate normals computed for 30 year periods are available at: `https://www.ncdc.noaa.gov/cdo-web`

[3]Data available at: `http://www.sercc.com`

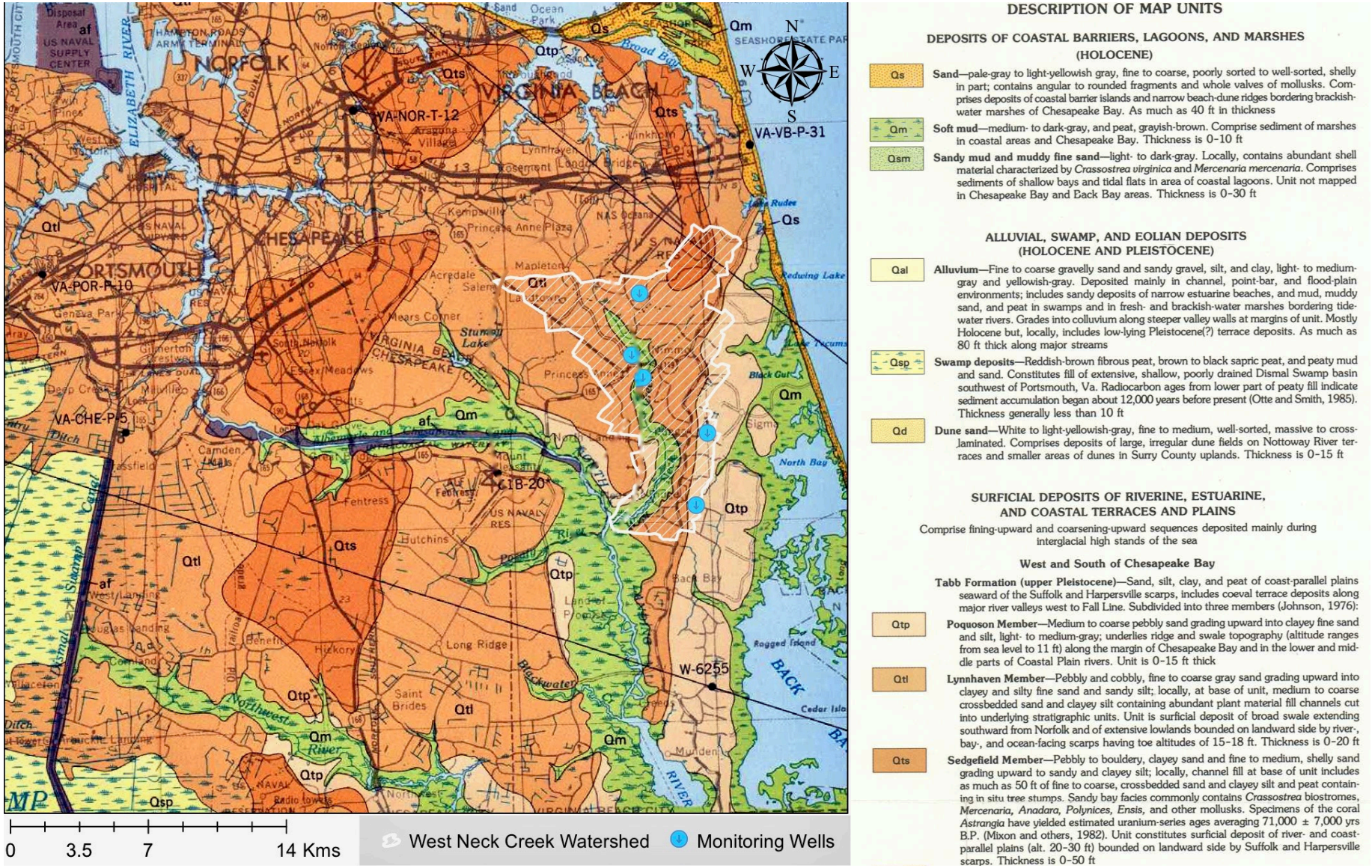

Figure 16: Geological map of Virginia Beach, Norfolk, and Chesapeake with study area outlined in white. Six shallow monitoring well locations are marked as blue circles (there are two at the northernmost location, only one is visible). Modified from Mixon et al. (1989).

thickens and deepens from 0 m in the west to 2000 m in the east (Fig. 17). These layers were formed by long-term sea level fluctuations of the Atlantic Ocean that alternate generally between fluvial and marine deposits overtop a crystalline bedrock. This variation has produced a complicated network of permeable aquifers and less permeable to impermeable confining zones.

A further complication was introduced when a large meteor or comet crashed into the Atlantic during the Tertiary Period, about 35 million years ago (Ma) ago. This impact caused a large crater that filled with mixed debris and turned part of a shallow coastal shelf system into a deep ocean one (Koeberl et al. 1996; Powars & Bruce 1999; Poag et al. 2004). Seawater is thought to have been trapped in this breccia and been chemically transformed into a hyper-saline brine as the initial heat from the collision dissipated (Sanford 2003). The top of the crater ring is currently located about 300 m below land surface (Koeberl et al. 1996).

The aquifer system under WNC consists of alternating aquifers and confining layers until the bedrock basement, about 600 m below mean sea level (MSL) (Fig. 17). However, only the shallow aquifer system, which extends to about 80 m below MSL to the St. Marys confining zone is hydraulically connected to the surficial water table (Powars & Bruce 1999). The shallowest layer of this system is the surficial aquifer, which is underlain by the Yorktown confining zone and the deeper Yorktown-Eastover aquifer (Meng & Harsh 1988; McFarland & Bruce 2006).

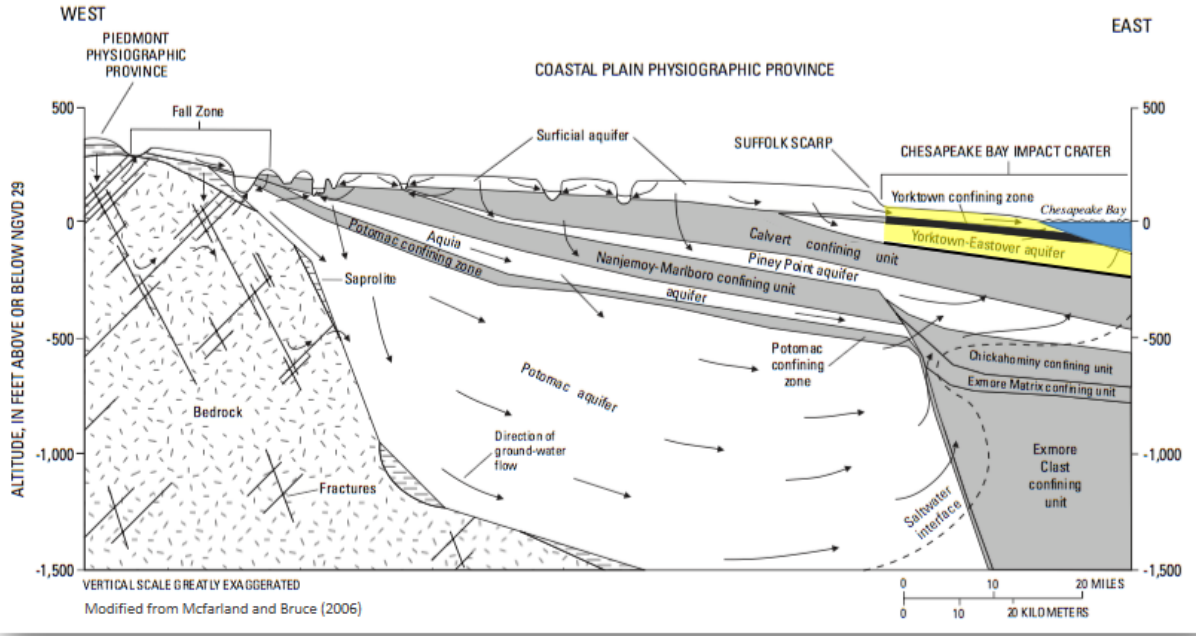

Figure 17: Hydrogeologic framework of the Virginia Coastal Plain Aquifer system. This study only focuses on the shallow aquifers colored (yellow), and shallow confining units (black). Adapted from McFarland & Bruce (2006).

The surficial aquifer is primarily unconfined and consists of Quaternary sands; however, it is heterogeneous and laterally extensive deposits of clay can cause confining conditions. The water table forms the top of the aquifer and its shape mimics the land surface. It is mainly recharged by precipitation in excess of ET, varies seasonally, and is within a meter of the surface beneath lowlands (McFarland & Bruce 2006).

The Yorktown confining zone is a leaky unit that extends throughout the Coastal Plain (Meng & Harsh 1988; Powars & Bruce 1999). In most areas it is some tens of meters thick and is comprised of silts and clays that retard GW flow. However, the Yorktown confining unit is not lithologically uniform, and under WNC watershed there exists interbeds of sand that contain water (Smith & Harlow 2002).

The deepest layer of the shallow system is the Yorktown-Eastover aquifer, which is heterogeneous and consists of fine-grained sediments interspersed with coarse-grained glauconitic and fossiliferous quartz sands. It is 30 m or more thick under southern Virginia Beach, and overlies the Saint Marys confining unit, which hydraulically separates the shallow aquifer system from the deeper units below (McFarland & Bruce 2006).

4.3 DATA COLLECTION

Geospatial datasets were collected and processed using the GIS ArcGIS by Environmental Systems Research Institute (ESRI). Watershed boundaries and wetland locations were obtained from the National Hydrography Database (NHD), a vector dataset produced by the USGS.[4] Land-cover data comes from the most current (2010) Coastal Change Analysis Program (C-CAP) product (NOAA 2010). A 1 m digital elevation model (DEM) created from high resolution Light Detection and Ranging (LiDAR) data (Dewberry and Davis, LLC 2013) was provided by the Center for Geospatial & Visualization Computing at Old Dominion University (ODU).[5] The National Geographic World Map was used as a baselayer within ESRI ArcMap.[6] Soil data, specifically soil hydrologic groups, collected and maintained by the USGS in the Soil Survey Geographic database (SSURGO) database were processed into a convenient ArcGIS layer by ESRI and used for this study.

Climate and precipitation data from January 2011 through December 2012 collected at the Norfolk International Airport (ORF) are available through National Centers for Environmental Information (NCEI), a series of data centers operated by National Ocean and Atmospheric Administration (NOAA).[7] ORF was chosen due to its proximity to the study area, full data coverage, and the availability of both hourly precipitation and climate data consisting of daily minimum and maximum temperatures, and average daily wind speeds. Average evapotranspiration was generated for southern Virginia Beach using the WebWIMP modeling tool (Matsuura et al. 2009).

Subsurface information was derived mainly from 7 locations where continuous cores and downhole geophysical logs were collected in 2002 by the USGS (see Smith & Harlow 2002, figure 3). Average annual water level measurements at six water-level monitoring wells are obtained from the USGS's Active Groundwater Level Network (Fig. 16). The wells have sporadic measurements from the 1970s-2005 and daily intervals for later periods.[8]

Streamflow at the southern end of WNC measured by Caldwell (2001) from March, 1998

[4]Data available at: `http://nhd.usgs.gov`
[5]Data available at: `https://catalog.data.gov/dataset/2013-usgs-lidar-norfolk-va`
[6]Data available at: `http://www.arcgis.com/`
[7]Data available at: `https://www.ncdc.noaa.gov/cdo-web/`
[8]Data available at: `http://groundwaterwatch.usgs.gov/default.asp`

to July, 1999 is also obtained from the USGS.[9] NOAA has modeled future inundation at mean higher high water (MHHW) from SLR based on elevation and hydrologic connection to the ocean.[10] These will be used as a broad comparison against model outputs generated in this study. When applicable, data is converted to WGS84 UTM-18N coordinates, and/or NGVD-29 using the tide gauge at Sewell's Point.

[9]Data available at: `https://waterwatch.usgs.gov/?id=ww_past`
[10]Data available at: `https://coast.noaa.gov/digitalcoast/tools/slr`

CHAPTER 5

METHODS

5.1 INTRODUCTION

The techniques laid out in the following chapter are designed to enhance our understanding of the spatial and temporal distribution of GW head and runoff in response to SLR-induced GW rise and precipitation. The complete hydrologic cycle is captured by coupling two numerical models: subsurface dynamics are simulated using the MODFLOW-NWT, while land surface and atmospheric interactions are captured using the SWMM. Each model is solved separately, with solutions from SWMM used as an internal boundary condition for MODFLOW-NWT and vice - versa. A series of scripts written in the programming language Python (Version 2.7) operates the models and manages the data exchange.

The following sections detail the model discretization and parameterization of the data for MODFLOW-NWT and SWMM. Next, we document the coupling schematic, and explain how data flows through the models. Finally, we describe the the calibration and methodology for testing the model sensitivity.

5.2 MODFLOW-NWT

Initial model development was facilitated by the use of Model Muse (Winston 2009), a graphical user interface (GUI) for MODFLOW-NWT and several other hydrologic models. Subsequent development utilized a series of Python scripts called FloPy (Bakker et al. 2016) that created the MODFLOW-NWT input files, ran the MODFLOW-NWT program, and assisted in post-processing. The approach taken here was largely based on a larger-scale steady-state solution developed by Smith (2003) that encompasses several watersheds in southern Virginia Beach. Density-dependent flow is not simulated because the large majority of data available in Virginia Beach show negligible pressure gradients between the fresh and slightly saline waters of the study area (Smith 2003). These data also indicate steady-state conditions with respect to average global sea level. The following describes the development of a steady-state simulation, which served to establish the initial conditions for the coupled model.

5.2.1 DISCRETIZATION

The finite difference grid consists of 51 columns and 74 rows of 200 m x 200 m cells (Fig. 18). The active area of the grid, in which GW flow occurs, is confined to WNC watershed as delimited by the NHD. The active area is further constrained to cells that produce surface water runoff to another active cell, resulting in 1459 cells where GW flow occurs. The grid is rotated 19° counterclockwise about the upper left corner, which is located at 400232.64777 E, 4072436.50165 N to best match the natural geometry of WNC.

The land surface elevation of each model cell was calculated from the mean elevations of the digital elevation model (DEM) using the Zonal Statistics tool in the spatial analysis extension of ArcGis. The model structure consist of seven layers: the surficial and Yorktown-Eastover

aquifers are each split into equal top and bottom portions to enable accurate representation of differing hydraulic conductivities. The Yorktown-Eastover confining unit is divided into three units: upper and lower confining zones with an aquifer in between, reflective of the interbedded sands indicated by the geophysical logs taken by Smith & Harlow (2002). The geometry of these layers matches that of Smith (2003), which was interpolated using linear variogram Kriging of the geophysical data described above.

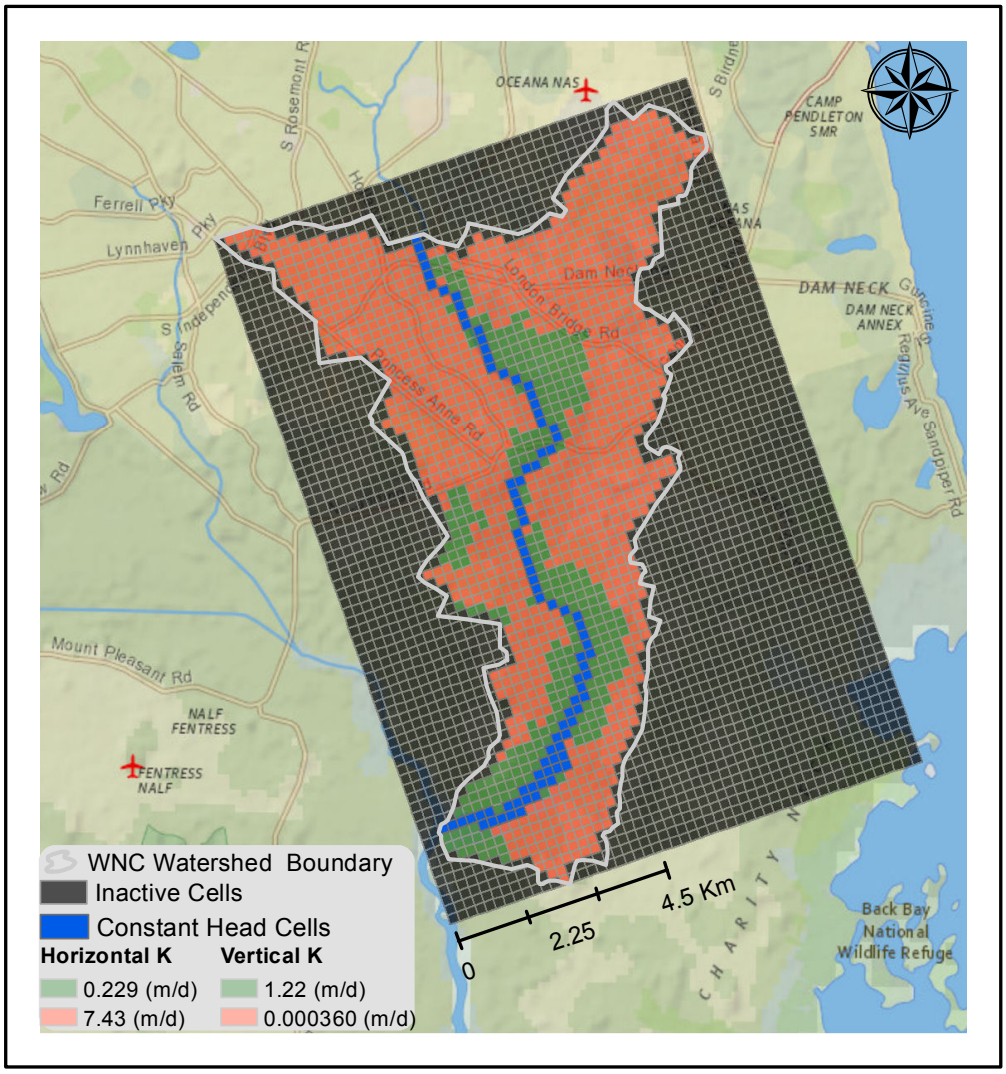

Figure 18: MODFLOW-NWT discretization and hydraulic conductivities in Layer 1. Green cells represent wetlands, red represent uplands, and blue are the surface water body WNC (base map source: National Geographic et al. 2017).

No-flow boundaries surround the watershed and serve as the basement of the Yorktown-Eastover aquifer. WNC, the tidal creek for which the watershed is named, was digitized manually from the NatGeo/Esri base map. The model cells through which it passes are represented as specified head boundaries that do not change within a simulation. The specified, or constant, head boundary cells are initially set to 0.3048 m above NGVD-29, reflecting the average tidal level of the estuary.

5.2.2 PARAMETERS

Horizontal and vertical hydraulic conductivities are usually the greatest sources of uncertainty in GW models due to the spatial heterogeneity of the subsurface, and the difficulty of measuring it. However, in southern Virginia Beach they can be considered generally constrained by previous analyses (see Smith 2003, table 2,3). Horizontal hydraulic conductivity is assumed to be greater than vertical due to the stratified hydrogeology of the Atlantic Coastal Plain. This study follows the approach taken by Smith (2003) to specify separate conductivity rates for wetlands and lowlands in the surficial aquifer, and for each unique layer using the UPW package of MODFLOW-NWT (Fig. 18). Horizontal conductivities ranged from 0.22 m/d to 60 m/d, while vertical conductivities ranged from 0.00039 m/d to 1.219 m/d (Table 1). Aquifers are assumed homogeneous and isotropic, greatly simplifying the calculations needed. Aquifer parameters of specific yield, 0.25, and effective porosity 0.30, are based on the generally sandy soils that characterize WNC watershed (Johnson 1967; Smith 2003).

Table 1: Hydraulic Conductivities (meters/day)

Layers	Horizontal	Vertical
Layer 1: Upland	7.43	0.000360
Layer 1: Wetland	0.229	1.22
Layer 2	60.0	0.208
Layer 3	6.10	0.00904
Layer 4	16.0	0.00122
Layer 5	6.10	0.00904
Layer 6	7.60	0.008
Layer 7	1.00	0.00122

GW flow is connected to land surface processes using the UZF1 package, described in Section 3.3. Infiltration is applied to the land surface and the MODFLOW-NWT flag NUZTOP is set to 3 so that GW recharge to and discharge from occurs at the highest active cell in each vertical column, and specified head cells prevent recharge (Winston 2010).

Saturated vertical hydraulic conductivity within the UZ, flag VKS, is set to 0.12 m/d to ensure infiltration is not limited by soil properties, which is accounted for in SWMM. Surface depth is set to 0.3048 m, determining the depth at which interaction between the land surface and UZ occurs. A constant Brooks-Corey exponent of 3.75 influences the relationship between infiltration rate and water content, and minimizes the initial condition error (see Chapter 7.2, p. 58). Extinction water depth, the distance into the subsurface over with evapotranspiration can occur, is set at 3.0 m, based on the vegetative and climate conditions typical of WNC watershed (Shah et al. 2007). An extinction water content of 0.1 reflects the field capacity for the generally sandy soils of the surficial aquifer. The MODFLOW-NWT flag IUZOPT is set to 3, so that a file is written and updated for every active cell and stress period. The file contains simulation time, GW hydraulic head, UZ thickness, and a series of depths and water contents in the UZ.

The governing GW equation is solved in MODFLOW-NWT using the Newton Linearization

Method (see Section 3.3, p. 21). Parameters are set to the defaults used in FloPy[11]. These include the 'COMPLEX' option, which is used because of the nonlinear nature and intricate SW/GW interactions of the study area.

5.3 SWMM

The EPA provides SWMM as a binary executable with a GUI, and/or source and make files for compiling it as a command-line executable, Dynamic-Link Library (DLL) (Windows) or Shared-Object Library (SOL) (UNIX-like). The GUI was used for initial model development before compiling SWMM as a SOL. A Python program was written that accesses and operates the C-functions compiled in the SOL. This program was largely based on a similar program designed to run the SWMM DLL (Riaño-Briceño et al. 2016).

5.3.1 DISCRETIZATION

SWMM is discretized to match the MODFLOW-NWT grid as closely as possible (see Fig. 19, p. 37). It consists of 1455 200 m x 200 m subcatchments, four less than active MODFLOW-NWT grid cells. Two of the 4 cells represent an engineered water body, Sherwood Lakes, as storage units. The other two represent as outfalls an industrial operation that has artificially lowered the land surface and water table.

ArcGIS Flow Direction tool was used to determine outfall locations along the watershed boundary. This tool uses the elevation of each grid cell to calculate its steepest downslope neighbor, an idealized representation of surface water flow direction. If the resulting direction is to an inactive MODFLOW-NWT cell, the location is designated an outfall in SWMM and GW flow is not simulated.The elevations of the subcatchments are the same as those used by active MODFLOW-NWT cells. The bottom elevations of the storage units are set to 3 m below National Geodetic Vertical Datum of 1929 (NGVD 29) (Hankerson 2016) and all outfalls inverts are set to NGVD 29, 0 m.

WNC is designated by 90 trapezoidal conduits with a maximum depth of 2 m, sides of 0.5 m, and lengths of 200 m to match the MODFLOW-NWT cell width. The creek was digitized to a polyline using the NatGeo/ESRI base map described above. The width of each conduit was estimated by manually measuring it at its widest location within ArcGis. The conduits are joined together by 91 junction nodes, one per constant-head MODFLOW-NWT cell, and an additional one at each endpoint (inactive cells in MODFLOW-NWT) that serve as final discharge nodes. DEM raster values beneath WNC at each segment were extracted using the Extract by Mask tool. The median value was then calculated using the Zonal Statistics tool and set to the invert elevation of the associated junction. Where necessary to ensure continuous flow through WNC, the conduit inlet offset was raised or lowered above the invert elevation.

[11] See: `https://modflowpy.github.io/flopydoc`

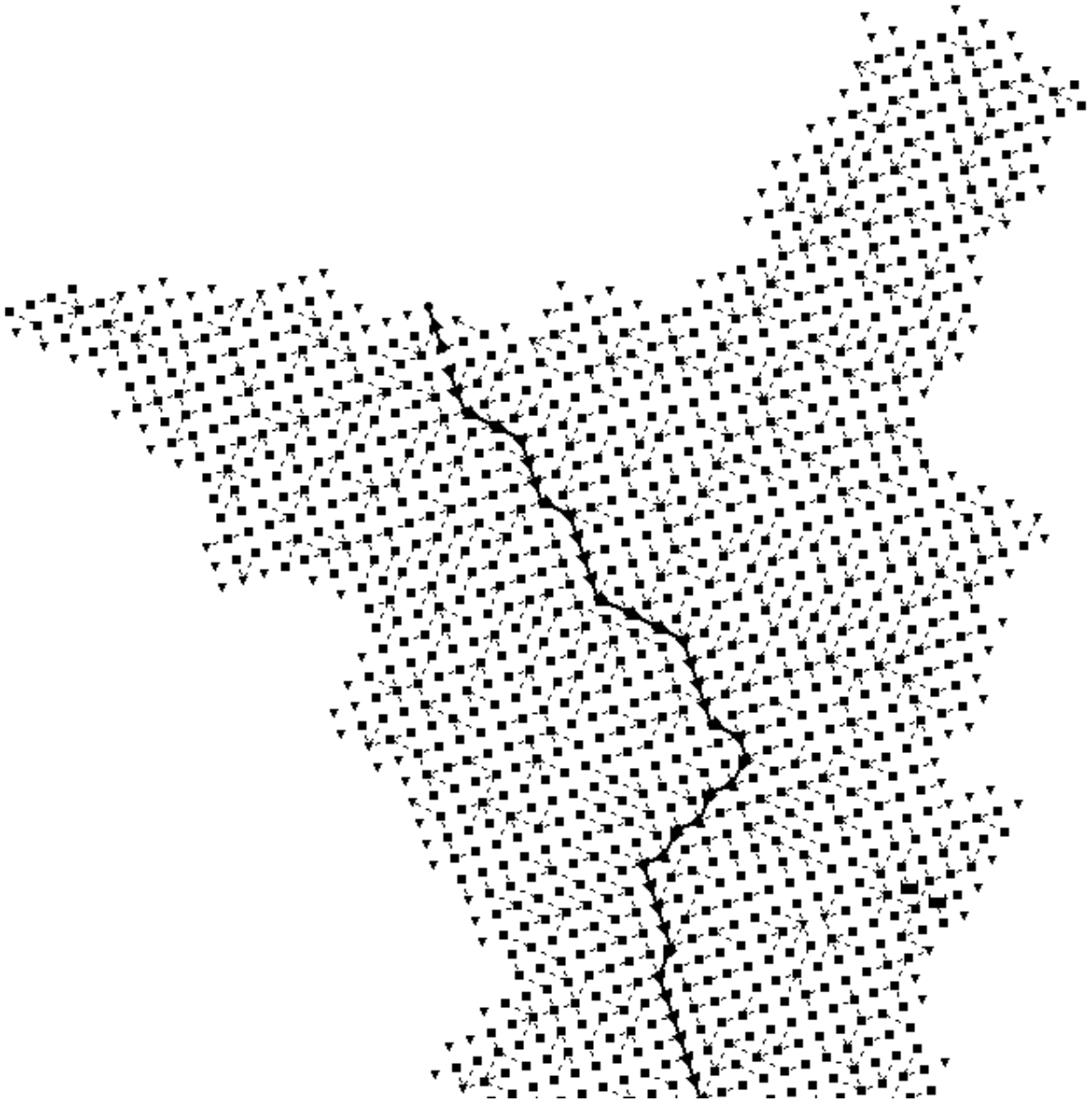

Figure 19: SWMM discretization of the northern portion of WNC watershed. Subcatchments are shown as squares. WNC runs approximately north/south through the center and is shown as a black line with arrows. Outfall nodes are symbolized as triangles, stream junctions as circles, and storage units as inverted hats near the bottom right. The dashed lines connected to subcatchments indicate overland runoff is exchanged between them, and the arrows on WNC show flow direction.

Each junction node receives a constant dry weather inflow to simulate tidal influx. A depth of 0.3048 m is used to reflect the average tidal height of WNC and raised in each SLR scenario, matching MODFLOW-NWT specified head cells. Tidal depth is converted to flow rate in cubic meters per second using the channel depth and width of the conduit, which begins at each junction.

5.3.2 PARAMETERS

The entire simulation spans July 1, 2011 through December 31, 2012. However, the time from July 1, 2011 to December 1, 2011 was not subject to analysis as it contains unrealistic effects due to the initial forcing (see Section 7.2, p. 34). Hourly time steps are used for both wet and dry periods to enable coupling to MODFLOW-NWT at regular intervals. The kinematic wave option for flow routing is deemed sufficient for the purposes of this study, which is not concerned with streamflow of the tidal creek. Evaporation is calculated from the daily climate data collected at ORF using the Hargreaves method (Hargreaves & Samani 1985).

Rainfall, as measured at ORF, drives the simulation. It does not vary spatially in the model, which would add unnecessary complexity. The outlet where runoff is directed to was calculated using the aforementioned Flow Direction tool in ArcGIS. The width of the overland flow path is 200 m, the length of the subcatchment. Percent slope is the mean in the subcatchment, as calculated from the DEM using the Slope tool in ArcGIS.

C-CAP is used with the Zonal Statistics tool to calculate the majority land-cover type in each subcatchment. The majority is used to estimate the Manning roughness coefficient for overland flow according to Rossman & Huber (2016, Table 3-5). It is also used to estimate depression storage, the amount of excess precipitation that ponds in a subcatchment before running off or is intercepted by vegetation (also known as initial abstraction) (Rossman 2015, Table A.5). C-CAP was then used with the NOAA Impervious Surface Analyis Tool (ISAT) to determine the percent of impervious surface of each grid cell. A Manning coefficient of 0.011 and depression storage of 0 were used for impervious surfaces based on soil type (Rossman & Huber 2016).

Infiltration was simulated using the Horton Method, an empirical model that predicts the exponential decay in infiltration capacity over time (Section 2.2, p. 8). This method enabled precipitation to be partitioned into runoff and infiltration based on surface properties alone, and thus does not overlap with infiltration and recharge calculated in the UZF1 package. Infiltration parameters are extremely variable in space and time, an only general estimates are able to be made using the soil properties. Here, the maximum infiltration rate was set to 50 mm/hr, the decay coefficient is 4, and the drying time is 7 days. The minimum infiltration rate is determined by the majority soil hydrologic group at each subcatchment. It is then assigned the minimum rate in the range determined by Musgrave (1955) (see Rossman & Huber 2016, table 4-4).

The aquifer compartment and GW elements of SWMM mimic the parameter configuration of MODFLOW. Each subcatchment has a GW zone in which GW head and soil moisture content (SMC) vary spatially and temporally. All subcatchments share one aquifer compartment that is designed in accordance with the surficial aquifer of the study area. Matching MODFLOW exactly, porosity is set to 0.3%, saturated vertical hydraulic conductivity to 0.12 m/d, field content is equivalent to specific yield of 0.25%, wilting point is equal to extinction water content of 0.1%, and extinction water depth is 3 m. The fraction of total evaporation available for evapotranspiration in the upper UZ is set to 50% to maintain an even proportion of evaporation from the upper (unsaturated) and lower (saturated) GW zones. The slope of the logarithm of hydraulic conductivity versus moisture deficit curve is set to 25 mm/hr based on

the predominantly sandy soils of the study area. GW flow coefficient A1 was set to 0.0001 m to enable intradaily flow within SWMM that is very similar to the rate of daily steady-state GW flow simulated in MODFLOW

The Manning roughness coefficient for the open channeled conduits was set to 0.02. A hydrograph at link 46 was generated, and annual flow was compared to the USGS streamflow gage described above to ensure general accuracy.

Initial and maximum depths of the junction nodes are not used in kinematic wave flow routing, as flow is computed based on the inflow and outflow at the nodes rather than the depths of water present. The ponded area at each junction is set to 40,000 m^2, the area of the MODFLOW-NWT CHD boundary cell. This area realistically reflects the wetlands and tidal influence around WNC.

Each storage unit has a maximum depth of 4 m, and an initial depth of 1 m (Hankerson 2016). The saturated hydraulic conductivity acts as the rate of vertical seepage from the bottom of the storage unit to the underlying aquifer, and so is set to the steady-state infiltration rate of 0.28 mm/d. Outfalls serve only as terminal nodes in the network, removing all water they receive. Thus their parameter configuration has no effect on the results.

5.4 COUPLED

SWMM and MODFLOW-NWT are coupled sequentially such that the output calculated at each model time serves as the input boundary conditions for the other (Fig. 20).

SLR is simulated by raising the Constant-Head (CHD) boundary of WNC, following the method used separately by Masterson (2004), Bjerklie et al. (2012), and most recently by Habel et al. (2017). Simulations are run for 0 m (current conditions), 1 m, and 2 m SLR scenarios. The next section describes how data flows between the models. The following sections details the modifications to the source code that enabled this. Finally, the nuances that occur at the boundaries are explained.

Initial GW heads and SMC for SWMM are determined by running a calibrated steady-state MODFLOW-NWT simulation. SWMM then simulates 24 hour long time steps, in which it calculates, among other things, infiltration and GW ET rates. MODFLOW-NWT operates on a transient, daily stress period, so the infiltration and ET rates that drive them are summed and written to files. MODFLOW-NWT uses these files to solve the governing GW flow equation, determining GW head and SMC in the UZ. When GW head comes within a specified distance to the land surface (parameter SURFDEP), the UZF1 package calculates discharge of GW to land as discussed in Section 3.3 (p. 23). A formatted ASCII file containing head information, and a binary file with the discharge rates are updated at time step. For each grid cell that doubles as a SWMM subcatchment, a 'gage' file is updated that contains the SMC of the unsaturated zone. These values are extracted from the files and passed to SWMM for use in the subsequent 24, hour-long time steps.

The MODFLOW-NWT source Fortran code was modified such that it would wait for the SWMM simulation to write the infiltration and GW ET rates, and write a file to signify that it had completed a stress period. The former was achieved by simply having the program wait until

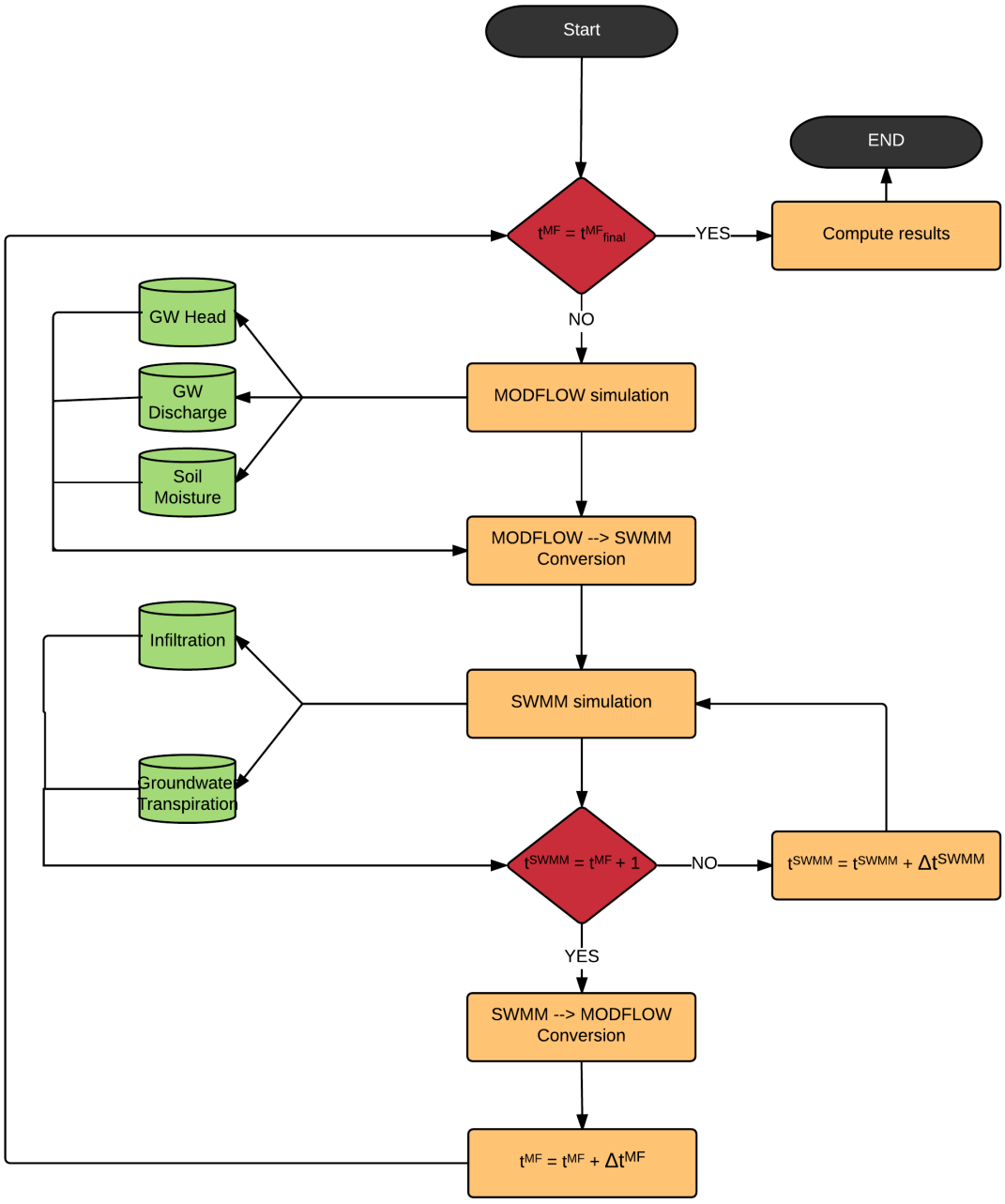

Figure 20: Flowchart of coupled programs. Each daily MODFLOW-NWT time step calculates hydraulic head, GW discharge, and SMC which are converted to SWMM input values. 24 hourly SWMM time steps use these to calculate infiltration and GW ET. Once the smaller SWMM time steps are equivalent to the MODFLOW-NWT time step, these values are passed to MODFLOW-NWT and the simulation time continues.

a file was written to disk in conjunction with the GFortran SLEEP function. The files containing the head results, as well as those containing the UZ results, needed to be flushed in order for SWMM to obtain the complete results (the file was truncated otherwise). This was accomplished using the gfortran FLUSH function within the gwf2bas7_NWT.f and gwf2uzf1_NWT.f source codes. It is also noteworthy that MODFLOW-NWT holds all files open for the duration of the simulation. This made it necessary to increase the open file limit of the operating system (MacOS Sierra).

The SWMM source C code was extended with a variety of 'cosimulation' functions developed by Riaño-Briceño et al. (2016) to interact with the SWMM simulation at each time step. These functions were not directly applicable to the coupling designed here, but provided the foundation on which to build the necessary methodology. Several functions were developed which access the structures in SWMM of each subcatchment that hold the pertinent data: GW head, UZ moisture content, infiltration and GW ET. A member was added to the GW structure to hold the GW discharge rates calculated by the UZF1 package, converted to SWMM units. It is then added to the ponded depth member of the subcatchment's pervious subarea structure, where it evaporates or contributes to runoff.

SWMM was compiled as a SOL, and a Python script was written utilizing the built-in ctypes library which enables calling functions in external libraries. Thus, SWMM was controlled entirely using Python programs, which greatly facilitated the exchange of data between the two models. After running a day of hourly timesteps in SWMM, Python accessed the C structures to obtain and write to disk the infiltration and ET rates, and subsequently wrote the file MODFLOW-NWT needed to simulate a stress period. The files written by MODFLOW-NWT were then read into the Python program, formatted and passed into the C structures before running the next 24 hourly time steps in SWMM.

Special consideration has to be taken when the GW head gets within a specified distance of the land surface (controlled by the surface depth parameter mentioned above). First, the SMC of the UZ is set to porosity in SWMM, since there is no UZ - the subsurface is fully saturated. Second, GW 'leaks' to the land surface and the GW head drops accordingly. This water is removed from the MODFLOW-NWT simulation and the GW head value that is passed to SWMM is artificially lowered below the land surface. The inconsistency is due to the time step differences in the two models: the hours in which GW head should be at the land surface in SWMM is masked by the daily value calculated in MODFLOW.

This is accounted for by passing SWMM the GW head value 0.05 m below land surface instead of the value calculated by MODFLOW-NWT when a location is experiencing surface leakage (Fig. 21). The 0.05 m 'surface threshold' (Table 2) is set to prevent numerical instability that arises in SWMM when the GW head is exactly equal to the land surface.

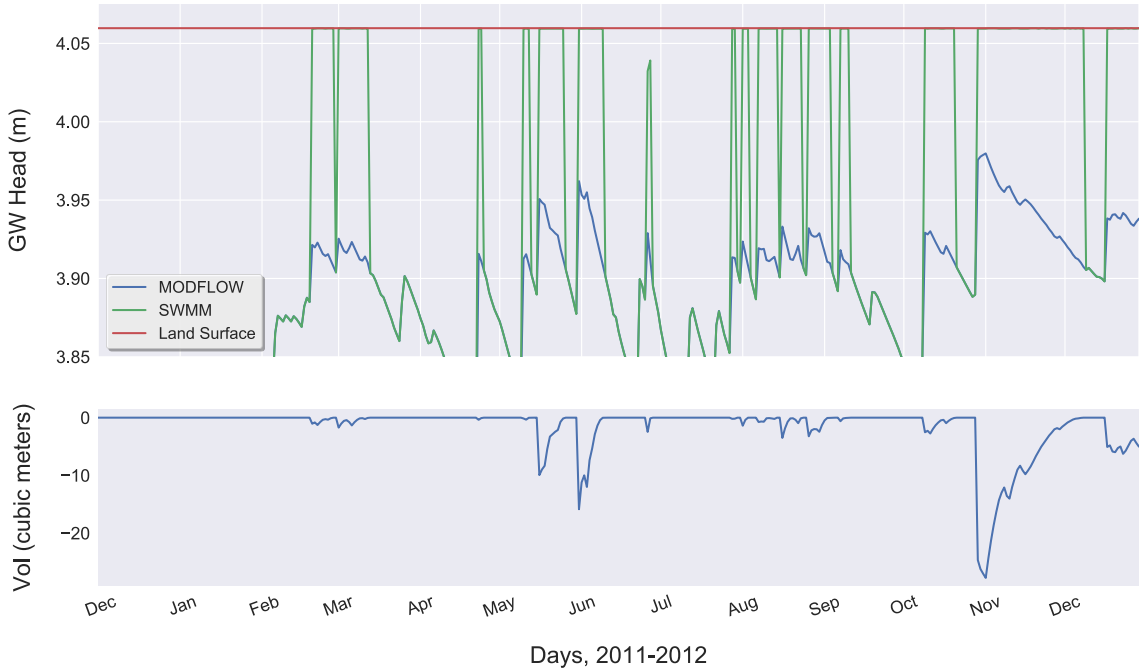

Figure 21: Head comparison between SWMM and MODFLOW-NWT. The top panel shows GW head in MODFLOW-NWT and SWMM diverging when the GW head approaches the land surface. This is caused by surface leakage, shown in the bottom panel, in which GW is discharging from MODFLOW-NWT model cells to the land surface. Hydraulic head in SWMM is manually forced to be near the land surface to overcome the artificial decrease caused by time step resolution differences in the two models.

5.5 CALIBRATION AND SENSITIVITY

The configurations described above represent the best estimates based on available data. However, as most of the data are estimates themselves or lumped representations of varying characteristics, this model representation of the real world is subject to uncertainty. To overcome some of this uncertainty, each model is calibrated separately for a SLR scenario of 0.0 m, which is representative of current conditions. The calibrated model, which had a root mean square error (RMSE) of 0.692 m calculated by subtracting each measured water level from the equivalent simulated water level, is then tested for sensitivity by varying individual parameters (Table 2). A rigorous calibration and sensitivity analysis were beyond the scope of this study, and would have required the collection of a variety of data, such as shallow GW head and stream discharge (for better quantifying the rainfall-runoff relationship and infiltration rates). However, this does not negate the usefulness of the model for understanding the relationship between sea level rise, water table location and runoff.

Smith (2003) calibrated conductivities to water levels in 38 wells using the parameter estimation software WinPEST® (Doherty 2004), achieving a RMSE of 0.607 m of measured to simulated water levels for a steady-state simulation. These conductivities served as the initial estimates for this study, but were manually adjusted to best match simulated water levels to the average water levels of the six monitoring wells within WNC watershed (Fig. 18, p. 34). The adjustments stayed near the bounds estimated by previous methods (see Smith 2003, table

2.3).

The SWMM simulation used GW heads and SMC as computed by the calibrated steady-state MODFLOW-NWT simulation as starting GW head and SMC. SWMM was then calibrated simply by comparing the ET, runoff, and infiltration calculated to the overall expected water budget for southern Virginia Beach. ET was calculated using the WebWimp tool, described in Section 4.3 (p. 31). Infiltration was based on the steady-state GW recharge rate previously calibrated by Smith (2003). Surface runoff is then the difference between precipitation, ET and GW recharge.

Sensitivity of the coupled model to hydraulic conductivities was tested by raising and lowering the bulk rates by 15%. Thus, the spatial variance of the rates was not tested and is an area ripe for further analysis. Sensitivity to specific SWMM and MODFLOW-NWT parameters was tested by altering an individual parameter and running a full, coupled simulation. It was not feasible to simulate every parameter due to the ∼24 hour computer run-time of one SLR scenario. Thus, parameters were chosen based on their relevance to infiltration and ET, the primary model forcings. Total infiltration and ET are used to assess the sensitivity of the forcings to the changed parameter. Total runoff is used to assess the sensitivity of the model results, both of runoff and as a proxy for GW head at the land surface since given the same precipitation, change in runoff is only caused by a change in UZ storage.

Table 2: Parameters Tested for Sensitivity

ID	Parameter	Low	Med	High
M1	Horizontal Hydraulic Conductivity[12]	85%	100%	115%
M2	Vertical Hydraulic Conductivity[12]	85%	100%	115%
M3	Surface Threshold	0.025	0.05	0.1
S1	% Impervious [12]	75%	100%	125%
S2	Subcatchment Width	100 (m)	200 (m)	400 (m)
S3	Conductivity Slope	5	25	45
S4	% GW ET from UZ	0.25%	0.5%	0.75%
S5	Max Infiltration Volume	30 (mm)	Unlimited	NA
S6	Infiltration Decay Coefficient	2	4	8
S7	Infiltration Dry Time	1 (day)	7 (days)	14 (days)
S8	Manning Coefficient	50%	100%	200%
S9	Storage Depth	50%	100%	200%
U1	Brooks-Corey Epsilon	2.5	3.75	5
U2	Porosity	0.25%	0.30%	0.35%
U3	Specific Yield	0.21%	0.25%	0.29%
U4	ET Extinction Water Content	0.05	0.1	0.15
U5	ET Extinction Depth	1.5 (m)	3 (m)	4.5 (m)
U6	Saturated Vertical Conductivity	0.06 (m/d)	0.12 (m/d)	0.18 (m/d)
U7	Surface Leak Depth	0.1524 (m)	0.3048 (m)	0.6096 (m)

[12]The spatial distribution is maintained.

CHAPTER 6

RESULTS

6.1 INTRODUCTION

This chapter presents the results generated by the coupled MODFLOW-NWT/SWMM simulation. The overall objective of this work was to investigate the influence of SLR on the temporal and spatial variations of GW over the course of a year. From this, insights were gleaned into the effects on runoff generation and the distance from the land surface to the GW table (DTW).

This chapter is divided into four main sections. Section 6.2 summarizes the model results, giving a general overview of the effects of SLR on GW recharge, ET, and position of the GW table. Second, changes in runoff generation in WNC over time are presented. The third section, shows the effects of SLR on the DTW. Finally, the sensitivity of these results are demonstrated by showing how they change as a result of the model parameterization. We explore the changes in time and space separately, which enables a better understanding of the challenges posed to the built and natural environments.

6.2 GENERAL

Precipitation and ET are the main forcings that drive GW recharge in the WNC watershed. Recharge contributes to the flow of GW, determining water table position and runoff production by saturation excess. Figure 22 shows how these drivers change over the time period of a year in response to SLR. As expected, recharge reflects the precipitation pattern, and ET oscillates seasonally in response to temperature. Recharge is subdued in higher SLR scenarios as a higher water table prevents surficial infiltration and subsequent percolation. The effect of SLR is most apparent during intense or prolonged precipitation, such as between May and August. In September, when there is a relatively small amount of precipitation, there is little difference in GW recharge between scenarios because GW head is not impacting the UZ.

Inversely, GW ET increases with SLR as there is more moisture available to meet the demand for water by plants performing photosynthesis. SLR has the greatest impact during the peak summer months July and August, when this ET demand is highest. The effect of SLR is all but negligible during the winter months when the full ET demand is met by the current conditions (no SLR).

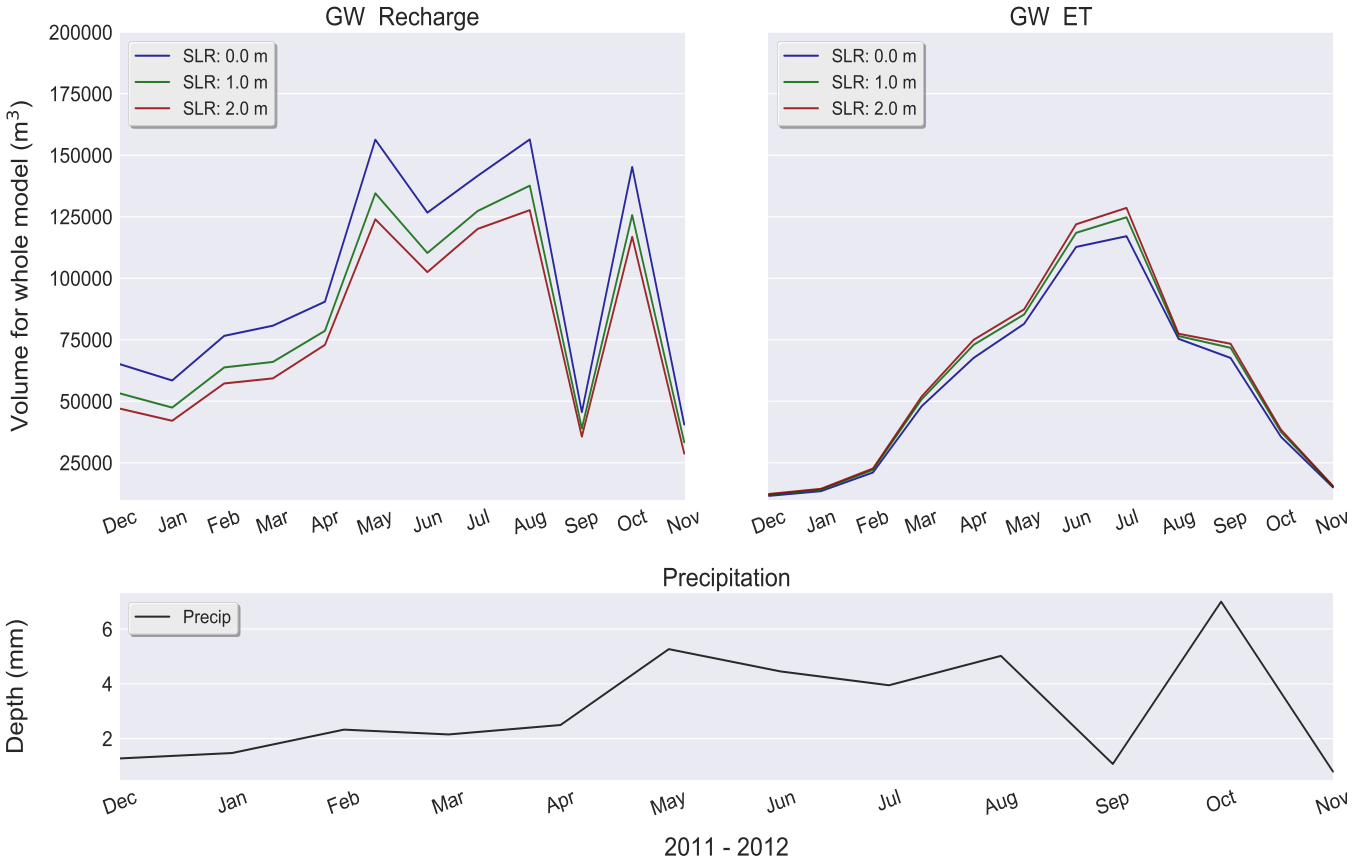

Figure 22: Monthly changes in GW recharge and ET due to SLR. From December 1, 2011 to November 30, 2012.

Both GW recharge and GW ET show a more pronounced effect from a 0 m to 1 m change in SLR than from a 1 m to 2 m change. This difference is caused by the hypsometry of WNC watershed. As shown in Figure 23, there are a large number of cell counts less than 1 m above NGVD 29.

As expected, these low elevation areas surround WNC estuary (Fig. 24). With a 1 m SLR, many of these locations experiences changes in the UZ zone, permitting the GW table to interact with the land surface, and affecting GW recharge and ET. A 2 m SLR, while extending further horizontally than a 1 m SLR, does not contribute a great deal more because the majority of impacted cells had an UZ small enough that a 1 m SLR scenario shrank it to 0. Had a 3 m or 4 m SLR scenario been simulated, there would likely have been a substantial impact due to the large amount of land with elevations in this range.

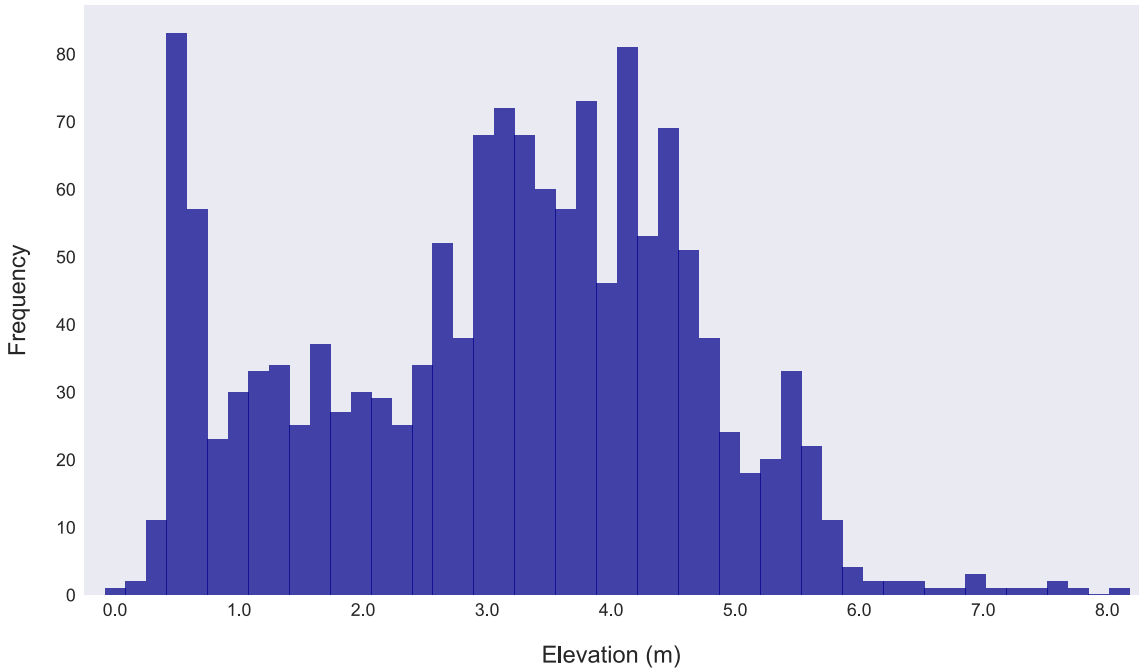

Figure 23: Frequency distribution of land surface elevations.

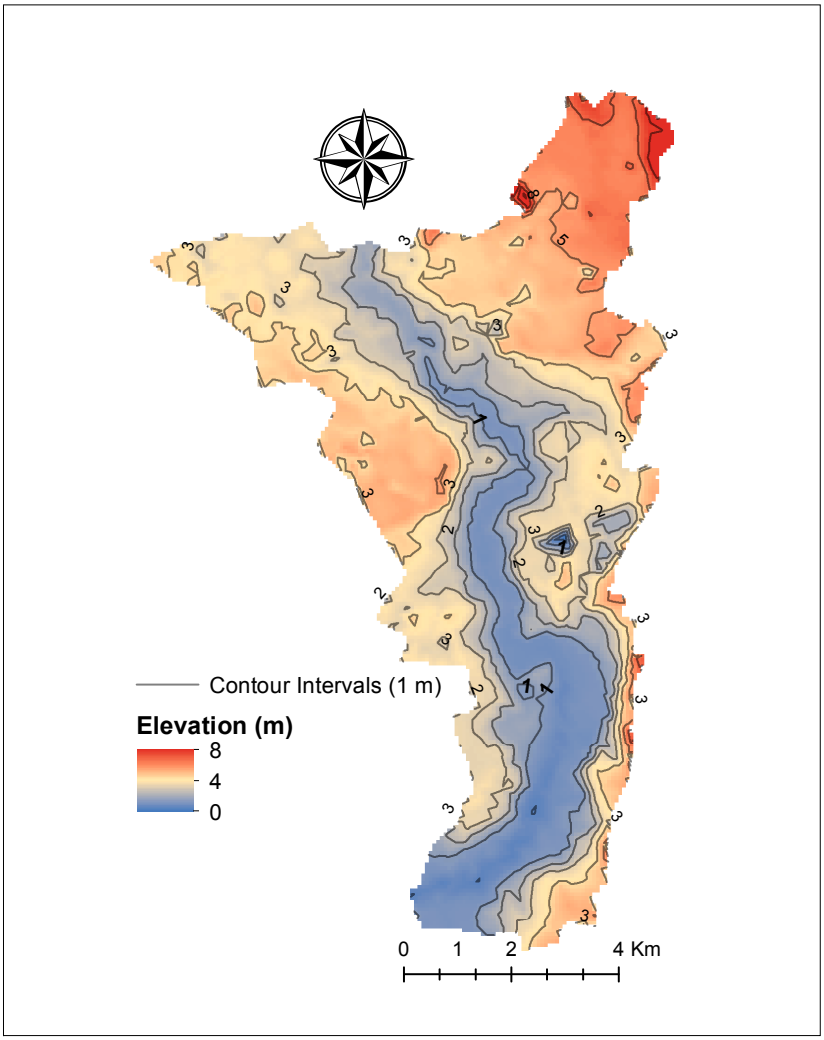

Figure 24: Land surface elevations within WNC watershed.

Figure 25 shows how the average GW head changes over the course of a year. Simulated SLR raises the overall GW head in WNC watershed. The most notable change is the increase in head of the maximum frequencies. This increase occurs mainly for heads below ∼3 m, which are located in the low lying area surrounding WNC.

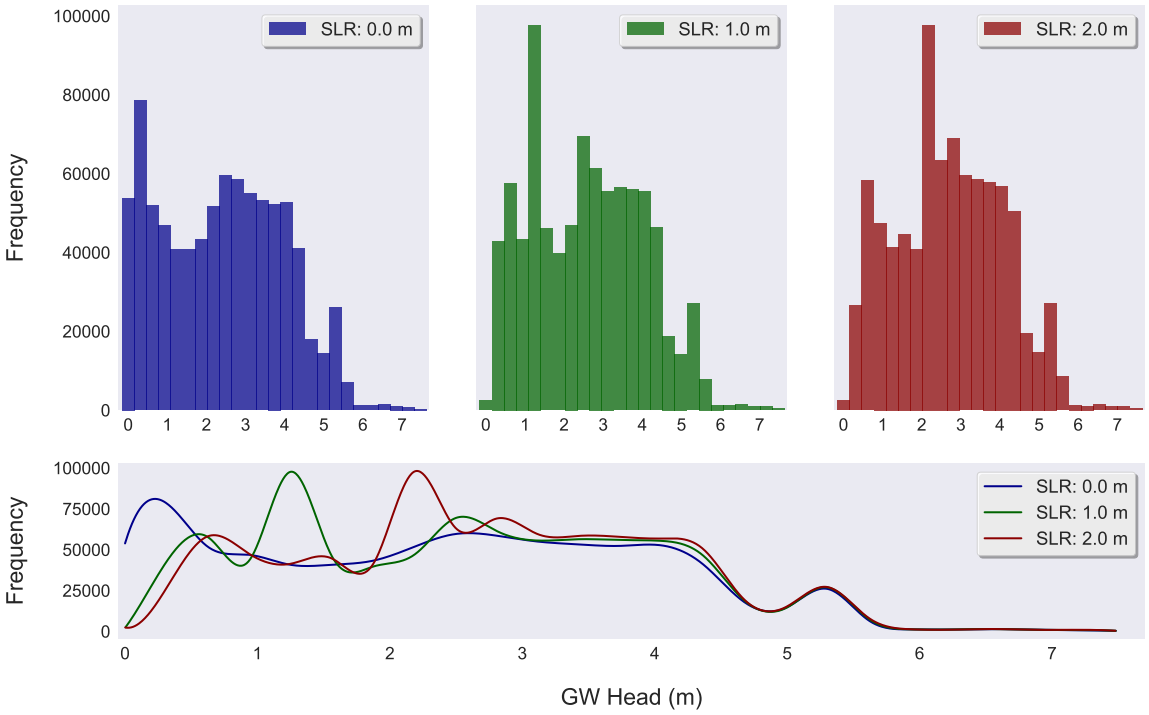

Figure 25: Frequency distribution of average annual GW head for each SLR scenario. The top panel shows the histogram for each scenario separately. In the bottom panel, the frequencies of the GW head occurrences for each scenario are plotted against one another, highlighting the shift in maximum frequencies and the negligible effects of SLR on heads greater than ∼3 m

Figure 26 shows the effects of the simulated SLR on the spatial distribution of GW head. GW head decreases with distance from tidal boundary, as described in Chapter 2 (p. 10). As with the changes in GW recharge and ET, there is a more pronounced change from a 0 m to 1 m SLR than from a 1 m to 2 m SLR due to the topography of the watershed (Fig. 23).

The spatial pattern of head changes reflect the wetland configuration of hydraulic conductivities, which have a higher vertical, and lower horizontal, rate than the nonwetland (upland) configuration (Fig. 18, p. 34). The faster vertical conductivity rates of these cells permit greater infiltration, recharge, and subsequently higher GW head at these locations than the majority of the watershed. This indicates a high impact of conductivity rates on the results, amplifying the importance of sensitivity testing (Section 6.5).

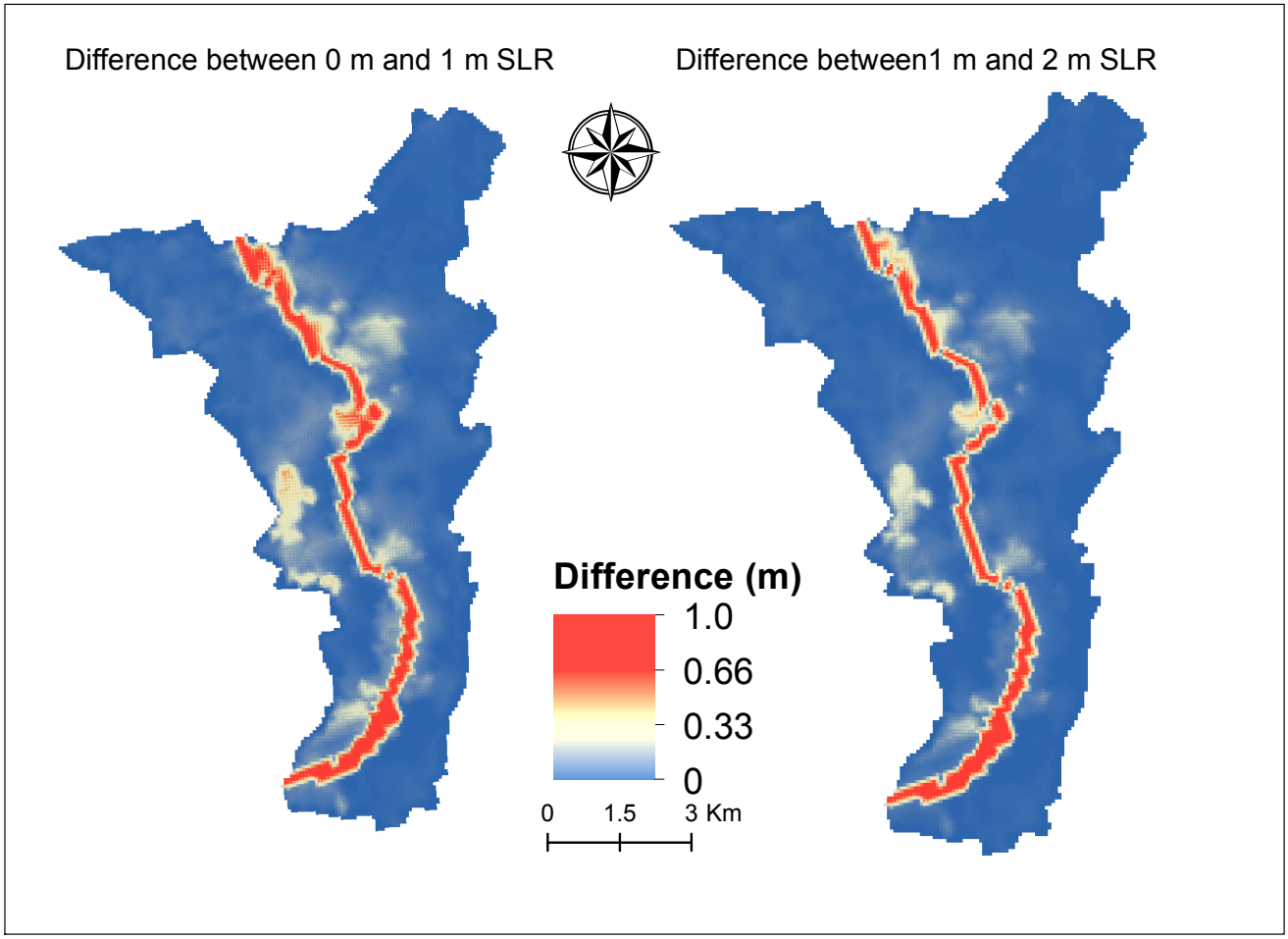

Figure 26: Difference in average GW head resulting from simulated SLR.

6.3 RUNOFF

The effects of SLR on total runoff can be seen in Figure 27. Clearly, SLR has a minimal effect on runoff generation. WNC is characterized by soils with slow infiltration rates. Thus, runoff is mainly caused by precipitation rates that exceed the infiltration capacity of the soils.

The spatial distribution of how runoff changes with SLR is shown in Figure 28. Thus, the changes in runoff reflect the locations that experienced changes in GW head (Fig. 26, p. 49), and this result is likewise sensitive to the spatial distribution of hydraulic conductivity and topography. SLR contributes to runoff via saturation excess, by reducing the storage capacity of the UZ to 0.

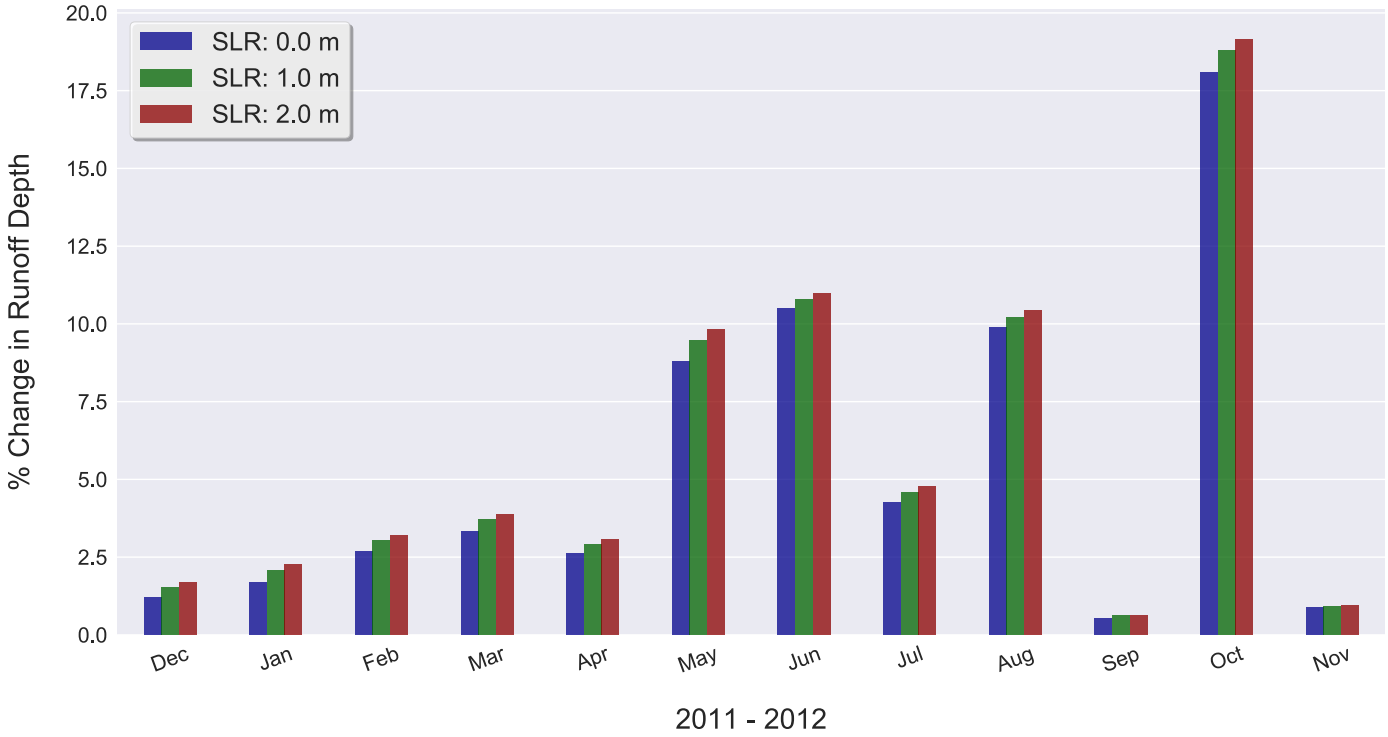

Figure 27: Monthly averaged runoff rate from December 1, 2011 to November 30, 2012.

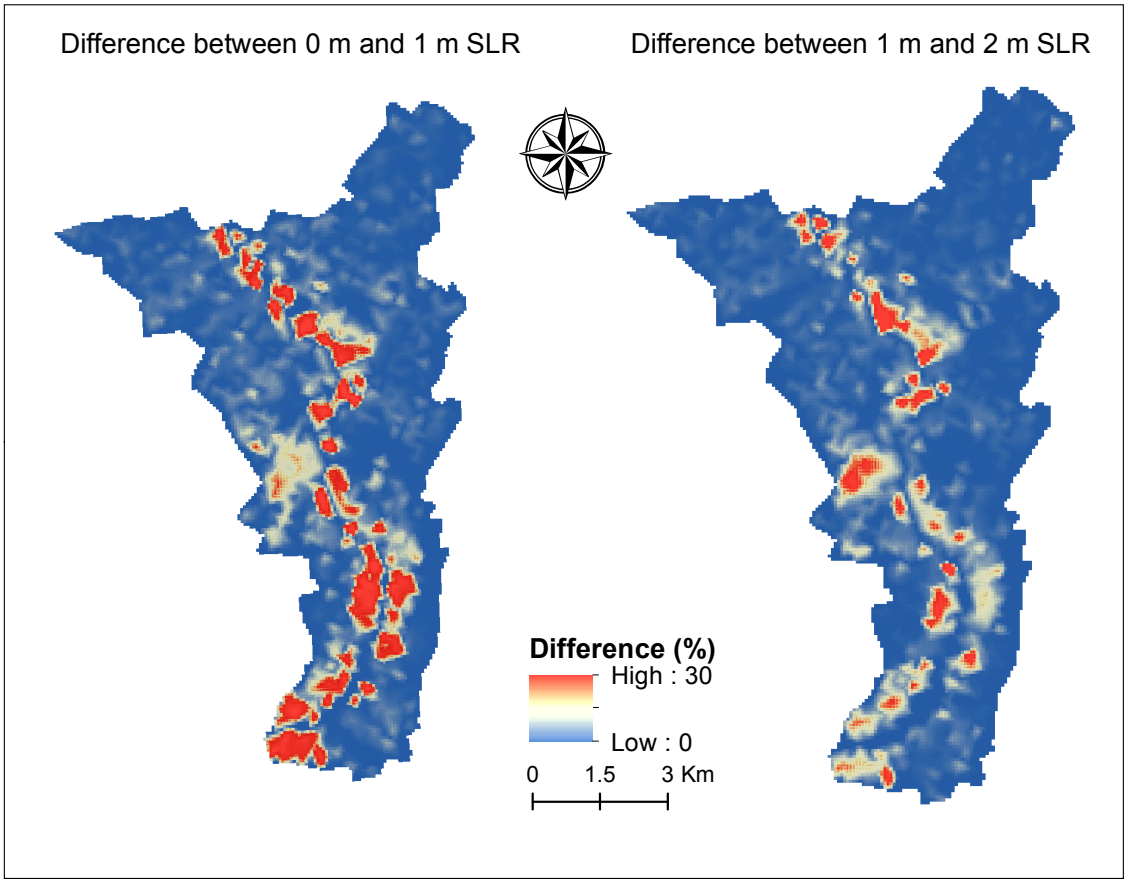

Figure 28: Difference in average runoff volume resulting from simulated SLR.

6.4 DEPTH TO WATER

Figure 29 shows the effects of SLR on DTW. Each panel shows the amount of time over the course of a year that the GW table is within a specified distance of the land surface. The top two panels, which represent the shallowest depth to the water tables of 0.1524 m (6 in) and 0.3048 m (12 in) respectively, exhibit notable changes. First, a SLR of 1 m substantially increases the amount of area that is permanently within 0.1524 m (0.5 ft). For the 0.3048 (1 ft) DTW case, there is a less pronounced, but still prominent increase in the amount of area affected for the 4000 - 7000 hour range. Where these changes are occurring has important implications for the built and natural environment (Chapter 7).

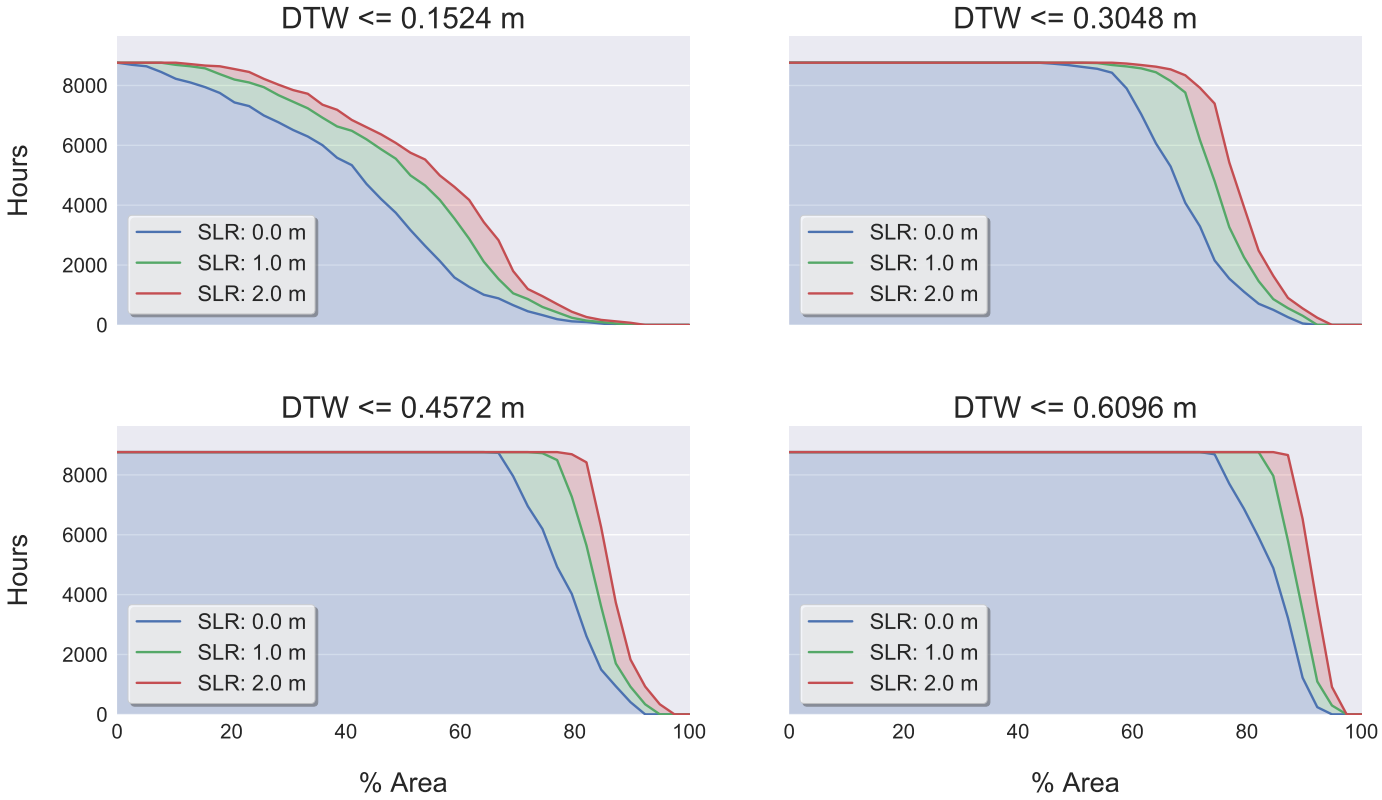

Figure 29: Distance from land surface to the GW table expressed as time per percent of the study area.

6.5 SENSITIVITY

Figure 30a shows that infiltration is most sensitive to the percentage of ET occurring in the UZ relative to that occurring in the saturated zone (S4). With less ET occurring in the UZ, more water is able to remain in the UZ as infiltration rather than being lost as ET. Intuitively, total infiltration is also greatly impacted by setting a hard limit on the maximum infiltration volume (S5). With increased SLR scenarios, infiltration becomes more sensitive to porosity (U2). As porosity and DTW decrease, water is more often prevented from entering the soil as infiltration.

As shown in Figure 30b, ET is more sensitive to parameter configurations than infiltration. It is most sensitive to lowering the maximum possible infiltration volume (S5), which causes more runoff and thus surface water that is more easily evaporated than subsurface infiltration. Similar to infiltration ET is also sensitive to the amount of ET occurring in the UZ relative to the saturated zone (S4); water is more easily transpired from the shallower UZ than from deeper GW. ET is also increased substantially by decreasing porosity (U2) and increasing specific yield/field capacity (U3H). The former, similar to lowering the maximum possible infiltration volume, causes more runoff that is more easily evaporated than subsurface water. Increasing specific yield and field capacity increases the amount of water held in the subsurface and allows for additional ET. Finally, altering vertical hydraulic conductivity (M3) has a noticeable effect on ET. Increasing the conductivity lowers infiltration because the infiltrating water can percolate through the UZ and beyond the root zones of plants at faster rates.

Results from parameter configuration S4 are show in Figures 31 and 32. The S4 parameter controls how much ET comes from the unsaturated zone as compared to the saturated zone. Since both both infiltration (Fig. 30a) and ET (Fig. 30b) are highly sensitive to S4, it is used to demonstrate the general effects of a changed parameter on the results shown in Figures 27 and 29.

Figure 31 shows the percent change between the original and altered parameter simulation. Change in runoff depth decreases as SLR increases because some runoff is already being produced by the shallower DTW during higher SLR scenarios, thus mitigating the impact of changed ET. Importantly, there are some drastic differences between this and the default scenario, around 40% in some cases, which demonstrates the importance of sensitivity testing.

Much more of the study area experiences higher groundwater levels in the new scenario (Fig. 32). Since more ET is being pulled from the UZ, rather than the saturated zone, there is greater porosity in the UZ, and thus the water table is free to rise. For the situation shown (DTW $\leq$ 0.1524 m and DTW $\leq$ 0.4572 m), there is a substantial effect from this parameter change.

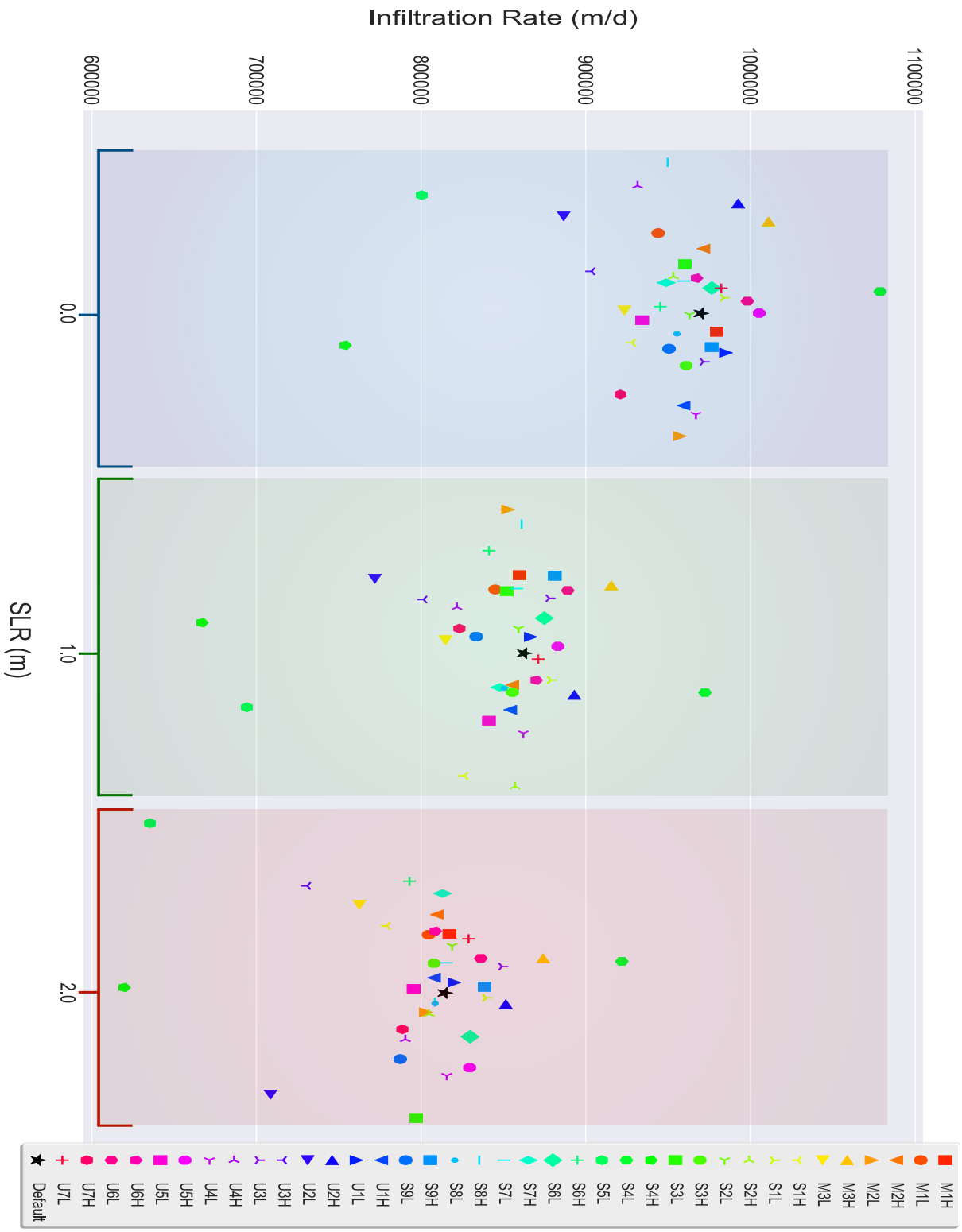

(a) Sensitivity of total infiltration from Dec 1, 2011 to Nov 31, 2012. Each marker type indicates a simulation with a changed parameter. The markers have been jittered for easier visualization. See Table 2 in Chapter 5 (p. 44) for a full description of the ID in the legend. The ID is followed by an H or L indicating the high or low scenario.

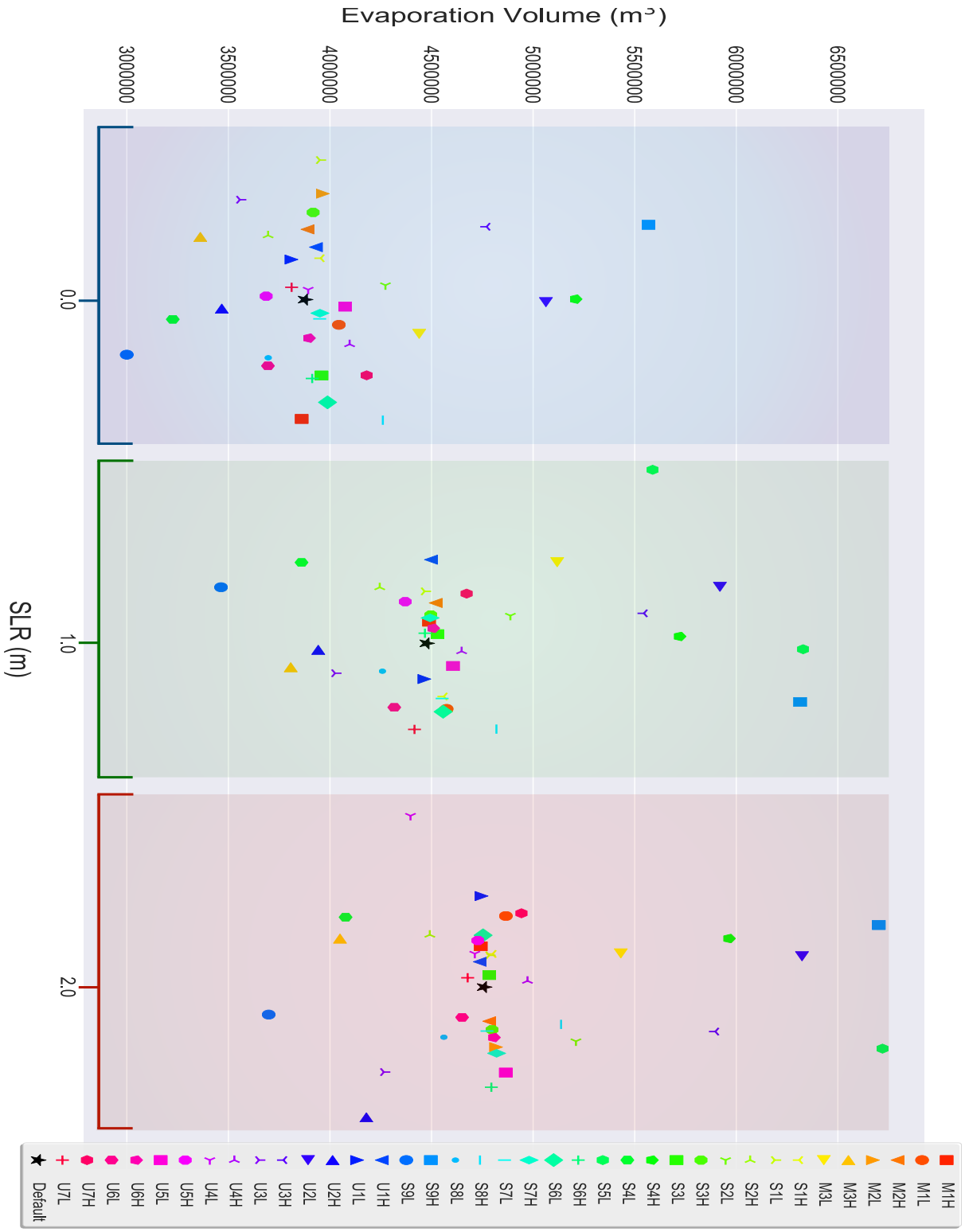

(b) Sensitivity of total evaporation from Dec 1, 2011 to Nov 31, 2012. Note that total evaporation is the sum of GW ET and surface water ET.

Figure 30: Sensitivity of model forcings to individual parameters.

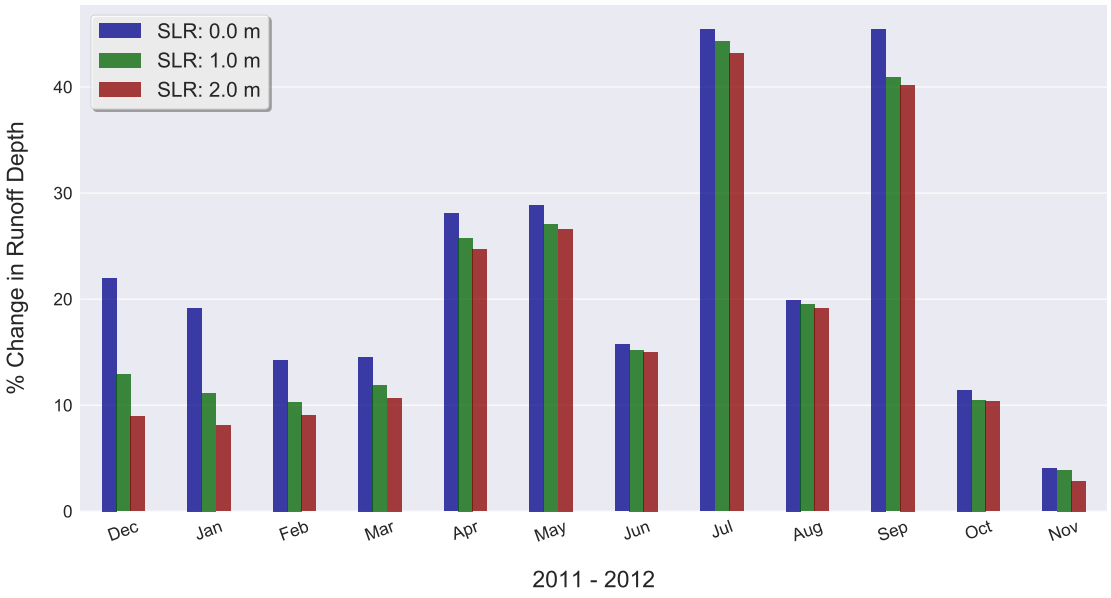

Figure 31: Change in runoff rate between default and S4H parameter configuration.

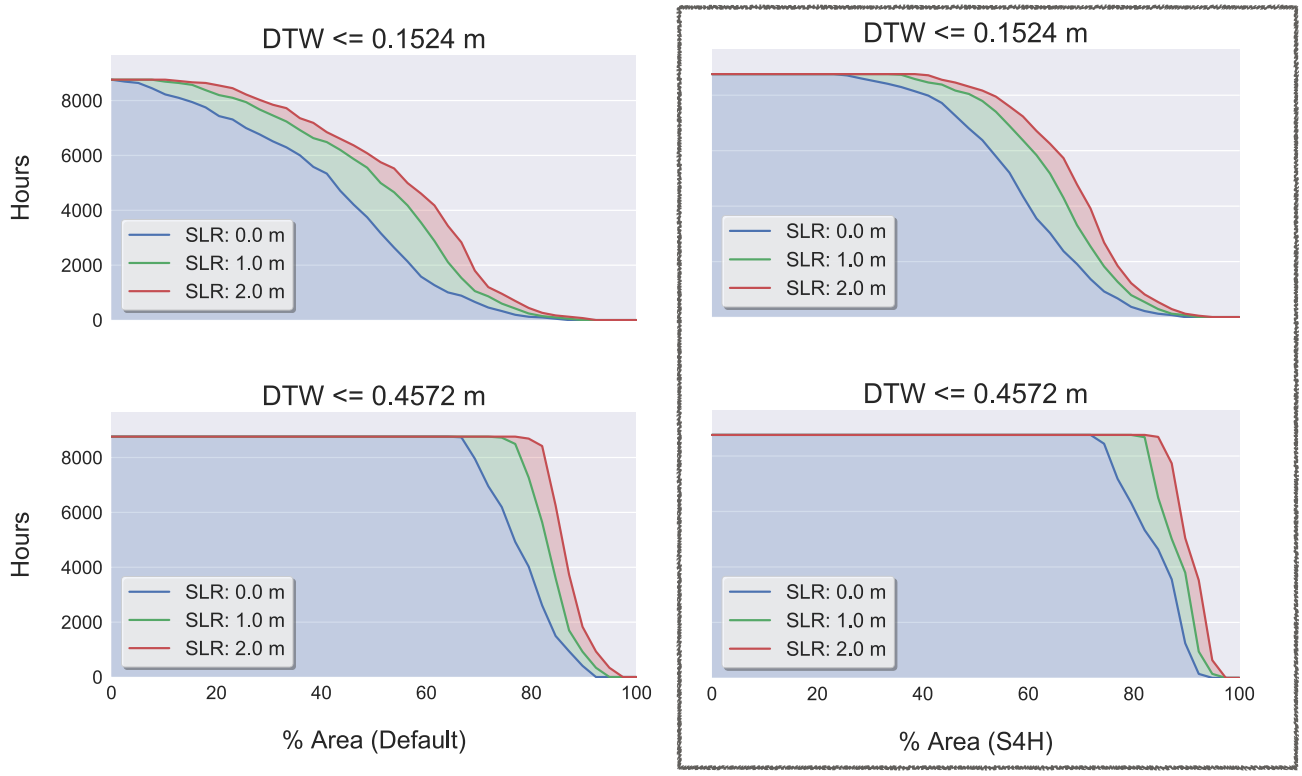

Figure 32: Comparison of DTW expressed as time per percent of the study area between Default (left) and S4H (right) scenarios.

CHAPTER 7

DISCUSSION

7.1 SIGNIFICANCE OF FINDINGS

The results presented above demonstrate the potential for the often under-appreciated effects of SLR-induced GW rise to become a damaging hazard to WNC communities and ecosystems. However, the possible futures simulated in this research serve as a first step in developing foresight. Most of these potential damages arise from the increased interactions of GW levels with subsurface infrastructure. Additional runoff is less of a concern because of the prevalent soils in WNC, which have slow infiltration rates. This causes most of the runoff to be produced by these soil properties rather than higher water tables reducing UZ storage to 0. The sensitivity analysis generally provides encouraging results, in that changes in most parameters do not have excessively large effects on forcing variables.

Several previous studies have compared the relative contributions of marine (tidal) and groundwater inundation to coastal flooding for future possible SLR scenarios (see: Rotzoll & Fletcher (2012); Manda et al. (2015); Moss (2016)). They have separately found that groundwater inundation contributes as much as, if not more, to flooding than does tidal flooding. These circumstances was investigated here by comparing the results from the coupled MODFLOW-NWT-SWMM model to data from the NOAA SLR-Viewer

First, we explored the spatial extent of the average annual DTW by locating cells where SLR had caused changes to the GW table that brought it within 0.3048 m (1 ft) of the land-surface. This was considered a hazardous depth with the potential to interact with multiple types of infrastructure as well as the roots of a variety of plant species. The 1 m scenario was chosen to demonstrate these effects because it has a more pronounced effect (see Section 6.2, p. 45), and is likely of more immediate concern. Next, we compared cells that met these criteria to tidal flooding for a 3 foot[13] SLR by overlaying the NOAA SLR-Viewer data in ArcGIS.

Figure 33 shows two groups of cells that experienced relatively large changes in DTW that brought the water table within 0.3048 m (1 ft) of the land-surface. The left inset map area is characterized by residential developments, while the right inset is mainly comprised of freshwater forested wetlands. The light blue shaded area indicates the horizontal extent of inundation by WNC at MHHW for the three foot SLR scenario modeled by the NOAA Sea-Level Rise Viewer. This result demonstrates the potential for GW head to not only interact with subsurface components of the environment, but also to extend beyond the influence of tidally induced flooding.

[13]The NOAA SLR-Viewer data is in US customary units.

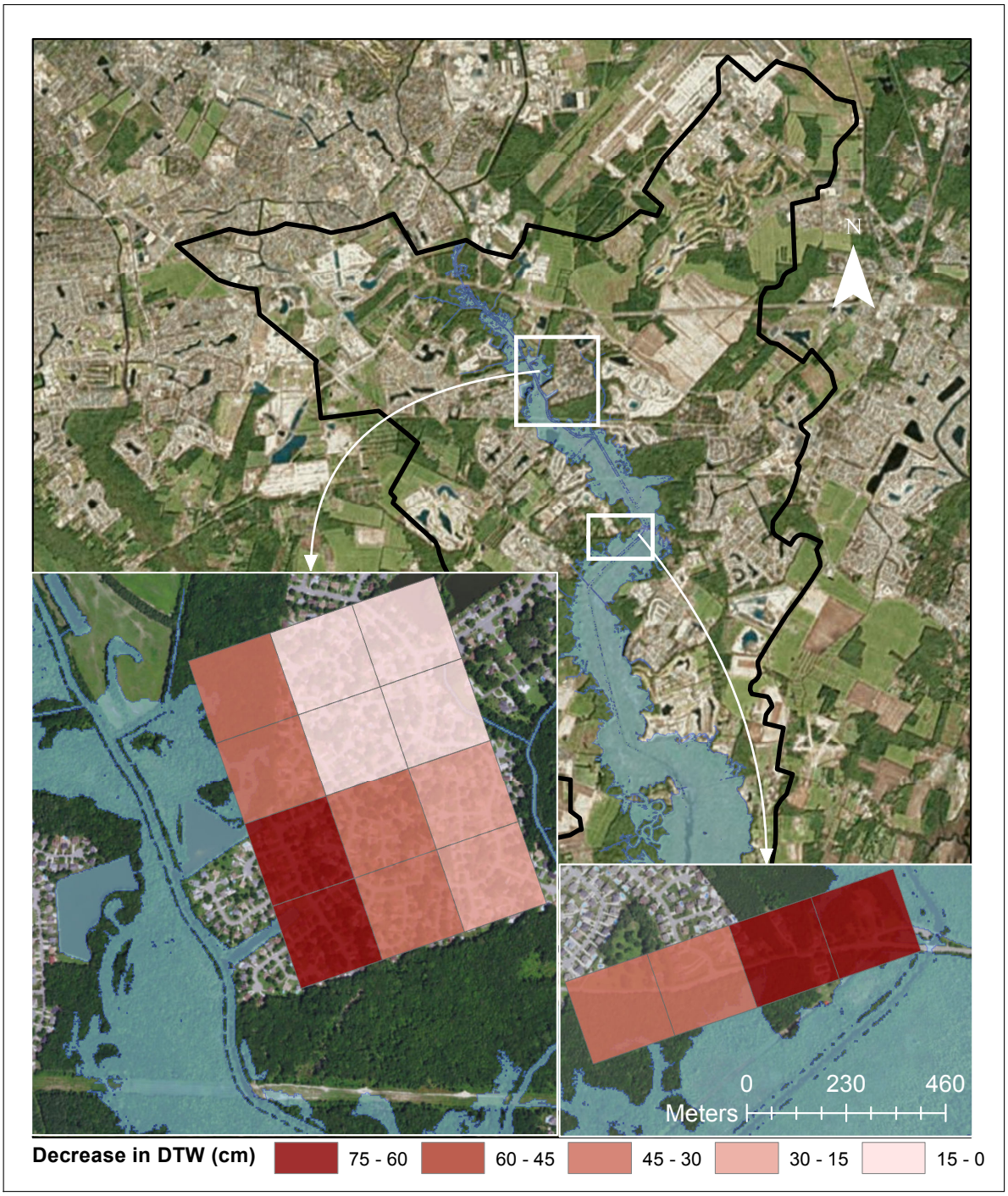

Figure 33: A selection of cells whose DTW is brought within 0.3048 m (1 ft) of the land-surface by SLR. The left inset is focused on a residential area, while the right is comprised mainly of a freshwater forested wetland. The blue shading indicates areas experiencing tidal flooding at MHHW for a 0.9144 m (3 ft) SLR scenario (base map source: ESRI et al. 2017).

These results are particularly important for stakeholders within ∼1 km of the tidal water bodies, those that will be most affected by GW rise. Sewage networks should be constructed to handle greater capacities, to account for both higher tides and the possibility of higher tides occurring with more intense rainfalls. Materials for important subsurface infrastructure, such

as utility lines and septic tanks should be tolerant of salt, as they will be increasingly exposed to brackish and saline waters. Residential developers must recognize that structural foundations and basements may be continuously subject to corrosion and flooding.

Further, longer term adaptation strategies should begin to be contemplated, especially as new research continues to increase the severity of future SLR projections (Sweet et al. 2017). As SLR expands the extent of tidal water bodies, the potential for negative consequences of GW rise migrates inland, further affecting the built and natural environment.

The results from the sensitivity analysis are essential for guiding future data collection efforts to assist in these concerns. Primarily, as indicated by the sensitivity of model results to parameter S4 (see Fig. 31, p. 55 and Fig. 32, p. 55) a better understanding of ET rates in the UZ and the subsurface geology will greatly alleviate uncertainties in these results. The former will require a high-resolution analysis of vegetation and soil properties within WNC watershed. The heterogeneity of hydraulic conductivities is particularly important for better quantifying GW flow, and thus the lateral extent of influence of the tidal boundary. A network of shallow water monitoring wells is needed to understand the initial position of the water table, and moreover, how it fluctuates in response to precipitation events. This would then enable a better representation of the partitioning of precipitation events into infiltration and runoff. A grid of stream-gages monitoring flow through WNC would be of great use for understanding the movement of water overland, enabling further insight into the rainfall/runoff relationship within WNC.

An important consideration in choosing WNC watershed as the study area for this research was that it is representative a typical watershed of the Atlantic Coastal Plain. Stretching from the New York Bight to Georgia and Florida, most of the aquifer systems in this physiographic province have been shaped by successive sea level rise and fall over geologic time scales (Powars et al. 2016). They therefore resemble WNC watershed, with alternating layers of fine clay confining units and vast sandy aquifers. The land surface is similarly characterized by low elevations and little relief, and thus it is reasonable to infer that the rainfall/runoff relationship and GW flow rates will reflect those of WNC. While further work would need to be done to use this model in urban environments, such as incorporating water management infrastructure, this is feasible with the flow-routing capabilities of SWMM. Thus, though the results shown in this work are not valid for the entire region they serve as a proof-of-concept and a starting point of inquiry for local water management concerns along the Atlantic Coast.

7.2 LIMITATIONS

A main shortcoming of this study was the inability to better represent the surficial properties of WNC watershed. By discretizing SWMM into 40000 m^2 cells to match the MODFLOW-NWT grid, heterogeneities in topography, soil type, and many other parameters were effectively 'lumped' together, masking their potential influence on infiltration and/or runoff. However, as discussed in Chapter 3 (p. 15), even the highest resolution models assume homogeneous units at the scale of discretization. Because this study was mainly focused on the movement of GW, the representative element size was chosen to better match the relatively smaller spatial scale

of GW flow, rather than surface water processes.

A second source of uncertainty implicit in hydrological modeling is the effect of the initial conditions on the simulation. At the start of a model run, antecedent soil-moisture conditions and DTW are important in determining how the catchment will respond, but data on their spatial patterns are generally lacking (Ivanov et al. 2004; Noto et al. 2008; Ajami et al. 2014). This study assumed steady-state conditions, with groundwater recharge equal to groundwater discharge over a multiyear period, as a starting point following Smith (2003). This overcame some of the difficulties identified by Ajami et al. (2014), but the effects of the initial forcings can be seen in the Figure 34. The transient simulation has a ~6 month 'initialization' period before stabilizing with respect to forcing via precipitation and infiltrating recharge. This initialization period was therefore excluded in the analysis of the model results.

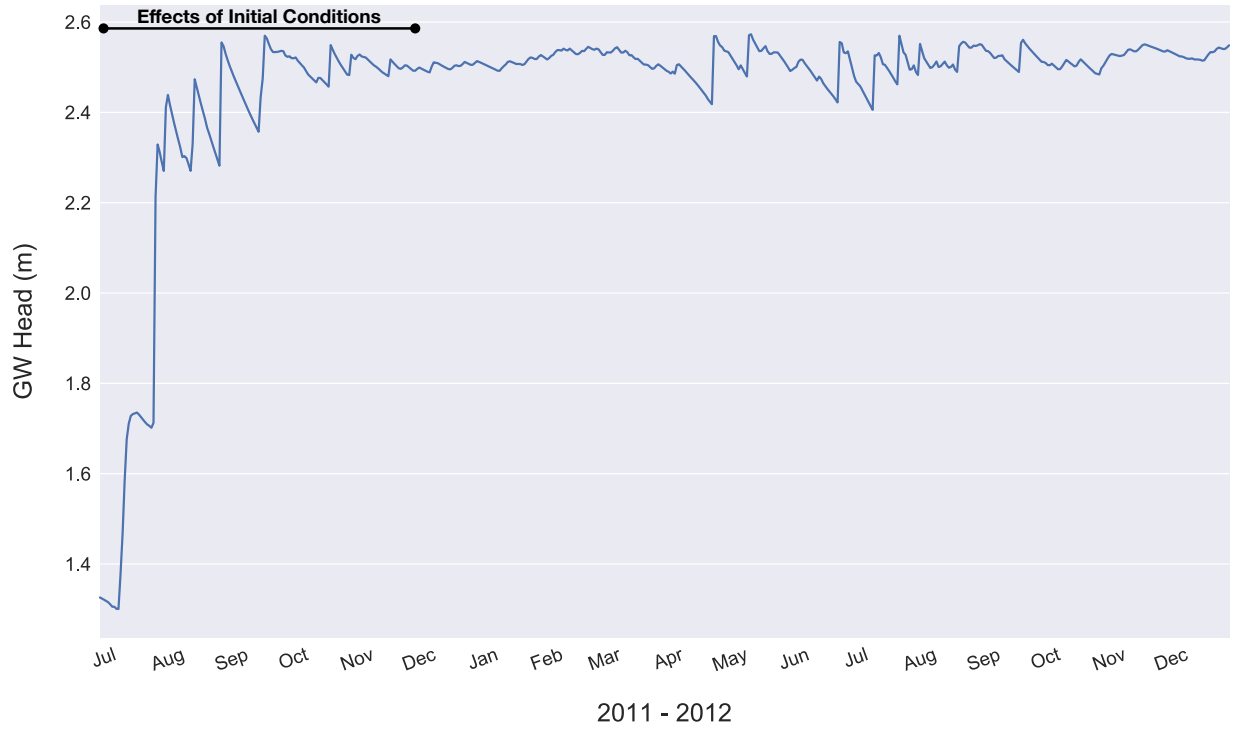

Figure 34: Effects of initial conditions on GW head. Only results after December 1, 2012 were used in this research.

A third source of uncertainty is that this study modeled WNC as a static boundary, instead of simulating oscillating tides. In reality, WNC will expand laterally with SLR, inundating wetland areas and driving expansion of new. This in turn extends the extent SLR impacts GW levels, potentially affecting a much larger area than these results indicate.

7.3 CONCLUSIONS

These limitations highlight the need, as with all scientific studies, for future work. This study focused on an undeveloped watershed with a sole tidal creek influenced by SLR. We took a modeling approach, that coupled the GW flow model MODFLOW-NWT and the rainfall-

runoff model SWMM to simulate the full hydrologic cycle. Using these models enabled us to create a robust tool that can be used in diverse settings, and can capture the spatial variability of a study area better than a simple analytical model. Since the most important finding was the increase of the water table surrounding WNC, future work should focus on developed areas with infrastructure near tidal bodies. Norfolk, Virginia is a prime area for such work as it is primarily urban and abuts the Chesapeake Bay with a number of estuaries that extend inland from it, most notably the Elizabeth River. However to model SLR-induced GW-rise and the resulting interactions with subsurface with enough accuracy to make sound decisions requires a large data collection effort which would include dense measurements of hydraulic conductivity and a well established network of shallow GW monitoring wells.

Under even the best case scenarios, SLR will be an increasing threat to coastal communities, and by extension, inland communities, for decades and centuries to come. Successful mitigation of, and adaptation to, these hazards relies on sound decision making based on the best scientific information available. The results of this study, while only a preliminary investigation, contribute to this information and serve as a basis for future inquiries. The effects of SLR, combined with historic precipitation, are shown to have the potential to cause GW levels to rise to levels that pose risks to underground infrastructure and ecosystems in the tidal watershed of WNC in Virginia Beach. Going forward, all stakeholders, from private citizens to elected officials, must work together to use the knowledge available, while co-creating the knowledge necessary to effectively manage the all important resource of water now, and in the future.

REFERENCES

Ahlfeld, D. P., Barlow, P. M., & Mulligan, A. E., 2005. GWM-A ground-water management process for the U.S. Geological Survey modular ground-water model (MODFLOW-2000), Open-File Report 2005-1072, U.S. Geological Survey.

Ajami, H., Evans, J., McCabe, M., & Stisen, S., 2014. Reducing the spin-up time of integrated surface water-groundwater models, *Hydrology and Earth System Sciences*, **18**(12), 5169–5179.

Alley, R. B., Anandakrishnan, S., Christianson, K., Horgan, H. J., Muto, A., Parizek, B. R., Pollard, D., & Walker, R. T., 2015. Oceanic forcing of ice-sheet retreat: West Antarctica and more, *Annual Review of Earth and Planetary Sciences*, **43**(1), 207–231.

Anderson, W. P. J., 2002. Aquifer salinization from storm overwash, *Journal of Coastal Research*, **18**(3), 413–420.

Anderson, W. P. J., 2014. Coastal environments and global change, in *Coastal Groundwater*, edited by R. Gehrels & G. Masselink, Wiley-Blackwell, 1st edn.

Arnold, J. G., Moriasi, D. N., Gassman, P. W., Abbaspour, K. C., White, M. J., Srinivasan, R., Santhi, C., Harmel, R. D., van Griensven, A., Van Liew, M. W., Kannan, N., & Jha, M. K., 2012. SWAT: Model use, calibration, and validation, *Transactions of the ASABE*, **55**(4), 1491–1508.

Ataie-Ashtiani, B., Werner, A. D., Simmons, C. T., Morgan, L. K., & Lu, C., 2013. How important is the impact of land-surface inundation on seawater intrusion caused by sea-level rise?, *Hydrogeology Journal*, **21**(7), 1673–1677.

Bakker, M., Schaars, F., Hughes, J. D., Langevin, C. D., & Dausman, A. M., 2013. Documentation of the seawater intrusion (SWI2) package for MODFLOW, Techniques and Methods 6-A46, U.S. Geological Survey, Reston, VA.

Bakker, M., Post, V., Langevin, C. D., Hughes, J. D., White, J. T., Starn, J. J., & Fienen, M. N., 2016. Scripting MODFLOW model development using Python and FloPy, *Groundwater*, **54**(5), 733–739.

Barco, J., Wong, K. M., & Stenstrom, M. K., 2008. Automatic calibration of the U.S. EPA SWMM model for a large urban catchment, *Journal of Hydraulic Engineering*, **134**(4), 466–474.

Barlow, P. M., 2003. Ground water in freshwater-salt water environments of the Atlantic Coast, Circular 1262, U.S. Geological Survey, Reston, Virginia.

Barlow, P. M. & Harbaugh, A. W., 2006. USGS directions in MODFLOW development, *Groundwater*, **44**(6), 771–774.

Bear, J., 1999. *Seawater intrusion in coastal aquifers*, Springer Science & Business Media.

Beven, K., 1989. Changing ideas in hydrology–the case of physically-based models, *Journal of Hydrology*, **105**(1), 157–172.

Beven, K., 1993. Prophecy, reality and uncertainty in distributed hydrological modelling, *Advances in Water Resources*, **16**(1), 41–51.

Beven, K., 2002. Towards an alternative blueprint for a physically based digitally simulated hydrologic response modelling system, *Hydrological Processes*, **16**(2), 189–206.

Beven, K., Kirkby, M., Schofield, N., & Tagg, A., 1984. Testing a physically-based flood forecasting model (TOPMODEL) for three U.K. catchments, *Journal of Hydrology*, **69**(1), 119 – 143.

Beven, K. J., 2011. *Rainfall-runoff modelling: The primer*, John Wiley & Sons.

Bjerklie, D., Mullaney, J., Stone, J., & Skinner, B., 2012. Preliminary investigation of the effects of sea-level rise on groundwater levels in New Haven, Connecticut, Open-File Report 2012–1025, U.S. Geological Survey.

Bouwer, H. & Maddock III, T., 1997. Making sense of the interactions between groundwater and streamflow: Lessons for water masters and adjudicators, *Rivers*, **6**(1), 19–31.

Box, G. E. & Draper, N. R., 1987. *Empirical model-building and response surfaces*, Wiley, New York.

Brooks, R. H. & Corey, A. T., 1966. Properties of porous media affecting fluid flow, *Journal of the Irrigation and Drainage Division*, **92**(2), 61–90.

Brunner, P. & Simmons, C. T., 2012. Hydrogeosphere: A fully integrated, physically based hydrological model, *Groundwater*, **50**(2), 170–176.

Bulatewicz Jr, T. F., 2006. *Support for model coupling: An interface-based approach*, Ph.D. thesis, University of Oregon.

Caldwell, W. S., 2001. Hydrologic and salinity characteristics of Currituck Sound and selected tributaries in North Carolina and Virginia, 1998-99, Water-Resources Investigations Report 01–4097, U.S. Geological Survey.

Carr, P. & Van Der Kamp, G., 1969. Determining aquifer characteristics by the tidal method, *Water Resources Research*, **5**(5), 1023–1031.

Chen, C. W. & Shubinski, R. P., 1971. Computer simulation of urban storm water runoff, *Journal of the Hydraulics Division*, **97**(2), 289–301.

Crawford, N. H. & Linsley, R. K., 1966. Digital simulation in hydrology: Stanford watershed model 4, Stanford University.

Dahl, K., Spanger-Siegfried, E., Caldas, A., & Udvardy, S., 2017. Effective inundation of continental United States communities with 21st century sea level rise, *Elem Sci Anth*, **5**(37), 1–21.

Darcy, H., 1856. *Les fontaines publiques de la ville de Dijon*, Paris: Victor Dalmont.

Davis, J., Rohrer, C., & Roesner, L., 2007. Calibration of rural watershed models in the North Carolina Piedmont ecoregion, in *World Environmental and Water Resources Congress 2007: Restoring Our Natural Habitat*, pp. 1–10.

Dewberry and Davis, LLC, 2013. USGS LiDAR: Norfolk (VA), Retrieved from `https://catalog.data.gov/dataset/2013-usgs-lidar-norfolk-va`.

Diersch, H., 2002. FEFLOW: Finite element subsurface flow and transport simulation system, Retrieved from `www.feflow.com`.

Doble, R., Brunner, P., McCallum, J., & Cook, P. G., 2012. An analysis of river bank slope and unsaturated flow effects on bank storage, *Groundwater*, **50**(1), 77–86.

Doherty, J., 2001. Improved calculations for dewatered cells in MODFLOW, *Groundwater*, **39**(6), 863–869.

Doherty, J., 2004. Manual for PEST, *Watermark Numerical Computing*, Brisbane, Queensland, Australia, Retrieved from `http://www.pesthomepage.org/Downloads.php`.

Downer, C. W. & Ogden, F. L., 2002. GSSHA user's manual, gridded surface subsurface hydrologic analysis version 1.43 for wms 6.1, Engineer Research and Development Center, Vicksburg, USA.

Dunne, T. & Black, R. D., 1970. An experimental investigation of runoff production in permeable soils, *Water Resources Research*, **6**, 478–490.

Dunne, T. & Leopold, L. B., 1978. *Water in Environmental Planning*, Macmillan.

Earman, S. & Dettinger, M., 2011. Potential impacts of climate change on groundwater resources – A global review, *Journal of Water and Climate Change*, **2**(4), 213–229.

Eggleston, J. & Pope, J., 2013. Land subsidence and relative sea-level rise in the southern Chesapeake Bay region, Circular 1392, U.S. Geological Survey.

Ellis, J. B., 2001. Sewer infiltration/exfiltration and interactions with sewer flows and groundwater quality, *Interactions between Sewers, Treatment Plants and Receiving Waters in Urban Areas – INTERUBA II*, pp. 311–319.

Epstein, J. M., 2008. Why model?, *Journal of Artificial Societies and Social Simulation*, **11**(4), 12.

ESRI, DigitalGlobe, GeoEye, i-cubed, USDA FSA, USGS, AEX, Getmapping, Aerogrid, IGN, IGP, swisstopo, & GIS User Community, 2017. World Imagery base map, Retrieved from `https://services.arcgisonline.com/ArcGIS/rest/services/NatGeo_World_Map/MapServer`.

Ezer, T., Atkinson, L. P., Corlett, W. B., & Blanco, J. L., 2013. Gulf Stream's induced sea level rise and variability along the U.S. Mid-Atlantic coast, *Journal of Geophysical Research*, **118**(2), 685–697.

Feldman, A. D., 2000. *Hydrologic modeling system HEC-HMS: Technical reference manual*, U.S. Army Corps of Engineers, Hydrologic Engineering Center.

Feltgen, A. H., 2015. South Florida winning war against saltwater intrusion, but it's not cheap, Retrieved from `http://www.floridabulldog.org/2015/06/south-florida-winning-war-against-saltwater-intrusion-but-its-not-cheap`.

Ferguson, G. & Gleeson, T., 2012. Vulnerability of coastal aquifers to groundwater use and climate change, *Nature Climate Change*, **2**(5), 342–345.

Feseker, T., 2007. Numerical studies on saltwater intrusion in a coastal aquifer in Northwestern Germany, *Hydrogeology Journal*, **15**(2), 267–279.

Feth, J. H., 1973. Water facts and figures for planners and managers, Circular 601-1, US Geological Survey.

Fetter, C. W., 2014. *Applied Hydrogeology*, Prentice Hall.

Fleckenstein, J. H., Krause, S., Hannah, D. M., & Boano, F., 2010. Groundwater-surface water interactions: New methods and models to improve understanding of processes and dynamics, *Advances in Water Resources*, **33**(11), 1291–1295.

Fordyce, E., 2014. *Groundwater dynamics of a shallow coastal aquifer*, Master's thesis, University of Otago.

Freeze, R. & Harlan, R., 1969. Blueprint for a physically-based, digitally-simulated hydrologic response model, *Journal of Hydrology*, **9**(3), 237–258.

Furman, A., 2008. Modeling coupled surface-subsurface flow processes: A review, *Vadose Zone Journal*, **7**(2), 741–756.

Gironás, J., Roesner, L. A., Davis, J., Rossman, L. A., & Supply, W., 2009. *Storm water management model applications manual*, National Risk Management Research Laboratory, Office of Research and Development, U.S. Environmental Protection Agency Cincinnati, OH.

Gleick, P. H., 1996. Water resources, in *Encyclopedia of Climate and Weather*, edited by H. Schneider, vol. 2, pp. 817–823, Oxford University Press, New York.

Glover, R. E., 1959. The pattern of fresh-water flow in a coastal aquifer, *Journal of Geophysical Research*, **64**(4), 457–459.

Govindaraju, R. S. & Kavvas, M. L., 1991. Dynamics of moving boundary overland flows over infiltrating surfaces at hillslopes, *Water Resources Research*, **27**(8), 1885–1898.

Green, W. H. & Ampt, G., 1911. Studies on soil phyics, *The Journal of Agricultural Science*, **4**(01), 1–24.

Gregory, M. A., Cunningham, B. A., Schmidt, M. F., & Mack, B. W., 1999. Estimating soil storage capacity for stormwater modeling applications, in *Proceedings of the 6th Biennial Conference on Stormwater Research and Watershed Management, Southwest Florida, FL, USA*, vol. 1417.

Gupta, H. V., Sorooshian, S., & Yapo, P. O., 1998. Toward improved calibration of hydrologic models: Multiple and noncommensurable measures of information, *Water Resources Research*, **34**(4), 751–763.

Gupta, V. K. & Sorooshian, S., 1985. The relationship between data and the precision of parameter estimates of hydrologic models, *Journal of Hydrology*, **81**(1), 57–77.

Habel, S., Fletcher, C. H., Rotzoll, K., & El-Kadi, A. I., 2017. Development of a model to simulate groundwater inundation induced by sea-level rise and high tides in Honolulu, Hawaii, *Water Research*, **114**, 122–134.

Hankerson, M., 2016. Why is Virginia Beach still pumping down water in the Sherwood Lakes neighborhood?, Retrieved from `https://pilotonline.com/news/local/environment/q-a-why-is-virginia-beach-still-pumping-down-water/article_a7543b0e-512e-5d3d-815c-2c2b13e57e6e.html`.

Hansen, J., Sato, M., Hearty, P., Ruedy, R., Kelley, M., Masson-Delmotte, V., Russell, G., Tselioudis, G., Cao, J., Rignot, E., Velicogna, I., Tormey, B., Donovan, B., Kandiano, E., von Schuckmann, K., Kharecha, P., Legrande, A. N., Bauer, M., & Lo, K.-W., 2016. Ice melt, sea level rise and superstorms: Evidence from paleoclimate data, climate modeling, and modern observations that 2° C global warming could be dangerous, *Atmospheric Chemistry and Physics*, **16**(6), 3761–3812.

Harbaugh, A. W., 2005. *MODFLOW-2005, the U.S. Geological Survey modular ground-water model: The ground-water flow process*, U.S. Department of the Interior, U.S. Geological Survey Reston, VA, USA.

Hargreaves, G. H. & Samani, Z. A., 1985. Reference crop evapotranspiration from temperature, *Applied Engineering in Agriculture*, **1**(2), 96–99.

Healy, R. W. & Cook, P. G., 2002. Using groundwater levels to estimate recharge, *Hydrogeology Journal*, **10**(1), 91–109.

Heywood, G., 1997. Accounting for infiltration: A more explicit approach, Paper presented at the Chartered Institute of Water and Environmental Management, London Metropolitan Branch Meeting, London.

Hill, M. C., Banta, E. R., Harbaugh, A. W., & Anderman, E. R., 2000. MODFLOW-2000, the U.S. Geological Survey modular ground-water model; user guide to the observation, sensitivity, and parameter-estimation processes and three post-processing programs, Open-File Report 2000-184, U.S. Geological Survey.

Holdahl, S. R. & Morrison, N. L., 1974. Regional investigations of vertical crustal movements in the u.s., using precise relevelings and mareograph data, *Tectonophysics*, **23**(4), 373 – 390.

Holding, S. & Allen, D. M., 2015. From days to decades: Numerical modelling of freshwater lens response to climate change stressors on small low-lying islands, *Hydrology and Earth System Sciences*, **19**(2), 933–949.

Holly, M. A., Russoniello, C. J., & Byron, L. A., 2013. Global assessment of vulnerability to sea-level rise in topography-limited and rechargelimited coastal groundwater systems, *Water Resources Research*, **49**, 2228–2240.

Horn, D. P., 2002. Beach groundwater dynamics, *Geomorphology*, **48**(1), 121–146.

Horton, R. E., 1933. The role of infiltration in the hydrologic cycle, *EOS*, **14**(1), 446–460.

Horton, R. E., 1941. An approach toward a physical interpretation of infiltration-capacity, *Soil Science Society of America*, **5**(C), 399–417.

Huisman, P., Cramer, W., Van Ee, G., Hooghart, J., Salz, H., & Zuidema, F., 1998. *Water in the Netherlands*, NHV.

Hunt, R. J. & Feinstein, D. T., 2012. MODFLOW-NWT: Robust handling of dry cells using a Newton formulation of MODFLOW-2005, *Groundwater*, **50**(5), 659–663.

Illangasekare, T., Tyler, S. W., Clement, T. P., Villholth, K. G., Perera, A. P. G. R. L., Obeysekera, J., Gunatilaka, A., Panabokke, C. R., Hyndman, D. W., Cunningham, K. J., Kaluarachchi, J. J., Yeh, W. W., van Genuchten, M. T., & Jensen, K., 2006. Impacts of the 2004 tsunami on groundwater resources in Sri Lanka, *Water Resources Research*, **42**(W05201), 1–9.

Ivanov, V. Y., Vivoni, E. R., Bras, R. L., & Entekhabi, D., 2004. Catchment hydrologic response with a fully distributed triangulated irregular network model, *Water Resources Research*, **40**(W11102), 1–23.

Jacob, C., 1950. Flow of ground water, in *Engineering Hydraulics*, edited by H. Rouse, p. 321, John Wiley, New York.

Jang, S., Cho, M., Yoon, J., Yoon, Y., Kim, S., Kim, G., Kim, L., & Aksoy, H., 2007. Using SWMM as a tool for hydrologic impact assessment, *Desalination*, **212**(1), 344–356.

Johanson, R. C. & Davis, H. H., 1980. Users manual for Hydrological Simulation Program-Fortran (HSPF), Research Reporting Series 600, Environmental Research Laboratory, Office of Research and Development, U.S. Environmental Protection Agency.

Johnson, A. I., 1967. Specific yield: Compilation of specific yields for various materials, Water-Supply Paper 1662-D, U.S. Geological Survey.

Johnson, G. H. & Berquist, C., 1989. *Geology and mineral resources of the Brandon and Norge Quadrangles, Virginia*, vol. 87, Commonwealth of Virginia, Dept. of Mines, Minerals and Energy, Division of Mineral Resources.

Johnson, S., Barry, D., Christofi, N., & Patel, D., 2001. Potential for anaerobic biodegradation of linear alkylbenzene cable oils: Literature review and preliminary investigation, *Land Contamination and Reclamation*, **9**(3), 279–291.

Khaled, I. M., Tsuyoshi, M., Kohei, N., Taku, N., & Hiromi, I., 2011. Experimental and modeling investigation of shallow water table fluctuations in relation to Reverse Wieringermeer Effect, *Open Journal of Soil Science*, **01**(02), 17–24.

Kidmose, J., Refsgaard, J., Troldborg, L., Seaby, L., & Escrivà, M., 2013. Climate change impact on groundwater levels: Ensemble modelling of extreme values, *Hydrology and Earth System Sciences*, **17**, 1619–1634.

Kleinosky, L. R., Yarnal, B., & Fisher, A., 2006. Vulnerability of Hampton Roads, Virginia to storm-surge flooding and sea-level rise, *Natural Hazards*, **40**(1), 43–70.

Koeberl, C., Poag, C. W., Reimold, W. U., & Brandt, D., 1996. Impact origin of the Chesapeake Bay structure and the source of the North American Tektites, *Science*, **271**(5253), 1263–1266.

Konikow, L. F., Goode, D. J., & Hornberger, G. Z., 1996. A three-dimensional method-of-characteristics solute-transport model (moc3d), Water-Resources Investigations Report 96-4267, U.S. Geological Survey.

Kundzewicz, Z. W. & Doell, P., 2009. Will groundwater ease freshwater stress under climate change?, *Hydrological Sciences Journal*, **54**(4), 665–675.

Lerner, D. N. & Barrett, M. H., 1996. Urban groundwater issues in the United Kingdom, *Hydrogeology Journal*, **4**(1), 80–89.

Li, H., Lin, L., & Burks-Copes, K. A., 2012. Modeling of coastal inundation, storm surge, and relative sea-level rise at Naval Station Norfolk, Norfolk, Virginia, USA, *Journal of Coastal Research*, **29**(1), 18–30.

Li, L., Barry, D., Stagnitti, F., & Parlange, J.-Y., 1999. Submarine groundwater discharge and associated chemical input to a coastal sea, *Water Resources Research*, **35**(11), 3253–3259.

Li, Q., Unger, A., Sudicky, E., Kassenaar, D., Wexler, E., & Shikaze, S., 2008. Simulating the multi-seasonal response of a large-scale watershed with a three-dimensional physically-based hydrologic model, *Journal of Hydrology*, **357**(3), 317–336.

Liu, G., Craig, J. R., & Soulis, E. D., 2010. Applicability of the Green-Ampt infiltration model with shallow boundary conditions, *Journal of Hydrologic Engineering*, **16**(3), 266–273.

Loague, K., ed., 2010. *Benchmark Papers in Hydrology: Rainfall–Runoff Modelling*, IAHS Press, Wallingford UK.

Manda, A. K., Sisco, M. S., Mallinson, D. J., & Griffin, M. T., 2015. Relative role and extent of marine and groundwater inundation on a dune-dominated barrier island under sea-level rise scenarios, *Hydrological Processes*, **29**(8), 1894–1904.

Markstrom, S. L., Niswonger, R. G., Regan, R. S., Prudic, D. E., & Barlow, P. M., 2008. GSFLOW-Coupled ground-water and surface-water flow model based on the integration of the Precipitation-Runoff Modeling System (PRMS) and the Modular Ground-Water Flow Model (MODFLOW-2005), Techniques and Methods 6-D1, U.S. Geological Survey.

Markstrom, S. L., Regan, R. S., Hay, L. E., Viger, R. J., Webb, R. M., Payn, R. A., & LaFontaine, J. H., 2015. PRMS-IV, the precipitation-runoff modeling system, Version 4, Techniques and Methods 6-B7, U.S. Geological Survey.

Masterson, J., 2004. Simulated interaction between freshwater and saltwater and effects of ground-water pumping and sea-level change, lower Cape Cod aquifer system, Massachusetts, Scientific Investigations Report 2004-5014, U.S. Geological Survey.

Masterson, J. P. & Garabedian, S. P., 2007. Effects of sea-level rise on ground water flow in a coastal aquifer system, *Groundwater*, **45**(2), 209–217.

Masterson, J. P., Fienen, M. N., Thieler, E. R., Gesch, D. B., Gutierrez, B. T., & Plant, N. G., 2014. Effects of sea-level rise on barrier island groundwater system dynamics–ecohydrological implications, *Ecohydrology*, **7**(3), 1064–1071.

Matsuura, K., Willmott, C., & Legates, D., 2009. WebWIMP: The web-based, water-budget, interactive, modeling program, Retrieved from `http://climate.geog.udel.edu/~wimp/`.

McFarland, E. & Bruce, T., 2006. The Virginia Coastal Plain hydrogeologic framework, Professional Paper 1731, U.S. Geological Survey.

McFarlane, B., 2011. Climate change in Hampton Roads Phase II: Storm surge vulnerability and public outreach, Hampton Roads Planning District Commission, Chesapeake, Virginia.

McFarlane, B., 2012. Climate change in Hampton Roads Phase III: Sea-level rise in Virginia, Hampton Roads Planning District Commission, Chesapeake, Virginia.

Meng, III, A. A. & Harsh, J. F., 1988. Hydrogeologic framework of the Virginia Coastal Plain, Professional Paper 1404-C, U.S. Geological Survey.

Mixon, R. B., Berquist Jr., C. R., Newell, W. L., Johnson, G. H., Powars, D. S., Schindler, J. S., & Rader, E. K., 1989. Geological map and generalized cross sections of the coastal plain and adjacent parts of the Piedmont, Virginia, IMAP 2033, U.S. Geological Survey.

Morita, M. & Chie Yen, B., 2000. Numerical methods for conjunctive two-dimensional surface and three-dimensional sub-surface flows, *International Journal for Numerical Methods in Fluids*, **32**(8), 921–957.

Morris, S., Cobby, D., Zaidman, M., & Fisher, K., 2015. Modelling and mapping groundwater flooding at the ground surface in Chalk catchments, *Journal of Flood Risk Management*.

Morrison, P. J. & Taylor, R., 1994. Foundations in a rising groundwater environment, in *Groundwater problems in urban areas*, edited by W. Wilkonson, pp. 342–354, Thomas Telford Services Ltd, London, U.K.

Moss, A., 2016. *Coastal water table mapping: Incorporating groundwater data into flood inundation forecasts*, Master's thesis, Duke University.

Musgrave, G., 1955. How much of the rain enters the soil?, in *Water, Yearbook of Agriculture*, pp. 151–159, U.S. Department of Agriculture.

National Geographic, Esri, DeLorme, HERE, UNEP-WCMC, USGS, NASA, ESA, METI, NRCAN, GEBCO, NOAA, & increment P Corp., 2017. National Geographic base map, Retrieved from `https://services.arcgisonline.com/ArcGIS/rest/services/NatGeo_World_Map/MapServer`.

Neitsch, S. L., Arnold, J. G., Kiniry, J. R., & Williams, J. R., 2001. Soil and water assessment tool theoretical documentation, Version 2000, Texas Water Resources Institute Technical Report 406, Grassland, Soil and Water Research service.

Nicklow, J. W., Boulos, P. F., & Muleta, M. K., 2006. *Comprehensive urban hydrologic modeling handbook for engineers and planners*, MWH Soft, Incorporated.

Niswonger, R. G. & Prudic, D. E., 2005. Documentation of the streamflow-routing (SFR2) package to include unsaturated flow beneath streams–a modification to SFR1, Techniques and Methods 6-A13, U.S. Geological Survey.

Niswonger, R. G., Prudic, D. E., & Regan, R. S., 2006. Documentation of the unsaturated-zone flow (UZF1) package for modeling unsaturated flow between the land surface and the water table with MODFLOW-2005, Techniques and Methods 6-A19, U.S. Geological Survey.

Niswonger, R. G., Panday, S., & Ibaraki, M., 2011. MODFLOW-NWT, a Newton formulation for MODFLOW-2005, Techniques and Methods 6–A37, U.S. Geological Survey.

NOAA, 2010. Coastal Change Analysis Program (C-CAP) regional landcover, Retrieved from `https://coast.noaa.gov/ccapatlas`.

NOAA, 2017. Sea levels online – Sea level variations of the United States derived from national water level observation network stations, Retrieved from `https://tidesandcurrents.noaa.gov/sltrends/sltrends.html`.

Noto, L. V., Ivanov, V. Y., Bras, R. L., & Vivoni, E. R., 2008. Effects of initialization on response of a fully-distributed hydrologic model, *Journal of Hydrology*, **352**(1), 107–125.

Oreskes, N., Shrader-Frechette, K., & Belitz, K., 1994. Verification, validation, and confirmation of numerical models in the earth sciences, *Science*, **263**(5147), 641–646.

Oude Essink, G. H., 2001. Salt water intrusion in a three-dimensional groundwater system in the netherlands: A numerical study, *Transport in Porous Media*, **43**(1), 137–158.

Oude Essink, G. H., van Baaren, E. S., & de Louw, P. G. B., 2010. Effects of climate change on coastal groundwater systems: A modeling study in the Netherlands, *Water Resources Research*, **46**(W00F04), 1–16.

Penman, H. L., 1961. Weather, plant and soil factors in hydrology, *Weather*, **16**(7), 207–219.

Peterson, E. W. & Wicks, C. M., 2006. Assessing the importance of conduit geometry and physical parameters in karst systems using the storm water management model (SWMM), *Journal of Hydrology*, **329**(1), 294–305.

Pinault, J.-L., Amraoui, N., & Golaz, C., 2005. Groundwater-induced flooding in macropore-dominated hydrological system in the context of climate changes, *Water Resources Research*, **41**(W05001), 1–16.

Poag, C. W., Koeberl, C., & Reimold, W. U., 2004. *The Chesapeake Bay Crater: Geology and geophysics of a Late Eocene submarine impact structure*, Springer.

Powars, D. S. & Bruce, T., 1999. The effects of the Chesapeake Bay impact crater on the geological framework and correlation of hydrogeologic units of the lower York-James Peninsula, Virginia, Professional Paper 1622, U.S. Geological Survey, Washington DC.

Powars, D. S., Edwards, L. E., Johnson, G. H., & Berquist, C. R., 2016. Geology of the Virginia Coastal Plain: New insights from continuous cores and geophysical surveys, in *The Geology of Virginia*, edited by C. M. Bailey, W. C. Sherwood, L. S. Eaton, & D. S. Powars, Special Publication 18, Virginia Museum of Natural History.

Prudic, D. E., Konikow, L. F., & Banta, E. R., 2004. A new streamflow-routing (SFR1) package to simulate stream-aquifer interaction with MODFLOW-2000, Techniques and Methods 6-A40, U.S. Geological Survey.

Refsgaard, J. C. & Henriksen, H. J., 2004. Modelling guidelines–terminology and guiding principles, *Advances in Water Resources*, **27**(1), 71–82.

Reilly, T. & Goodman, A., 1987. Analysis of saltwater upconing beneath a pumping well, *Journal of Hydrology*, **89**(3-4), 169–204.

Rekker, J., 2012. The South Dunedin Coastal Aquifer and effect of sea level fluctuations, Otaga Regional Council.

Riaño-Briceño, G., Barreiro-Gomez, J., Ramirez-Jaime, A., Quijano, N., & Ocampo-Martinez, C., 2016. MatSWMM—An open-source toolbox for designing real-time control of urban drainage systems, *Environmental Modelling and Software*, **83**, 143–154.

Richards, L. A., 1931. Capillary conduction of liquids through porous mediums, *Journal of Applied Physics*, **1**(5), 318–333.

Richey, A. S., Thomas, B. F., Lo, M.-H., Reager, J. T., Famiglietti, J. S., Voss, K., Swenson, S., & Rodell, M., 2015. Quantifying renewable groundwater stress with GRACE, *Water Resources Research*, **51**(7), 5217–5238.

Robinson, C., Li, L., & Barry, D., 2007. Effect of tidal forcing on a subterranean estuary, *Advances in Water Resources*, **30**(4), 851–865.

Rockstrom, J., Steffen, W., Noone, K., Persson, A., Chapin, F. S., Lambin, E. F., Lenton, T. M., Scheffer, M., Folke, C., Schellnhuber, H. J., Nykvist, B., de Wit, C. A., Hughes, T., van der Leeuw, S., Rodhe, H., Sorlin, S., Snyder, P. K., Costanza, R., Svedin, U., Falkenmark, M., Karlberg, L., Corell, R. W., Fabry, V. J., Hansen, J., Walker, B., Liverman, D., Richardson, K., Crutzen, P., & Foley, J. A., 2009. A safe operating space for humanity, *Nature*, **461**(7263), 472–475.

Rodriguez-Iturbe, I., Porporato, A., Laio, F., & Ridolfi, L., 2001. Plants in water-controlled ecosystems: Active role in hydrologic processes and response to water stress, *Advances in Water Resources*, **24**(7), 695–705.

Romah, T., 2012. *Advanced methods in sea level rise vulnerability assessment*, Master's thesis, Florida Atlantic University.

Rossman, L. A., 2015. *Storm water management model user's manual, Version 5.1*, National Risk Management Research Laboratory, Office of Research and Development, U.S. Environmental Protection Agency Cincinnati.

Rossman, L. A. & Huber, W. C., 2016. *Storm water management model reference manual, Volume I - Hydrology - Revised*, National Risk Management Research Laboratory, Office of Research and Development, U.S. Environmental Protection Agency Cincinnati.

Rotzoll, K. & Fletcher, C. H., 2012. Assessment of groundwater inundation as a consequence of sea-level rise, *Nature Climate Change*, **3**(5), 477–481.

Rowan, A., 2001. *Development of the multiple model broker, a system integrating stormwater and groundwater models of different spatial and temporal scales using embedded GIS functionality*, Ph.D. thesis, PhD Dissertation. Rutgers, The State University of New Jersey: New Brunswick, NJ.

Rozell, D. J. & Wong, T.-f., 2010. Effects of climate change on groundwater resources at Shelter Island, New York State, USA, *Hydrogeology Journal*, **18**(7), 1657–1665.

Saint-Venant, A. d., 1871. Theorie du mouvement non permanent des eaux, avec application aux crues des rivieres et a líintroduction de marees dans leurs lits.íí, *Comptes rendus des seances de líAcademie des Sciences*, **36**, 174–154.

Sanford, W., 2003. Heat flow and brine generation following the Chesapeake Bay bolide impact, *Journal of Geochemical Exploration*, **78–79**, 243–247.

Sanford, W. E., Pope, J. P., & Nelms, D. L., 2009. Simulation of groundwater-level and salinity changes in the Eastern Shore, Virginia, Scientific Investigations Report 2009-5066, U.S. Geological Survey, Washington DC.

Schroeder, P. R., Dozier, T. S., Zappi, P. A., McEnroe, B. M., Sjostrom, J. W., & Peyton, R. L., 1994. The hydrologic evaluation of landfill performance (HELP) model: Engineering documentation for Version 3, *Environmental Protection Agency, United States*.

Scott, T. W., Swift, D. J., Whittecar, G. R., & Brook, G. A., 2010. Glacioisostatic influences on virginia's late pleistocene coastal plain deposits, *Geomorphology*, **116**(1), 175 – 188.

Sejna, M. & Simunek, J., 2007. HYDRUS (2D/3D): Graphical user interface for the HYDRUS software package simulating two-and three-dimensional movement of water, heat, and multiple solutes in variably-saturated media, technical manual, Version 1.0, `https://www.pc-progress.com/en/default.aspx?hydrus-3d`.

Serrano, S. E., 2004. Modeling infiltration with approximate solutions to Richard's equation, *Journal of Hydrologic Engineering*, **9**(5), 421–432.

Shah, N., Nachabe, M., & Ross, M., 2007. Extinction depth and evapotranspiration from ground water under selected land covers, *Groundwater*, **45**(3), 329–338.

Sherif, M. M. & Singh, V. P., 1999. Effect of climate change on sea water intrusion in coastal aquifers, *Hydrological Processes*, **13**(8), 1277–1287.

Sherman, L. K., 1932. Streamflow from rainfall by the unit-graph method, *Engineering News Record*, **108**, 501–505.

Singh, V. P. & Woolhiser, D. A., 2002. Mathematical modeling of watershed hydrology, *Journal of Hydrologic Engineering*, **7**(4), 270–292.

Small, C., 2003. A global analysis of human settlement in coastal zones, *Journal of Coastal Research*, **19**(3), 584–599.

Smith, B., 2003. Ground-water flow and saline water in the shallow aquifer system of the southern watersheds of Virginia Beach, Virginia, Water-Resources Investigations Report 03-4258, U.S. Geological Survey.

Smith, B. & Harlow, G., 2002. Conceptual hydrogeologic framework of the shallow aquifer system at Virginia Beach, Virginia, Water-Resources Investigations Report 01-4262, U.S. Geological Survey.

Smith, R. E. & Woolhiser, D. A., 1971. Overland flow on an infiltrating surface, *Water Resources Research*, **7**(4), 899–913.

Sophocleous, M., 2002. Interactions between groundwater and surface water: The state of the science, *Hydrogeology Journal*, **10**(1), 52–67.

Sophocleous, M., 2004. Groundwater recharge, *Encyclopedia of Life Support Systems (EOLSS)*.

Steffen, W., Richardson, K., Rockström, J., Cornell, S. E., Fetzer, I., Bennett, E. M., Biggs, R., Carpenter, S. R., de Vries, W., de Wit, C. A., Folke, C., Gerten, D., Heinke, J., Mace, G. M., Persson, L. M., Ramanathan, V., Reyers, B., & Sörlin, S., 2015. Planetary boundaries: Guiding human development on a changing planet, *Science*, **347**(6223).

Sweet, W., Kopp, R., Weaver, C., Obeyskera, J., Horton, R., Thieler, E., & Zervas, C., 2017. Global and regional sea level rise scenarios for the United States, NOS CO-OPS 083, National Oceanographic and Atmospheric Administration, Silver Spring, MD.

Tal, E., 2016. Diagram of the Water Cycle, Retrieved from `https://commons.wikimedia.org/wiki/File%3ADiagram_of_the_Water_Cycle.jpg`.

Temprano, J., Arango, Ó., Cagiao, J., Suárez, J., & Tejero, I., 2005. Stormwater quality calibration by SWMM: A case study in Northern Spain, *Water SA*, **32**(1), 55–63.

Theis, C. V., 1938. The significance and nature of the cone of depression in ground-water bodies, *Economic Geology*, **33**(8), 889–902.

Therrien, R. & Sudicky, E., 1992. *Three-dimensional analysis of variably-saturated flow and solute transport in discretely-fractured porous media*, Ph.D. thesis, University of Waterloo, Waterloo, Ontario.

Thoms, R. B., Johnson, R. L., & Healy, R. W., 2006. User's guide to the Variably Saturated Flow (VSF) process to MODFLOW, Techniques and Methods 6-A18, U.S. Geological Survey.

Tian, Y., Zheng, Y., Wu, B., Wu, X., Liu, J., & Zheng, C., 2015. Modeling surface water-groundwater interaction in arid and semi-arid regions with intensive agriculture, *Environmental Modelling and Software*, **63**, 170 – 184.

Toth, J., 1963. A theoretical analysis of groundwater flow in small drainage basins, *Journal of Geophysical Research*, **68**(16), 4795–4812.

Tsihrintzis, V. A. & Hamid, R., 1998. Runoff quality prediction from small urban catchments using SWMM, *Hydrological Processes*, **12**(2), 311–329.

Turner, I. L., 1998. Monitoring groundwater dynamics in the littoral zone at seasonal, storm, tide and swash frequencies, *Coastal Engineering*, **35**(1), 1–16.

Uchrin, C., Ahn, H. C., Mun, Y., Rowan, A., & Belton, T., 2002. A watershed mathematical model for assessing septic impacts to Cranberry Lake, NJ, in *Proceedings 34th Mid-Atlantic Industrial and Hazardous Waste Conference, MM Haggblom*, edited by K. Lee & D. Fennel, pp. 282–284, Rutgers University.

U.S. Census Bureau, 2012. 2010 census of population and housing, *Population and Housing Unit Counts*, CPH-2-48, Virginia U.S. Government Printing Office, Washington, DC, Retrieved from `http://www.census.gov/prod/cen2010/cph-2-48.pdf`.

van Gaalen, J., Kruse, S., Lafrenz, W., & Burroughs, S., 2013. Predicting water table response to rainfall events, Central Florida, *Groundwater*, **51**(3), 350–362.

Vandenbohede, A., Luyten, K., & Lebbe, L., 2008. Effects of global change on heterogeneous coastal aquifers: A case study in Belgium, *Journal of Coastal Research*, **24**, 160–170.

Vázquez-Suñé, E., Sánchez-Vila, X., & Carrera, J., 2005. Introductory review of specific factors influencing urban groundwater, an emerging branch of hydrogeology, with reference to Barcelona, Spain, *Hydrogeology Journal*, **13**(3), 522–533.

Veihmeyer, F. & Hendrickson, A., 1931. The moisture equivalent as a measure of the field capacity of soils., *Soil Science*, **32**(3), 181–194.

Viswanathan, M., 1983. The rainfall/water-table level relationship of an unconfined aquifer, *Groundwater*, **21**(1), 49–56.

Watson, T. A., Werner, A. D., & Simmons, C. T., 2010. Transience of seawater intrusion in response to sea level rise, *Water Resources Research*, **46**(W12533), 1–10.

Wehrmann, H. A., 2008. Enhancing groundwater recharge for water supply, Retrieved from `http://pcgcd.org/recharge-enhancement`.

Werner, A. D. & Simmons, C. T., 2009. Impact of sealevel rise on sea water intrusion in coastal aquifers, *Groundwater*, **47**(2), 197–204.

Winston, R., 2010. Online guide to MODFLOW, Retrieved from `https://water.usgs.gov/nrp/gwsoftware/modflow2000/MFDOC`.

Winston, R. B., 2009. *ModelMuse–A graphical user interface for MODFLOW-2005 and PHAST*, U.S. Geological Survey.

Winter, T. C., 1999. Relation of streams, lakes, and wetlands to groundwater flow systems, *Hydrogeology Journal*, **7**(1), 28–45.

Winter, T. C. & Rosenberry, D. O., 1998. Hydrology of prairie pothole wetlands during drought and deluge: A 17-year study of the Cottonwood Lake wetland complex in North Dakota in the perspective of longer term measured and proxy hydrological records, *Climatic Change*, **40**(2), 189–209.

Wong, P. P., Losada, I. J., Gattuso, J.-P., Hinkel, J., Khattabi, A., McInnes, K. L., Saito, Y., & Sallenger, A., 2014. IPCC, 2014: Contribution of Working Group II to the Fifth Assessment Report of the Intergovernmental Panel on Climate Change. Climate Change 2014: Impacts, Adaptation, and Vulnerability. Part A: Global and Sectoral Aspects. Coastal systems and Low-lying areas.

Wright, K. M. & Hogan, C., 2008. The potential impacts of global sea level rise on transportation, Part 1: Methodology, IFC, U.S. DOT Center for Climate Change and Environmental Forecasting, Retrieved from `http://climate.dot.gov/impacts-adaptations/pdf/entire.pdf`.

Xu, C.-Y. & Singh, V. P., 1998. A review on monthly water balance models for water resources investigations, *Water Resources Management*, **12**(1), 20–50.

Yapo, P. O., Gupta, H. V., & Sorooshian, S., 1996. Automatic calibration of conceptual rainfall-runoff models: Sensitivity to calibration data, *Journal of Hydrology*, **181**(1-4), 23–48.

Yergeau, S. E., 2010. *Development and application of a coupled SWMM/MODFLOW model for an urban wetland*, Ph.D. thesis, Rutgers University-Graduate School-New Brunswick.

Zervas, C. E., 2009. Sea level variations of the United States, 1854-2006, NOS CO-OPS 053, National Oceanic and Atmospheric Administration.

VITA

Brett A. Buzzanga

Department of Ocean, Earth, and Atmospheric Sciences
4600 Elkhorn Ave. Norfolk, VA 23508
Center for Coastal Physical Oceanography
4111 Monarch Way Norfolk, VA 23508
Old Dominion University

EDUCATION

Master of Science — Ocean, Earth, and Atmospheric Sciences
December 2017 — Concentration: Hydrological Science
Old Dominion University

Thesis: Precipitation and sea level rise impacts on groundwater levels in Virginia Beach, Virginia

Associate of Science
December 2013 — Concentration: Math/Science
Brookdale Community College

Bachelor of Arts — School of Arts and Sciences
May 2011 — Concentration: Political Philosophy
Rutgers University

PUBLICATIONS

Bekaert, D.P.S., Hamlington, B.D., **Buzzanga, B.**, & Jones, C.E., 2017. Spaceborne synthetic aperture radar survey of subsidence in Hampton Roads, Virginia (USA). *Nature Scientific Reports*, **7**(1), 14752.

PRESENTATIONS

Buzzanga, B., 2016. Sea level rise impacts on precipitation-induced flooding. Poster presentation at the *American Geophysical Union, Fall Meeting*, San Francisco, California.

Buzzanga, B., Plag, H.P., 2016. Linking earth observations and models to societal information needs: The case of coastal flooding. Oral presentation at the *American Geophysical Union, Fall Meeting*, San Francisco, California.

Roberts-Pierre, B., **Buzzanga, B.**, Pasco, M., Charlam, B., Patrick, J., 2015. Sensing the Sounds: An updated land use/landcover classification of the Albemarle and Pamlico Sounds. Oral presentation at *NASA Langley*, Langley Air Force Base, Hampton, VA.